A STUDY OF A SUPERSONIC AXIAL FLOW COMPRESSOR

by

WU - WAI CHAO

S.B., National Tung-Chi University of China

(1943)

M.S., Massachusetts Institute of Technology

(1945)

SUBMITTED IN PARTIAL FULFILLMENT OF THE
REQUIREMENTS FOR THE DEGREE OF
DOCTOR OF SCIENCE

at the

MASSACHUSETTS INSTITUTE OF TECHNOLOGY

(1949)

Signature of Author Signature redacted .....
Department of Mechanical Engineering, January 1, 1949

Certified by Signature redacted .....
Thesis Supervisor

Signature redacted

.....
Chairman, Department Committee on Graduate Students

Professor Jacob P.Den Hartog
Chairman, Department Committee
on Graduate Students
Massachusetts Institute of Technology

Dear Sir:

In partial fulfillment of the requirements for the degree of Doctor of Science from the Massachusetts Institute of Technology, I hereby submit my thesis entitled " A STUDY OF A SUPERSONIC AXIAL FLOW COMPRESSOR "

Respectfully yours,

Signature redacted

TABLE OF CONTENTS

ACKNOWLEDGEMENT

ABSTRACT

NOMENCLATURE

page

I. INTRODUCTION 1

II. PRIMARY INVESTIGATIONS AT ONE RADIUS

1. General Analysis 4
2. Non-Dimensional Calculations of Performances at different Design points 9
3. Summary 16

III. NON-DIMENSIONAL ANALYSIS OF FLOW CHARACTERISTICS AT ONE RADIUS

1. Calculation of Flow Characteristics 18
2. Conditions of Choking 24
3. Summary and Discussion 26

IV. ANALYSIS OF A SINGLE STAGE COMPRESSOR OF CONSTANT CIRCULATION

1. Considerations of Radial Equilibrium 29
2. Considerations of Constant Circulation 32
3. Pressure Distributions 34
4. Blade Angles and Blade Height 37
5. Non-Dimensional Calculation of Performances 40
6. The Design Curve 46
7. The Effective Design Points 54
8. Summary and Discussion 56

V. OUTLET STATOR

1. Introduction 60
2. Limiting Contraction Ratio of Stator Passage 62
3. Non-Dimensional Calculations of Optimum Performances at Various Design Points 66
4. Supersonic Cascade for Stator Design 69
5. Summary 74

VI. EXPERIMENTAL FIELD ON THE SUPERSONIC CASCADE page

1. Introduction 76
2. Theory of Hydraulic Analogy 77
3. Resemblance of Normal Hydraulic Jump to the Normal Compression Shock 84
4. Analogy in Water Channel Width and Area of Compressible Flow Passage 88
5. Resemblance in Limiting Contraction Ratio and Experimental Tests 91
   a. Theory
   b. Experimental Tests
   c. Conclusions
6. Design of the Experimental Supersonic Cascade 102
7. Experimental Results on the Supersonic Cascade Tests in Water Channel 104
8. Starting Conditions 112
9. Summary and Conclusion 120

APPENDIX

I. PHOTOGRAPHS OF THE SUPERSONIC DIFFUSER TIPS AND CASCADE 125

II. PHOTOGRAPHIC RESULTS OF THE EXPERIMENT ON SUPERSONIC DIFFUSERS 126

III. PHOTOGRAPHIC RESULTS OF THE EXPERIMENT ON SUPERSONIC CASCADE 128

IV. Fig(1) TO Fig(45) 137

V. TABLES 182 to 212

REFERENCES

BIOGRAPHY OF AUTHOR

ACKNOWLEDGEMENT

The author wishes to express his deepest appreciation to Professor William R. Hawthrone for his advice and for his supervision of this thesis. He is also indebted to Professor Ascher H. Shapiro for his interest in this research.

ABSTRACT

An effective design range for the single stage axial flow compressor with supersonic stator is presented.

The compressor consists of a subsonic inlet guide fan, a subsonic rotor, and a supersonic stator.

Flow is considered being adiabatic and reversible except for the compression shock in stator. Radial equilibrium before and after rotor is considered with the assumption of constant circulation at all radii.

Construction of rotor resembles that of a conventional turbine, there is no pressure increase across it. Pure impulse type blading is adopted for rotor at tip radius. Hence low rotor losses can be expected.

Design of the supersonic stator is presented. Optimum performances are accomplished by controlling normal compression shock at throat section of stator passage. Calculated for all design possibilities under this condition, the efficiency drop in stator from shroud to hub shows less than 9%. Prevention of flow separation in the compression shock can be succeeded by installing suction slits. It also helps to stabilize

the position of normal compression shock.

The compressor performance depends mainly on the efficiency of stator. Experimental study of flow patterns for a two-dimensional cascade for stator design through hydraulic analogy is presented. It concluded that the contraction ratio of stator at any radius is a function of the entering flow Mach Number only. The establishment of supersonic flow in stator at design condition is preceded by a normal compression shock at stator entrance, similar to the supersonic diffusers.

Although the limiting contraction ratios for supersonic cascades and diffusers are the same at the same design Mach Numbers of approaching flow, the flow patterns during starting conditions are different. For that reason,the inevitable 'spill' condition of supersonic diffuser during the start is avoided by the supersonic cascade. Therfore the compressor should not offer any problem in starting.

The flow characteristics of the compressor will be just the opposite to that of a conventional one. Compression ratio and efficiency increase with increasing flow, until it reaches the design condition. Choking of the compressor starts at further increase

of mass flow, hence sharp drop in performance follows.

Such a compressor will be unstable,if it is connected with a conventional turbine. But it can be coupled with a turbine, which also has flow characteristics opposite to the conventional ones. Perhaps a supersonic turbine.

The analytical study is consistently non-dimensional. Therefore the results presented can be applied to any operating condition and compressor dimension.

The primary investigations start at one radius. The particular velocity diagram chosen is a result of the following considerations:

1. subsonic inlet and rotor condition, supersonic velocity entering stator.
2. maximum work done.
3. no pressue increase across rotor in order to keep rotor losses low.

Flow is assumed being steady, two-dimensional, adiabatic and reversible except the normal compression shock at stator entrance. The maximum turning angle in rotor, chosen $\theta = 120^{\circ}$, is based on the present knowledge of subsonic turning of flow. The maximum and minimum operating compressor Mach Number for each turning angle design in rotor are determined by the limits of sonic rotor and

stator condition respectively. The minimum turning angle in rotor is determined by the sonic rotor condition and a compression ratio not less than 2. Thus a design range is outlined. A complete survey of the design points within this range is presented. Flow characteristics for various design points are calculated.

The constant circulation design is adopted in order to fulfill the condition of radial equilibrium of flow before and after rotor. To keep rotor losses low, no compression of flow in rotor is attempted. Hence the velocity diagram in one-radius analysis is fitted to the tip radius of compressor.

Blade height is limited by the condition of sonic relative velocity leaving rotor at blade root. It is a function of the turning angle in rotor and compressor Mach Number at tip radius only. Consequently so is the mass flow.

The asymptode of mass flow function curves discloses that the maximum obtainable mass flow, hence also the corresponding turning angle in rotor tip, are both functions of the tip compressor Mach Number only.

A survey shows that the design points on the asymptode are the best, hence it is called the Design Curve. It concludes that the compressor design is a function of tip compressor Mach Number only, so are the compression ratio, efficiency, and mass flow function of

the compressor.

By eliminating impractically low mass flow functions and the average compression ratios less than 2:1, the compressor design conclusions range thus:

Tip Compressor Mach Number, $M_{ua} = (u_a/c_{1o})$	0.800	to	1.000
Turning angle in rotor at tip radius, θ_a.	75^o	to	97.5^o
Diameter Ratio of rotor, $\varsigma = (D_{hub}/D_a)$	0.851	to	0.893
Mass flow function, $(W\sqrt{T_{1o}}/\pi r_a^2 p_{1o})$	0.106	to	0.063
Compression ratio average	2.130	to	2.930
Thermal efficiency average	0.950	to	0.902
Radial efficiency drop in stator due to compression shock.	all less than 9%		

Details of the design range are plotted in Fig(38) in appendix.

Although the effects of friction are not being considered, but they are not important owing to the following considerations:

1. The Mach Number entering rotor does not exceed 0.7
2. Turning angle in rotor is not large

considering flow is accelerated through the rotor passage.

3. Boundary layer elimination can be accomplished by installing suction slits at throat section in the shroud and hub of stator to prevent flow seperation in the compression shock.

Therefore, by careful designing the compressor efficiency should be able to match that of the conventional subsonic axial type, and superior to the centrifugal type.

Although compared to the subsonic axial flow compressor it requires 2 to 4 of the frontal area depending on whether it has a compression ratio around 2:1 or 3:1, the former has to be much longer. Hence the total volume will probably result in favor of the compressor in discussion. Furthermore the cost of manufacturing many stages required for the subsonic axial flow compressor owing to its limitated stage pressure, around 1.2:1, is distinctly an unfavorable factor.

Compared to the centrifugal type besides its superior efficiency, it has less frontal area, and it is very possible that it can be designed in many stages.

An experimental compressor is urgently needed. The results of the present study should serve as a guide to its design. Also there is a possibility that the

contraction ratio of supersonic diffuser could be made equal to the critical area ratio of the design flow Mach Number, by installing suction slits at throat section. The establishment of supersonic flow in such a diffuser may be made possible by drawing off air from suction slits during its start. If this is possible, then the compression ratio and efficiency of compressor can be still greatly improved. This subject should be studied immediately.

NOMENCLATURE

SYMBOLS:

V	Absolute velocity, ft/sec
w	Velocity relative to rotor, ft/sec
u	Tangential velocity of rotor, ft/sec
p	Pressure, lbs/ft^2.
T	Absolute Temperature, F^{o}abs
W	Mass flow, lbs/sec.
r	Radius, ft.
θ	Angle of turn in rotor, degree, impulse blade.
α	Angle of absolute velocity from plane of rotor, degree
β	Angle of relative velocity from plane of rotor, degree
M	Mach Number
M'	Velocity/c_{1o}
c	Velocity of sound, ft/sec
ν	Velocity ratio = (V_x/u)
k	$c_p/c_v = 1.4$
g	Acceleration due to gravity, 32.2 ft/sec^2
R	Total compression ratio } Normal Shock
η	Thermal efficiency } at stator entrance
M_u	= (u/c)
M_u'	Compressor Mach Number = (u/c_{1o})
R'	Total compression ratio } Normal shock
η'	Thermal efficiency } at stator throat
A	Projection of area between two adjacent blades
A_o	Total annular area of inlet
A^*	Area of sonic throat
α_m	Mach angle, degree
ς	Ratio of radius to tip radius of rotor
v	Specific volume
ℓ	Depth of water from surface to bottom
h	Enthalpy
n	Ratio of water height across normal hydraulic jump
p_{3o}	Final stagnation pressure. Normal shock at stator entrance
p_{3o}'	Final stagnation pressure. Normal shock at stator throat.
V_x	Axial velocity component
M_x	= (V_x/c) in Chapter II only.

SUBSCRIPTS:

o	Stagnation condition
1o	Initial stagnation condition
2o	Stagnation condition at rotor exit, stator inlet
3o	Stagnation condition after normal compression shock
1	Guide fan outlet, rotor inlet
2	Rotor exit, stator inlet
3	Immediate downstream of normal compression shock
a	At tip radius
y	Immediate downstream of normal hydraulic jump
x	Immediate upstream of normal hydraulic jump

I. INTRODUCTION

In the conventional axial flow compressor design, the occurrence of supersonic velocities of flow results in large energy losses. Therefore the compressors are designed subsonic. With this restriction to the velocity diagram in compressor design, the obtainable pressure ratio per stage then is limited to about 1.25:1. Hence many stages are required to achieve higher pressure ratios for practical needs in industry.

The centrifugal type is capable of higher pressure ratio per rotor compared to the axial type. But its efficiency is much lower, and needs larger frontal area, hence its total volume is about the same as the axial type. Its pressure ratio per stage is limited by rotor stresses to about 3:1. Complications in piping and casings are not practical in adding stages to achieve higher pressure ratios.

The rotary type compressor has good efficiency, but it is rather bulky and requires careful design and manufacture to maintain its clearance.

Because of its superior efficiency, its low frontal area and the ease in obtaining higher pressure ratios by adding stages, the axial type compressor is steadily gaining favor. With the knowledge of recent development in aerodynamics that supersonic flow

velocities about blade rows are not neccessary to cause large energy losses if properly designed, and that even if the ultimate goal of isentropic deceleration of flow through the velocity of sound is not possible, good efficiencies through normal compression shock can be obtained at low supersonic velocities, say, below Mach Number 2. Avoiding the transonic range of speeds (from Mach Number 0.8 to 1.2) the compressor design can thus consider both subsonic and supersonic flow velocities. This means that the stage pressure ratio of axial type compressor could be greatly improved. Considerable amount of attention to the development of axial flow compressor designs involving supersonic velocities of flow has been attracted. The compressor of this type is called as supersonic.

The designs of the supersonic flow compressor can be classified as follows:

1. supersonic flow in rotor only
2. supersonic flow in stator only
3. supersonic flow in both rotor and stator.

The 1. type compressor is receiving a considerable amount of development by NACA under the direction of A. Kantrowitz[2]. An experimental single stage compressor has been constructed and tested in Freon-12. The pressure ratio and efficiency were

reported at 1.8:1 and 80% respectively.

An experimental single stage compressor of type 2. was constructed and tested in Germany under the direction of A. Weise[1]. Because of wartime conditions, the program was only partially completed . The maximum pressure ratio and efficiency tested were only around 1.4:1 and 40% respectively.

Type 3. compressor seems to be the ultimate goal of the supersonic compressor development because of its possibilty in both high compression ratio and flow capacity. But until the other two types are better understood, its development has to wait.

The purpose of this study is to explore the possibilities of the type 2 compressor.

II. PRIMARY INVESTIGATIONS AT ONE RADIUS

1. General Analysis

The velocity diagram and blade design consisting of the inlet guide fan, the rotor and the outlet stator are shown in Fig (1)a for different design radii.

In the inlet guide fan the axially entering subsonic flow is deflected with an angle α_1 through the exit. Leaving the inlet guide fan with the absolute velocity V_1, it enters the rotor with the relative velocity w_1. The inlet angle of flow to rotor is designed equal to the flow angle at guide fan exit $\beta_1 = \alpha_1$, hence $V_1 = w_1$. The twist of flow is to keep a subsonic rotor inlet condition but at the same time allow a sizable circumferential rotor speed in order to give a large work done. The rotor is of impulse design in order to avoid losses resulting from pressure conversion. Thus the flow is directed across the rotor with neither changes in pressure nor in axial velocity and $V_1 = w_1 = w_2$. In spite of the small relative velocity coming out of the rotor a supersonic absolute velocity is produced on account of the sizeable circumferential speed u of rotor. At the entrance of the outlet stator the supersonic velocity V_2 is decelerated to subsonic velocity V_3 through a normal compression shock and then diffused

in the stator.

With the advantage of no temperature change across the rotor, the velocity diagram also represents the diagram of Mach Numbers as shown in Fig $(1)_b$, where M_u is the ratio of the circumferential speed u of rotor to the local velocity of sound of gas flow. Thus the same trigonometric relations of velocities also apply to the Mach Numbers. By denoting subscript lo as the stagnation state of gas at inlet, subscripts 1 and 2 as the states of gas flow at rotor inlet and exit respectively, it follows;

$$M_1^2 = (\tfrac{1}{2}M_u)^2 + M_x^2 \qquad (1)$$

and

$$M_2^2 = (\tfrac{3}{2}M_u)^2 + M_x^2 \qquad (2)$$

where M_x is the ratio of axial component V_x of velocities to the local velocity of sound of gas flow.

By using the conventional notation of velocity ratio $\nu = (V_x/u)$, which is also equal to the ratio (M_x/M_u), equations (1) and (2) can be written as follows,

$$\frac{M_1}{M_u} = \sqrt{.25 + \nu^2} \qquad (1)'$$

$$\frac{M_2}{M_u} = \sqrt{2.25 + \nu^2} \qquad (2)'$$

also, $$\gamma = \tfrac{1}{2} \cot (\tfrac{1}{2}\theta)$$

where θ is the turning angle in rotor.

To keep subsonic flow in rotor and supersonic flow entering stator, by substituting $M_1 = 1$ into equation (1)' and $M_2 = 1$ into equation (2)', it follows,

$$(M_u)_{max} = \frac{1}{\sqrt{0.25 + \gamma^2}} \tag{3}$$

$$(M_u)_{min} = \frac{1}{\sqrt{2.25 + \gamma^2}} \tag{4}$$

or, $$\frac{1}{\sqrt{2.25 + \gamma^2}} \leq M_u \leq \frac{1}{\sqrt{0.25 + \gamma^2}} \tag{5}$$

this gives the theoretical limit of operating range of a compressor with a designed turning angle θ in rotor.

It is seen from the above equations that $(M_u)_{max}$ and also $(M_u)_{min}$ increases when the designed turning angle θ in rotor increases.

By eliminating the term γ from equations (3) and (4), it gives the relation between $(M_u)_{max}$ and $(M_u)_{min}$ independent of θ,

$$\frac{1}{(M_u)^2_{min}} - \frac{1}{(M_u)^2_{max}} = 2 \tag{6}$$

From the velocity diagram it is seen that the work done is directly proportional to the square of circumferential speed of rotor. Therefore in order to obtain high compression ratio it is necessary to operate compressor at high speed. From equation (3) it can been seen that a maximum designed turning angle θ in rotor will permit the highest operating speed. This maximum turning angle θ is limited by the difficulties in directing subsonic flow efficiently through large angle of turning. According to present knowledge it is limited to,

$$(\theta)_{max} = 120^{\circ}$$

or

$$\gamma_{min} = 0.289$$

For the same reason, in order to obtain useful compression ratio the compressor should operate above a certain limit of $(M_u)_{min}$. Since the value of M_1 should not exceed one, it is assumed that,

$$(M_1 / M_{u_{min}}) = 1$$

by substituting this condition into equation (1)' it gives the smallest turning angle θ in rotor to be considered in further analysis,

$$(\theta)_{min} = 60^{\circ}$$

or, $$\gamma_{max} = 0.866$$

Togeather with equations (3) and (4), the limitation of

$$60^{\circ} \leq (\theta) \leq 120^{\circ} \qquad (7)$$

gives a preliminary survey of the possible operating ranges and designs.

Numerical calculations based upon the above analysis are presented in Table (I) and plotted on Fig (2) and (3).

By assuming same initial stagnation conditions of gas flow at inlet,following conclusions can be drawn;

As the designed turning angle θ in rotor is increased,there are following advantages;

(1) higher limit of $(M_u)_{max}$ will be permitted hence higher compression ratio can be obtained,

(2) $(M_u)_{max} - (M_u)min$ increases ,hence larger permissible operating range will be provided, but the reductions in flow rate and stagger angle of outlet stator are disadvantageous.

2. Non-Dimensional Calculations of Performances at Different Design Points

a. Compression Ratio and Thermal Efficiency

To calculate the compression ratio and the thermal efficiency based upon the velocity diagram shown in Fig (1), the following premises are assumed;

Flow of perfect gas is directed adiabatically through the inlet guide fan and the rotor blades. No friction is considered and the normal compression shock formed at the entrance of the outlet stator is considered as the only source of energy loss. Flow is diffused adiabatically in the stator passage after the normal compression shock. So the process of changing states of the perfect gas flow throughout the compressor stage is adiabatic and reversible except the normal compression shock. It is expressed in the T-S diagram schematically shown in Fig $(1)_c$, where the stagnation states are denoted with subscript o, the states before and after the rotor blades are denoted with subscripts 1 and 2, and subscript 3 is used to denote the state after the normal compression shock in stator.

The compression ratio,denoted by R is defined as the ratio of the final stagnation pressure of gas flow coming out the compressor stage to its initial staganation pressure.

$$R = p_{3o} / p_{1o} \tag{8}$$

The thermal efficiency, denoted by η, is defined as the ratio of isentropic change of enthalpy of perfect gas between the initial stagnation state and the final stagnation pressure p_{3o}, to the total work imput.

$$\eta = \Delta h / W_x \tag{9}$$

Deriving the expression for R;
since there is neither change in temperature nor in pressure across the rotor, therefore,

$$\frac{P_{1o}}{P_1} = \frac{P_{1o}}{P_2} = \left(1 + \frac{K-1}{2} M_1^2 \right)^{\frac{K}{K-1}} \tag{10}$$

the pressure ratio of the pressure p_3 after the normal comression shock to the corresponding stagnation pressure p_{3o} in stator is,

$$\frac{P_3}{P_{3o}} = \left(1 + \frac{K-1}{2} M_3^2 \right)^{-\frac{K}{K-1}} \tag{11}$$

from equations (10) and (11), it follows,

$$\frac{P_{3o}}{P_{1o}} = \frac{P_3}{P_2} \left[\frac{1 + \frac{K-1}{2} M_3^2}{1 + \frac{K-1}{2} M_1^2} \right]^{\frac{K}{K-1}} \tag{12}$$

where subscripts 2 and 3 as mentioned previously, denote the states of gas flow immediately before and after the normal compression shock respectively, by substituting the perfect gas relation and the definition of the Mach Number into the continuity equation,

$$\frac{V_2}{v_2} = \frac{V_3}{v_3} \tag{13}$$

it follows,

$$\left(\frac{p_3}{p_2}\right)^2 = \left(\frac{T_3}{T_2}\right)\left(\frac{M_2}{M_3}\right)^2 \tag{14}$$

since there is no change in stagnation temperature across the normal shock , $T_{2o} = T_{3o}$,by substituting the energy equations before and after the shock into equation (14), it follwos,

$$\frac{p_3}{p_2} = \frac{M_2}{M_3}\cdot\sqrt{\frac{1+\frac{k-1}{2}M_2^2}{1+\frac{k-1}{2}M_3^2}} \tag{15}$$

from the momentum equation,

$$p_2 - p_3 = \frac{1}{g}\left(\frac{V_3^2}{v_3} - \frac{V_2^2}{v_2}\right) \tag{16}$$

with

$$\frac{V^2}{gv} = kpM^2$$

substituted,it follows,

$$\frac{p_3}{p_2} = \frac{1+kM_2^2}{1+kM_3^2} \tag{17}$$

by combining equations (15) and (17) it follows,

$$M_3^2 = \frac{M_2^2 + \frac{2}{K-1}}{\frac{2K}{K-1} M_2^2 - 1} \tag{18}$$

substitute equation (18) into (17),it gives,

$$\left(\frac{P_3}{P_2}\right) = \frac{K-1}{K+1}\left(\frac{2K}{K-1} M_2^2 - 1\right) \tag{19}$$

by substituting equations (18) and (19) into equation (12),it gives the expression of compression ratio R as a function of M_1 and M_2 only,

$$R = \left(\frac{K+1}{K-1}\right)^{\frac{1}{K-1}} \left[\frac{\left(\frac{K+1}{2}\right) M_2^2}{\left(1+\frac{K-1}{2} M_1^2\right)\left(\frac{2K}{K-1} M_2^2 - 1\right)^{\frac{1}{K}}}\right]^{\frac{K}{K-1}} \tag{20}$$

The expression for the thermal efficiency η can be written from its definition,

$$\eta = \frac{\Delta h}{W_x} = \frac{\left[R^{\frac{K-1}{K}} - 1\right]}{\left[\frac{T_{30}}{T_{10}} - 1\right]} \tag{21}$$

and since,

$$T_{20} = T_{30}, \quad T_1 = T_2, \quad \therefore \frac{T_{30}}{T_{10}} = \frac{1 + \frac{K-1}{2} M_2^2}{1 + \frac{K-1}{2} M_1^2} \tag{22}$$

hence it gives the expression of η also as a function of M_1 and M_2 only.

It was shown in the previous chapter that for a designed turning angle θ in the rotor, the Mach Numbers M_1 and M_2 are functions of M_u only. Therefore the compression ratio and thermal efficiency for a designed turning angle θ are also functions of M_u only. With the operating range of M_u determined for each designed turning angle θ in rotor and the value of θ chosen within the limit, $60^\circ \leq \theta \leq 120^\circ$ as discussed in previous analysis, possible compression ratios and thermal efficiencies are calculated in Table (III) and plotted in Fig (4), (5) and (6) versus the compressor Mach Number M_u'.

The Compressor Mach Number M_u' is defined as the ratio of the rotor circumferential speed u, to the velocity of sound of gas at the initial stagnation state,

$$M_u' = \frac{u}{c_{1o}} \qquad \text{where} \quad c_{1o} = \sqrt{k_g R T_{1o}}$$

since,

$$M_u = \frac{u}{c_1} \qquad \text{where} \quad c_1 = \sqrt{k_g R T_1}$$

therefore,

$$M_u' = M_u \cdot \sqrt{\frac{T_1}{T_{1o}}} \tag{22}$$

The advantage of defining M_u' as the Compressor Mach Number is, by assuming the same initial stagnation conditions M_u' directly represents the compressor operating speed and the comparison of performances can be easily seen from Fig (4), (5) and (6).

Fig(6) combines Fig(4) and (5) by adding further considerations on the conditions of subsonic inlet to the rotor and supersonic inlet of stator. The difficult transonic region is eliminated by the following limitations,

$$M_1 \leq 0.80$$
$$M_2 \geq 1.20$$

b. Mass Flow Rate

If the total annular area of inlet is denoted by A_0 and the total area perpendicular to the flow direction at the guide fan exit by A_{1o}, the relationship between A_0 and A_{1o} follows,

$$A_{1o} = A_0 \cdot \sin \alpha_1 \qquad (24)$$

Denoting W as the total mass flow rate in lbs./sec. across the compressor stage, then the rate of mass flow per unit area at the guide fan outlet is,

$$\frac{W}{A_{1o}} = \frac{V_1}{v_1} \qquad (25)$$

after introducing the perfect gas and isentropic relations in the above equation it follows,

$$\frac{W\sqrt{T_{10}}}{A_{10}P_{10}} = \sqrt{\frac{gK}{R}} \cdot \frac{M_1}{\left(1+\frac{K-1}{2}M_1^2\right)^{\frac{K+1}{2(K-1)}}}$$

or from equation (24),

$$\frac{W\sqrt{T_{10}}}{A_0 P_{10}} = \sqrt{\frac{gK}{R}} \cdot \frac{M_1}{\left(1+\frac{K-1}{2}M_1^2\right)^{\frac{K+1}{2(K-1)}}} \cdot \sin\alpha_1 \qquad (26)$$

Since that for a designed turning angle θ in rotor, M_1 is a function of the Compressor Mach Number M_U' only, therfore the right hand side of the above equation is also a function of M_U' only for a designed turning angle in rotor. By assuming the same total annular area A_0 and the same stagnation state of inlet for all design points, the left hand side of the equation (26) hence represents the rate of mass flow in non-dimensional form.

With $k = 1.4$, $g = 32.2$ and $R = 53.3$, numerical calculations of equation (26) are presented on table (II) and plotted in Fig(7) vs. the Compressor Mach Number M_U' for variuus values of θ.

3. Summary

The results of the above analysis are presented graphically in Fig (3), (6) and (7). It shows that :

(1) for each designed angle of turn θ in rotor, the compression ratio and mass flow rate increases as the operating speed increases, the efficiency decreases.

(2) for the same initial stagnation conditions of gas at inlet , at the same operating speeds design of large turning angle θ in rotor gives higher compression ratio and thermal efficiency but less flow than designs of smaller θ .

(3) the maximum permissible operating speed increases as the designed turning angle θ in rotor increases, hence a maximum compression ratio will be obtained at the largest designed turning angle θ .

Since in general the compression ratio and thermal efficiency are predominant factors rather than the rate of mass flow in compressor design, therefore it can be concluded that the angle of turn θ in rotor should be chosen at its maximum permissible value, 120°. A compression ratio of 4.145 togeather with an thermal efficiency at 72 % is calculated for instance for $\theta = 120^{\circ}$ operating at a compressor Mach Number $M_1 = 1.318$.

At sea level operating condition (520° Fabs. & 1 atm.) this Compressor Mach Number corresponds to an operating speed of 1503 feet/sec , which is still below the highest rotational speed currently being used (1600 ft/sec).

Summarized:

Turning Angle θ in Rotor		large	small
Same stagnation conditions of gas at inlet, at the same operating speeds, same total area of inlet.	Compression Ratio & Thermal Efficiency	high*	low
	Mass flow rate	low	high*
	Mach Number of flow entering rotor	low*	high
	Mach Number of flow entering stator	low*	high
Permissible Maximum Operating Compressor Mach Number $(M'_u)_{max}$		high*	low
Permissible Range of Operating Compressor Mach Numbers $(M'_u)_{max} - (M'_u)_{min}$		large*	small
Maximum Obtainable Compression Ratio		high*	low

Mark * indicates advantage

III NON-DIMENSIONAL ANALYSIS OF FLOW CHARACTERISTICS AT ONE RADIUS

1. Calculation of Flow Characteristics

If the rate of mass flow varies from that calculated from the operating condition of design as discussed previously, the velocity V_1 of flow coming out of the inlet guide fan will no longer hold the relationship with the rotor circumferential speed u, as stated in equation (1)' . Following the premise of subsonic inlet condition, V_1 will decrease or increase as the flow rate decreases or increases. If the rotor speed remains the same while the flow rate varies, the relative velocity w_1 of flow entering the rotor must change and its angle of attack to the rotor blades will no longer be zero, Fig $(8)_{b,c}$. Hence the cross sectional area of flow entering the rotor blades will not be the same as that of flow leaving the rotor blades, a change of axial velocity across the rotor results. This further effects the magnitute of flow velocity entering the outlet stator and cause a finite angle of attack of flow entering the stator blades, Fig $(8)_{b,c}$. By comparing the velocity diagrams in dicussion to that of design points, Fig $(8)_a$, it shows that the only factors which remain unchanged are the flow directions leaving the guide fan , rotor blades (α_1 & β_2) and the rotor

circumferential speed u ,others are all changed. Consequently the compression ratio and the thermal efficiency also change following the change of mass flow rate.

In order to enable the investigations of the general flow characteristics , problems such as the effects of friction and cascades are not considered in the analysis. Flow is assuned being isentropic except the normal compression shock formed at the entrance of the outlet stator.

Referring to Fig (8), the velocity diagrams should remain the same trigonometric relation if all the velocities in the same diagram are divided by a same denominator. For convenience,let a denominator be chosen $c_{1o}=\sqrt{kgRT_{1o}}$,the velocity of sound of gas flow at the stagnation state of inlet,and denote the ratios of velocities to c_{1o} with M', thus,

$$
\begin{aligned}
M'_1 &= V_1/c_{1o} = M_1 \cdot c_1/c_{1o} \\
M'_{w2} &= w_2/c_{1o} = M_{w2} \cdot c_2/c_{1o} \\
M'_{w1} &= w_1/c_{1o} = M_{w1} \cdot c_1/c_{1o} \\
M'_2 &= V_2/c_{1o} = M_2 \cdot c_2/c_{1o} \\
M'_u &= u/c_{1o} = M_u \cdot c_1/c_{1o}
\end{aligned}
\qquad (27)
$$

$$(M_u = u/c_1)$$

By choosing a certain value of M_u , the Mach Number M_1 of flow coming out of the inlet guide fan at the design point is determined from equation (1)' with an assumed value of turning angle θ in rotor. With M_1 known the ratio of c_1/c_{1o} and hence the operating Compressor Mach Number M_u' can also be calculated.

To compute the flow characteristic at the operating Compressor Mach Number thus determined, a series of values of M_1 in the vincinity of that at the design point are assumed. For each assumed value of M_1 following properties can be calculated; T_1/T_{1o}, p_1/p_{1o}, M_1' and the corresponding mass flow function $W\sqrt{T_{1o}}/A_o p_{1o}$.

With M_u' , M_1' and α_1 known, M_{w1}' and β_1' can be calculated from the trigonometric relation in Fig (8),

$$(M_{w1}')^2 = (M_u')^2 + (M_1')^2 - 2M_1' \cdot M_u' \cdot \cos \alpha_1$$

and $$\sin \beta_1' = (M_1'/M_{w1}') \cdot \sin \alpha_1$$

the relative Mach Number entering the rotor follows,

$$M_{w1} = M_{w1}' \cdot (c_{1o}/c_1)$$

by defining p_{or} and T_{or} as the stagnation pressure

and temperature of gas flow with respect to the rotor, the ratios,

$$p_1/p_{or} \ , \ T_1/T_{or} \ , \text{ and } \ A^*/A_{w1}$$

can be determined from known M_{w1} .

The ratio of the cross sectional area of flow entering the rotor blades A_{w1} to that of flow coming out of the rotor A_{w2} ,as shown in Fig (8) is,

$$A_{w1}/A_{w2} = \sin\beta_1' / \sin\alpha_1$$

hence the relative Mach Number M_{w2} of flow leaving the rotor can be determined from the isentropic flow equation by knowing M_{w1} and A_{w1}/A_{w2} since,

$$A^*/A_{w2} = (A_{w1}/A_{w2}) \cdot (A^*/A_{w1})$$

with M_{w2} known , the ratios T_2/T_{or} and p_2/p_{or} are also known , the ratios of temperature T_2 and pressure p_2 of gas flow at the rotor exit to its initial stagnation temperature T_{1o} and pressure p_{1o} at inlet guide fan can be calculated from,

$$p_2/p_{1o} = (p_2/p_1) \cdot (p_1/p_{1o})$$

and

$$T_2/T_{1o} = (T_2/T_1) \cdot (T_1/T_{1o})$$

With M'_{w2} known from knowing M_{w2} and c_2/c_{1o}, the value of M'_{2a} can be determined through the trigonometric relation from velocity diagram Fig(8),

$$(M'_{2a})^2 = (M'_{\omega_2})^2 + (M'_u)^2 + 2(M'_u)(M'_{\omega_2}) \cdot \cos\alpha_1$$

and from,

$$M_{2a} = M'_{2a} \cdot c_{1o}/c_2$$

the Mach Number M_{2a} of flow approaching the outlet stator is evaluated, the flow direction can be determined through the relation,

$$\sin\alpha_2' = \frac{M'_{\omega_2}}{M'_{2a}} \cdot \sin\alpha_1$$

also the ratios of T_2/T_{2o} and p_2/p_{2o} are known by knowing M_{2a} and so the ratios of T_{2o}/T_{1o} and p_{2o}/p_{1o} can be calculated.

Assuming that the flow is then directed isentropically into the outlet stator entrance, the Mach Number of flow entering the stator M_2 is then determined by the known approaching Mach Number M_{2a} and the change of flow area following the change of flow directions,

$$(A^*/A_2) = (A^*/A_{2a}) \cdot (\sin\alpha_2'/\sin\alpha_2)$$

where (A^*/A_{2a}) is a function of M_{2a}.

Assume that a normal compression shock is formed immeadiately at the stator entrance, with known Mach Number M_2 before the normal compression shock,

the stagnation pressure after and before the compression shock in p_{3o}/p_{2o} can thus be determined. Hence the Compression Ratio and the Thermal Efficiendy,

$$R = p_{3o}/p_{1o}$$

$$\eta = \frac{(R)^{\frac{K-1}{K}} - 1}{(\frac{T_{2o}}{T_{1o}}) - 1}$$

can also be determined.

A series of flow characteristics in non-dimensional form of R and η vs. $W\sqrt{T_{1o}}/A_o p_{1o}$, for designed turning angle in rotor at $\theta = 120^\circ$, 102.6° and 90° at different operating Compressor Mach Numbers are calculated in Table III, IV and V and plotted on Fig (9), (10) and (11).

2. Conditions of Choking

When the flow rate increases, the cross sectional area of flow entering the rotor blades enlarges with the increasing flow angle $\measuredangle\beta_1'$, Fig(8)$_c$. The exit angle of flow coming out of the rotor is being fixed by the blade angle $\measuredangle\beta_2$, therefore the flow will be accelerated through the rotor blades as the mass flow rate increases. The flow rate will reach its maximum limiting value when the relative velocity at the rotor exit reaches the local velocity of sound. This is the case when,

$$A^* / A_{w2} = 1 \qquad (28)$$

the flow reaches its choking condition, further increase in flow rate is impossible.

From the relation,

$$\frac{A^*}{A_{w2}} = \frac{A^*}{A_{w1}} \cdot \frac{A_{w1}}{A_{w2}}$$

and

$$\frac{A_{w1}}{A_{w2}} = \frac{\sin\beta_1'}{\sin\alpha_1} = \frac{M_1}{M_{w1}}$$

equation (28) can also be written as,

$$\frac{A^*}{A_{w1}} \cdot \frac{M_1}{M_{w1}} = 1 \qquad (28)'$$

since A^*/A_{w1} is a function of M_{w1} only, this equa-

tion gives the relation between M_1 and M_{w1} for conditions of choking. Numerical calculations of M_1 and M_{w1} of the choking conditions are carried out in Table VI and plotted on Fig (12).

By eliminating the term M_{w1} from the equation (28)' and the trigonometric relation ,

$$(M_u)^2 - 2 M_1 \cdot M_u \cdot \cos\alpha_1 + (M_1^2 - M_{\omega_1}^2) = 0$$

M_1 of choking conditions at different values of M_u for a designed turning angle θ in rotor can thus be determined. With M_1 known, the rate of mass flow in term of $(W\sqrt{T_{1o}}/A_o p_{1o})$ and also the Compressor Mach Number M_u' can be determined.

The calculated values of $(W\sqrt{T_{1o}}/A_o p_{1o})$ and M_1 of conditions of choking at various operating Compressor Mach Numbers M_u' for $\theta = 120°$, $102.6°$ and $90°$ are presented on Table VII and plotted in Fig (13). In the diagrams of flow characteristics the choking conditions thus determined are shown in dotted lines.

3. Summary and Discussion

An analysis of flow characteristics in non-dimensional form is presented. The results of the analysis which does not consider losses due to friction and cascade effects,are presented on Fig (9), (10) and (11) for $\theta = 120^{\circ}$, 102.6° and 90° respectively. It shows that :

(1) as the operating speed of design increases,the choking condition starts at a mass flow closer to the design mass flow.

(2) the optimum efficiency is obtained close to the condition where choking starts,thus at high operating speed,it falls at the design point,whereas at low operating speed,it is located somewhere in-between the design point and the point where choking starts.

(3) the compression ratio increases with the increasing mass flow. The increase is almost linear up to the design point,then rises rapidly to its peak value at the choking condition.

(4) further changes of conditions downstream in the outlet stator after the choking condition is reached do not effect the mass flow,sudden drop in efficiency and compression ratio will be

expected. It is represented by vertical lines on the diagram of flow characteristics.

(5) at the design points flow enters rotor and stator blades with zero angles of attack. When the mass flow is below that at design point, flow enters the rotor and stator blades with angles smaller than the blade angles. When the mass flow exceeds that at design point,flow angles entering the rotor and stator blades are larger than the blade angles.

Regarding the inlet conditions of subsonic flow entering the impulse type rotor,it is known that for a designed turning angle θ ,the condition of stall will be reached at certain flow angles of insidence. For instance for $\theta = 120^{\circ}$ they are around $\pm 10^{\circ}$. Therefore actually on the diagram of flow characteristics there shall be a surge line representing conditions of stall before the mass flow reaches the design mass flow. It could be plotted by knowing the corresponding angle of incidence on the diagram from experimental informations.

But similar informatioms concerning the supersonic flow entering the outlet stator are still lacking,therefore it is impossible to predict as how the conditions of stall downstream at the stator will effect the flow charateristics.

Further discussions of flow characteristics can be found in chapter VI.

IV ANALYSIS OF A SINGLE STAGE COMPRESSOR OF CONSTANT CIRCULATION

1. Considerations of Radial Equilibrium

Assume that the absolute velocity V of gas flow at any radius in the compressor has no radial component , hence it may be resolved into a tangential component V_t and an axial component V_x . Due to the tangential velocity component V_t , there is a centrifugal force acting on each element of gas flow proportional to

$$\frac{\rho V_t^2}{r \cdot g}$$

To establish radial equilibrium this force has to be balanced by a radial pressure gradient in the flow field,thus

$$\frac{dp}{dr} = \frac{\rho V_t^2}{r \cdot g} \qquad (29)$$

gives the condition of radial equilibrium.

Assume that flow issteady , adiabatic and reversible except the normal compression shock in the outlet stator, from the energy equation for steady flow neglecting the effect of gravity,

$$dQ = dh + d\left(\frac{V^2}{2g}\right) + d\bar{W}_x$$

and since

$$dh = T\,dS + v\,dp \ ,$$

$$dQ = v\,dp + d\left(\frac{V^2}{2g}\right) + T\,dS + d\bar{W}_x$$

for adiabatic and reversible flow,

$$v\,dp + d\left(\frac{V^2}{2g}\right) = -d\,\overline{W}_x$$

by assuming same initial stagnation conditions of flow at all radii, entropy will be independent of radius,

$$\frac{1}{\rho}\cdot\frac{dp}{dr} + \frac{d}{dr}\left(\frac{V^2}{2g}\right) = -\frac{d}{dr}\left(\overline{W}_x\right) \qquad (30)$$

by substitute equation (29) into the above equation it follows,

$$\frac{V_t^2}{rg} + \frac{d}{dr}\left(\frac{V^2}{2g}\right) = -\frac{d}{dr}\left(\overline{W}_x\right) \qquad (31)$$

or, since $V^2 = V_x^2 + V_t^2$,

$$\frac{V_t}{rg}\frac{d}{dr}(r\cdot V_t) + \frac{V_x}{g}\frac{d}{dr}(V_x) = -\frac{d}{dr}\left(\overline{W}_x\right) \qquad (32)$$

denoting the velocities before the rotor by subscript 1, since there $W_x = 0$

$$\frac{V_{t1}}{r}\cdot\frac{d}{dr}(r\cdot V_{t_1}) + V_{x_1}\frac{d}{dr}(V_{x1}) = 0 \qquad (33)$$

referring the velocities after the rotor with subscript 2, since $W_x = -\frac{1}{g}(V_{t2} - V_{t1})\cdot(\omega r)$ where ω is the angular velocity of rotor,

$$\frac{V_{t2}}{r}\cdot\frac{d}{dr}(r\cdot V_{t_2}) + V_{x_2}\frac{d}{dr}(V_{x_2}) = \frac{d}{dr}\omega r(V_{t_2}-V_{t_1}) \qquad (34)$$

multiplying both sides of equations (33) and (34) with r^2 and subtracting, it follows,

$$\frac{d}{dr} \cdot r^2 \frac{(V_{t_2}^2 - V_{t_1}^2)}{2} + r^2 \cdot \frac{d}{dr} \frac{(V_{x_2}^2 - V_{x_1}^2)}{2} = r^2 \cdot \frac{d}{dr} \omega r (V_{t_2} - V_{t_1}) \qquad (35)$$

It is seen that equation (35) is satisfied by the assumption of constant circulation at all radii since then V_x and $r \cdot V_t$ are all constant.

2. Considerations of Constant Circulation

Following the assumption of constant circulation for two dimensional steady flow , geometric relations of velocity diagram are determined by the following conditions for all radii,

(1) constant axial component of velocities, $V_x = V_{xa}$ = constant

(2) tangential component of absolute velocities are reversely proportional to the radius,

$$V_t = V_{ta} \cdot \frac{1}{\varsigma} \qquad (\varsigma = r/r_a)$$

where subscript a denotes any reference radius r_a .

Assuming that at $r = r_a$ the rotor blade section is of pure impulse design Fig(1). From the velocity diagram it follows,

$$\begin{aligned} V_{1t_a} &= \tfrac{1}{2} u_a \\ V_{2t_a} &= \tfrac{3}{2} u_a \end{aligned} \tag{36}$$

substitute the above relations into the conditions of constant circulation and $u = u_a$. it gives,

$$\begin{aligned} V_{1t} &= \tfrac{1}{2} \cdot \frac{u_a}{\varsigma} \\ V_{2t} &= \tfrac{3}{2} \cdot \frac{u_a}{\varsigma} \\ w_{1t} &= (\varsigma - \tfrac{1}{2\varsigma}) \cdot u_a \\ w_{2t} &= (\tfrac{3}{2\varsigma} - \varsigma) \cdot u_a \end{aligned} \tag{37}$$

Velocity diagrams for $\theta_a = 120^\circ$ at radii $\varsigma = 1.25$, 1.0 and 0.8 are illustrated in Fig(14) from calcutations of equation (37).

It is seen that the stagger angles of blades of inlet guide fan and the oulet stator increase as the radius increases,while the rotor blades are to be warped strongly from one direction to the other. For $\varsigma < 1$ flow is accelerated in the rotor blade passage and for $\varsigma > 1$ flow will be decelerated. For the reason that flow can be accelerated efficiently at widely different rates , but can be hardly diffused with good efficiency, especially when flow has to be directed through a large angle of turning at the same time as in the case when $r > r_a$,therefore pure impulse design will be chosen for the blade section at rotor tip.

It may be expected that the losses due to diffusion of flow in the rotor passage and the difficulties hence in rotor blade design of conventional axial flow compressors can be avoided.

In following discussions subscript a will be denoted all symbols referring to the tip radius At this radius velocity diagrams, limiting operating Compressor Mach Numbers and performances etc. have been thoroughly discussed in chapter (II).

3. Pressure Distributions

Assume that flow is directed isentropically from the inlet guide fan through the rotor passage and the initial stagnation conditions of flow at inlet are the same for all radii. The energy equations for flow before and after the rotor at radius r can be written,

$$T_{1o} = T_1 + \frac{V_1^2}{2gc_p}$$

$$T_{2o} = T_2 + \frac{V_2^2}{2gc_p} \tag{38}$$

since work done is the same at all radii,hence,

$$T_{2o} = T_{1o} + \frac{u_a^2}{gc_p} \tag{39}$$

the stagnation states of flow after the rotor are also the same at all radii.

before the rotor:

$$T_1 + \frac{V_1^2}{2gc_p} = T_{1a} + \frac{V_{1a}^2}{2gc_p} \tag{40}$$

since

$$V_{1a}^2 - V_1^2 = V_{1t_a}^2 - V_{1t}^2$$

and

$$V_{1t_a} = \frac{1}{2} u_a$$

$$V_{1t} = \frac{1}{2} \cdot \frac{u_a}{s}$$

it follows,

$$T_1 - T_{1a} = \frac{k-1}{8}\left(1 - \frac{1}{\varsigma^2}\right)\frac{u_a^2}{kgR}$$

dividing both sides of the equation by T_{1a} and rearranging

$$\left(\frac{T_1}{T_{1a}}\right) = 1 + \frac{k-1}{8}\left(1 - \frac{1}{\varsigma^2}\right) M_{ua}^2 \qquad (41)$$

similarily the temperature ratio after the rotor can be derived,

$$\left(\frac{T_2}{T_{2a}}\right) = 1 + \frac{\varsigma(k-1)}{8}\left(1 - \frac{1}{\varsigma^2}\right) M_{ua}^2 \qquad (42)$$

where $T_{1a} = T_{2a}$, $M_{ua} = \frac{u_a}{\sqrt{kgRT_{1a}}}$

The pressure ratios follow the isentropic relation of perfect gas,

$$\left(\frac{p_1}{p_{1a}}\right) = \left[1 + \frac{k-1}{8}\left(1 - \frac{1}{\varsigma^2}\right) M_{ua}^2\right]^{\frac{k}{k-1}} \qquad (43)$$

$$\left(\frac{p_2}{p_{2a}}\right) = \left[1 + \frac{\varsigma(k-1)}{8}\left(1 - \frac{1}{\varsigma^2}\right) M_{ua}^2\right]^{\frac{k}{k-1}} \qquad (44)$$

where $p_{1a} = p_{2a}$

The pressure ratios for different values of M_{ua} are calculated for ς from 0.8 to 1.0 in

Table (VIII) and plotted in Fig (15).

It is seen whereas the operating speed and so the value of M_{ua} is to be chosen within the range which is a function of θ_a ,as being discussed in chapter (II), the pressure distributions of flow at rotor inlet and exit are functions of M_{ua} and ς only.

Except at the tip radius where $\varsigma = 1$, there is no change in pressure across the rotor, there is a pressure drop across the rotor at all radii. And the rate of pressure drop increases as the operating speed of rotor is increased.

Along the radial direction ,both before and after the rotor,pressure drops with decreasing radius. Also the rate of pressure drop increases with increasing operating speed of rotor.

4. Blade Angles and Blade Height

The blade angles α_1 of guide fan exit, β_1 & β_2 of rotor inlet and exit and α_2 of outlet stator as shown in Fig (14) can be be calculated from equation (37) as functions of ξ and γ_a,

$$\tan \alpha_1 = \frac{V_{xa}}{V_{t_1}} = 2\xi\gamma_a$$

thus,
$$\alpha_1 = \tan^{-1}(2\xi\gamma_a) \tag{45}$$

$$\tan \beta_1 = \frac{V_{xa}}{\omega_{1t}} = \frac{\gamma_a}{(\xi - \frac{1}{2\xi})}$$

thus,
$$\beta_1 = \tan^{-1}\left(\frac{\gamma_a}{\xi - \frac{1}{2\xi}}\right) \tag{46}$$

$$\tan \beta_2 = \frac{V_{xa}}{\omega_{2t}} = \frac{\gamma_a}{(\frac{3}{2\xi} - \xi)}$$

thus,
$$\beta_2 = \tan^{-1}\left(\frac{\gamma_a}{\frac{3}{2\xi} - \xi}\right) \tag{47}$$

$$\tan \alpha_2 = \frac{V_{xa}}{V_{2t}} = \frac{2\xi}{3}\gamma_a$$

and
$$\alpha_2 = \tan^{-1}\left(\frac{2\xi}{3}\gamma_a\right) \tag{48}$$

The blade angles for $\theta_a = 120°$, 102.6° and 90° are calculated for ξ from 1.0 to 0.8 in Table(IX) and plotted on Fig (16), (17) and (18).

The blade angles of inlet guide fan and outlet stator α_1 and α_2 decrease with the decreasing radius. At the rotor blades, the outlet angle also

decreases with the decreasing radius but the inlet angle increase. The flow is increasingly accelerated in the rotor blade passage as the radius decreases. When the relative velocity of flow leaving the rotor w_2 reaches the local velocity of sound a choking condition of flow will be reached. This consideration therefore sets the limiting value of blade height or $(\varsigma)_{min}$ which is derived as follows,

$$w_2^2 = w_{2t}^2 + V_x^2 = u_a^2 \left[\left(\frac{3-2\varsigma^2}{2\varsigma} \right)^2 + \gamma_a^2 \right]$$

dividing both sides of the equation by $c_2^2 = \sqrt{kgRT_2}$,

$$M_{w_2}^2 = \frac{T_{2a}}{T_2} \cdot M_{ua}^2 \left[\left(\frac{3-2\varsigma^2}{2\varsigma} \right)^2 + \gamma_a^2 \right]$$

and from equation (42), it follows,

$$M_{w_2}^2 = \frac{\left[\left(\frac{3-2\varsigma^2}{2\varsigma} \right)^2 + \gamma_a^2 \right]}{\left[1 + \frac{\varsigma(k-1)}{8} \left(1 - \frac{1}{\varsigma^2} \right) M_{ua}^2 \right]} \cdot M_{ua}^2 \qquad (49)$$

for $M_{w2} = 1$ it gives,

$$\varsigma_{min}^2 + \frac{\varsigma(k-1)}{8\varsigma_{min}^2} = \frac{1}{M_{ua}^2} - \gamma_a^2 + \frac{3(3k+5)}{8} \qquad (50)$$

or with $k = 1.4$,

$$\varsigma_{min}^4 - \left(3.45 + \frac{1}{M_{ua}^2} - \gamma_a^2 \right) \cdot \varsigma_{min}^2 + 2.7 = 0 \qquad (51)$$

recall equations (3) and (4)

$$[M_{ua}]_{max} = \frac{1}{\sqrt{0.25 + \gamma_a^2}} \qquad (3)$$

$$[M_{ua}]_{min} = \frac{1}{\sqrt{2.25 + \gamma_a^2}} \qquad (4)$$

by substituting equation (3) in equation (51) it gives,

$$[\beta]_{MIN} = 1.0$$

substituting equation (4) into (51) it follows,

$$[\beta]_{MIN} = 0.722 \qquad (52)$$

Therfore the possible blade height designs are limited by the limiting ratios of hub radius to the tip radius :

$$0.722 \leq (\beta)_{MIN} \leq 1.0 \qquad (53)$$

$(\beta)_{min}$ for different designed θ_a, at different compressor Mach Number of tip radius M'_{ua} are calculated from equation (51) and tabulated in Table (X). Results are also plotted in Fig (19).

5. Non-Dimensional Calculation of Performances

Assume that flow of perfect gas at all radii in a compressor being two-dimensional,steady,adiabatic and reversible except the normal compression shocks formed at the entrance of oultlet stator,them the only loss involved will be that due to normal compression shocks. Pure impulse type design is adapted for the blade section at the tip of rotor,so the pressure and temperature there before and after rotor are the same;

$$p_a = p_{1a} = p_{2a}$$

$$T_a = T_{1a} = T_{2a}$$

Also assume that initial stagnation conditions of flow at all radii being the same,togeather with the assumption of constant circulation,hence the stagnation conditions of flow behind rotor are also the same independent of radius;

$$p_{1o} = \text{constant}$$

$$T_{1o} = \text{constant}$$

$$p_{2o} = \text{constant}$$

$$T_{2o} = \text{constant}$$

$$\text{Work done} = u_a^2/gc_p$$

from the energy equation and isentropic relation of perfect gas,

$$\frac{p_{10}}{p_a} = \left[1 + \frac{K-1}{2} M_{1a}^2 \right]^{\frac{K}{K-1}}$$

and since

$$M_{1a}^2 = \left(\frac{1}{4} + \gamma_a^2\right) M_{ua}^2 \qquad (1)'$$

it follows,

$$\frac{p_{10}}{p_a} = \left[1 + \frac{K-1}{2} \left(\frac{1}{4} + \gamma_a^2\right) M_{ua}^2 \right]^{\frac{K}{K-1}}$$

substituting equation (43), it gives,

$$\frac{p_1}{p_{10}} = \left[\frac{1 + \frac{K-1}{8}\left(1 - \frac{1}{S^2}\right) M_{ua}^2}{1 + \frac{K-1}{2}\left(\frac{1}{4} + \gamma_a^2\right) M_{ua}^2} \right]^{\frac{K}{K-1}} \qquad (54)$$

hence the Mach Number M_1 of flow leaving the guide fan,

$$M_1^2 = \frac{\left(\gamma_a^2 + \frac{1}{4S^2}\right) M_{ua}^2}{1 + \frac{K-1}{8}\left(1 - \frac{1}{S^2}\right) M_{ua}^2} \qquad (55)$$

similarily at tip radius behind rotor,

$$\frac{p_{20}}{p_a} = \left[1 + \frac{K-1}{2} M_{2a}^2 \right]^{\frac{K}{K-1}}$$

and since

$$M_{2a}^2 = \left(\frac{9}{4} + \gamma_a^2\right) M_{ua}^2$$

it follows,

$$\frac{p_{20}}{p_a} = \left[1 + \frac{K-1}{2} \left(\frac{9}{4} + \gamma_a^2\right) M_{ua}^2 \right]^{\frac{K}{K-1}}$$

substituting equation (44)

$$\frac{p_2}{p_{20}} = \left[\frac{1 + \frac{9(K-1)}{8}\left(1 - \frac{1}{S^2}\right) M_{ua}^2}{1 + \frac{K-1}{2}\left(\frac{9}{4} + \gamma_a^2\right) M_{ua}^2} \right]^{\frac{K}{K-1}} \qquad (56)$$

the Mach Number M_2 of flow entering the outlet stator follows,

$$M_2^2 = \frac{(\gamma_a^2 + \frac{9}{4\varsigma^2}) \cdot M_{ua}^2}{1 + \frac{9(K-1)}{8}(1 - \frac{1}{\varsigma^2}) M_{ua}^2} \tag{57}$$

the relative Mach Numbers of flow entering and leaving the rotor M_{w1} and M_{w2} can be derived from trigonometric relations of velocity diagram,

$$M_{w_1} = M_1 \cdot \sqrt{1 + \frac{(\varsigma^2 - 1)}{(\gamma_a^2 + \frac{1}{4\varsigma^2})}} \tag{58}$$

$$M_{w_2} = M_2 \cdot \sqrt{1 + \frac{(\varsigma^2 - 3)}{(\gamma_a^2 + \frac{9}{4\varsigma^2})}} \tag{59}$$

assuming that normal compression shock is formed at the entrance of outlet stator, M_2 being the Mach Number of flow immediately before the shock, then the Mach Number M_3 after the shock and the pressure ratio across the shock are given by equations (18) and (19) as functions of M_2 only. Hence the compression ratio $R = p_{3o}/p_{1o}$ and thermal efficiency at any radius r can be derived as functions of M_{ua}, γ_a and ς,

$$R_{at\,r} = f(M_{ua}, \gamma_a, \varsigma)$$

$$\eta_{at\,r} = \frac{\left[(R)_{at\,r}^{\frac{K-1}{K}} - 1\right]}{\left[\frac{T_{3o}}{T_{1o}} - 1\right]}$$

where, since $T_{30} = T_{20}$

$$\frac{T_{30}}{T_{10}} = 1 + \frac{u_a^2}{g \varphi T_{10}}$$

or
$$\frac{T_{30}}{T_{10}} = \left[1 + (K-1) M_{ua}'^2 \right] \tag{60}$$

where
$$M_{ua}' = \frac{u_a}{c_{10}} = M_{ua} \cdot \sqrt{\frac{T_a}{T_{10}}}$$
$$= \frac{M_{ua}}{\sqrt{1 + \frac{K-1}{2} (\varphi + V_a^2) M_{ua}^2}} \tag{61}$$

is the ratio of the circumferential speed at tip radius to the velocity of sound of gas at initial stagnation condition. It will be called the tip compressor Mach Number.

The compression ratio R and thermal efficiency η can thus be calculated at different radii as functions of M_{ua}', V_a and φ. The results of performances thus calculated for $\theta_a = 120°$, $102.6°$ and $90°$ are tabulated on Table (XI), (XII) and (XIII), plotted in Fig (20), (21) and (22).

The rate of mass flow (W), can be derived as follows; the flow equation at any radius r,

$$d\overline{W} = \frac{V_x}{v_1} \cdot dA \tag{62}$$

where V_x is the axial component of velocities, constant

at all radii, v_1 is the specific volume of gas flow before rotor and $dA = 2\pi r.dr$. Thus the equation can also be written,

$$d\bar{W} = \frac{V_{xa}}{v_{1a}} \cdot \frac{v_{1a}}{v_1} \cdot (2\pi r)\, dr$$

introducing $\varsigma = r/r_a$, equation (41) and the isentropic relation of perfect gas, it follows,

$$d\bar{W} = \left(\frac{V_{xa}}{v_{1a}}\right)(2\pi r_a^2)\left[1 + \frac{k-1}{8}\left(1 - \frac{1}{\varsigma^2}\right)M_{ua}^2\right]^{\frac{1}{k-1}} \cdot \varsigma\, d\varsigma$$

with $k = 1.4$,

$$d\bar{W} = (2\pi r_a^2)\cdot\left(\frac{V_{xa}}{v_{1a}}\right)\frac{\left[\varsigma^2(1+.05M_{ua}^2) - .05M_{ua}^2\right]^{5/2}}{\varsigma^4} \cdot d\varsigma$$

let

$$a^2 = \frac{.05 \cdot M_{ua}^2}{1 + .05M_{ua}^2} \qquad (63)$$

it follows,

$$d\bar{W} = (2\pi r_a^2)\left(\frac{V_{xa}}{v_{1a}}\right)\cdot(1+.05M_{ua}^2)^{5/2}\frac{(\varsigma^2 - a^2)^{5/2}}{\varsigma^4}\, d\varsigma$$

hence

$$\bar{W} = (2\pi r_a^2)\cdot\left(\frac{V_{xa}}{v_{1a}}\right)\cdot(1+.05M_{ua}^2)^{5/2}\int_{\varsigma=(\varsigma)_{MIN}}^{\varsigma=1}\frac{(\varsigma^2 - a^2)^{5/2}}{\varsigma^4}\, d\varsigma \qquad (64)$$

where $(\varsigma)_{min}$ is a function of operating speed and the turning angle θ_a in rotor at tip radius, as can be calculated from equation (51).

with $k = 1.4$, $g = 32.2$ and $R = 53.3$,

$$\left(\frac{V_{xa}}{V_{1a}}\right) = \frac{p_{10}}{\sqrt{T_{10}}} \cdot \frac{.92\, M_{1a}}{(1+.2\,M_{1a}^2)^3} \cdot \sin\alpha_{1a}$$

substituting into equation (64), it follows,

$$\frac{W\sqrt{T_{10}}}{(\pi r_a^2)\,p_{10}} = \frac{1.84\, M_{1a}(1+.05M_{ua}^2)^{5/2}\cdot\sin\alpha_{1a}}{(1+.2\,M_{1a}^2)^3} \int_{\beta=(\beta)_{MIN}}^{\beta=1} \frac{(\beta^2-a^2)^{5/2}}{\beta^4}\, d\beta$$

solving the integral,

$$\frac{W\sqrt{T_{10}}}{(\pi r_a^2)\,p_{10}} = \frac{1.84\cdot M_{1a}(1+.05M_{ua}^2)^{5/2}\cdot\sin\alpha_{1a}}{(1+.2M_{1a}^2)^3}\left[\frac{a^2(\beta^2-a^2)^{3/2}}{3\beta^3} + \frac{2a^2(\beta^2-a^2)^{1/2}}{\beta} + \frac{\beta(\beta^2-a^2)^{1/2}}{2} - \frac{5}{2}a^2\cdot\log|\beta+(\beta^2-a^2)^{1/2}|\right]_{\beta=(\beta)_{MIN}}^{\beta=1} \qquad (65)$$

recall equation (1)'

$$M_{1a} = (.25 + \gamma_a^2)^{1/2}\cdot M_{ua}$$

and $$\gamma_a = \tfrac{1}{2}\cot\left(\tfrac{1}{2}\theta_a\right), \quad \alpha_{1a} = \left(\frac{\pi}{2} - \frac{\theta_a}{2}\right),$$

$$M'_{ua} = \frac{M_{ua}}{[\,1+.2\,(.25+\gamma_a^2)\,M_{ua}^2\,]^{1/2}}$$

it can be seen that equation (65) gives the rate of mass flow in non-dimensional form as a function of M'_{ua} and θ_a . Once an operating speed and an angle of turn for the rotor at tip are chosen, the obtainable rate of mass flow can be determined.

6. The Design Curve

Equation (65) gives the exact solution of mass flow , but the process of calculation is rather lengthy. An approximate methode of assuming specific volume v_1 as constant independant of radius can simplify the calculation greatly. From equation (41) or from Fig (15) it can be seen that v_1 increases as the radius decreases, hence the approximate solution of mass flow can be obtained by taking v_1 equal to the specific volume of gas flow at mean radius r_m ;

$$v_1 = v_{1m}$$

it follows,

$$\overline{W} = \frac{\overline{V}_x}{v_{1m}} \cdot \pi r_a^2 (1 - \delta_{MIN}^2)$$

or,

$$\overline{W} = \frac{\overline{V}_x}{v_{1a}} \cdot \frac{v_{1a}}{v_{1m}} \cdot \pi r_a^2 (1 - \delta_{MIN}^2)$$

with

$$\frac{v_{1a}}{v_{1m}} = \left[1 + \frac{k-1}{8} \left(1 - \frac{1}{\delta_m^2}\right) M_{1a}^2 \right]^{\frac{1}{k-1}}$$

where

$$\delta_m = r_m / r_a = \frac{1 + \delta_{MIN}}{2}$$

and

$$\frac{\overline{V}_x}{v_{1a}} = \frac{\overline{V}_{1a}}{v_{1a}} \cdot \sin\alpha_{1a} = \frac{p_{10}}{\sqrt{T_{10}}} \cdot \sqrt{\frac{gk}{R}} \cdot \frac{M_{1a}}{\left(1 + \frac{k-1}{2} M_{1a}^2\right)^{\frac{k+2}{2(k-1)}}} \cdot \sin\alpha_{1a}$$

it gives,

$$\overline{W} = \frac{p_{10}}{\sqrt{T_{10}}} \cdot \sqrt{\frac{gk}{R}} \cdot \frac{M_{1a}}{\left(1 + \frac{k-1}{2} M_{1a}^2\right)^{\frac{k+2}{2(k-1)}}} \cdot \sin\alpha_{1a} \cdot \left[1 + \frac{k-1}{8} \left(1 - \frac{1}{\delta_m^2}\right) M_{1a}^2 \right]^{\frac{1}{k-1}} \cdot \pi r_a^2 (1 - \delta_{MIN}^2)$$

or in non-dimensional form,

$$\frac{W\sqrt{T_{10}}}{\pi r_a^2 \cdot p_{10}} = \left[\sqrt{\frac{gk}{R}} \cdot \underbrace{\frac{M_{1a}\cdot \sin\alpha_{1a}}{\left(1+\frac{k-1}{2}M_{1a}^2\right)^{\frac{k+2}{2(k-1)}}}}_{\phi\,(M'_{ua}\ \&\ \theta_a)}\right] \cdot \left[1+\frac{k-1}{8}\left(1-\frac{1}{\sigma_m^2}\right)M_{ua}^2\right]^{\frac{1}{k-1}} \cdot \left(1-\sigma_{MIN}^2\right) \tag{65}$$

for a chosen θ_a and M'_{ua} ;

$\phi\,(M'_{ua}\ \&\ \theta_a)$ can be read from Fig (7),

σ_{MIN} can be read from Fig (19),

$\sigma_m = \frac{1}{2}(1+\sigma_{MIN})$,

M_{ua} can be calculated from knowing M_{1a} from Fig (3) and (M_{1a}/M_{ua}) from Fig (2).

hence the rate of mass flow in non-dimensional form can be easily calculated.

For example, for $\theta_a = 120^\circ$ and a tip compressor Mach Number $M'_{ua} = 0.925$:

from Fig (7), $\phi\,(M'_{ua}\ \&\ \theta_a) = 0.212$

from Fig (19), $\sigma_{MIN} = 0.850$, hence

$\sigma_m = 0.925$

from Fig (3), $M_{1a} = 0.550$

Fig (2), $(M_{1a}/M_{ua}) = 0.577$

hence, $M_{ua} = 0.9547$

with k=1.4 , g = 32.2 and R = 53.3 substituted in

equation (65)' it follows,

$$\frac{W\sqrt{T_{1o}}}{\pi r_a^2 \cdot p_{1o}} = 0.060$$

the exact solution for this example calculated from equation (65) is 0.058 . The error introduced by the approximate methode is only 0.2 % .

Calculations of mass flow rate for various turning angles θ_a at various tip compressor Mach Numbers M'_{ua} are tabulated in Table (XVIII) and results are plotted in Fig (34). The asymptote in Fig (34) gives the relation of the maximum obtainable mass flow rate at certain tip compressor Mach Number M'_{ua}. Hence it also gives the minimum value of θ_a for design at any chose operating tip compressor Mach Number. From Fig(34) it gives,

$(\theta_a)_{min}$ for design	120^o	102.6^o	90^o	79.6^o	71^o
M'_{ua}	1.582	1.055	0.926	0.840	0.770

the maximum θ_a for design at all tip compressor Mach Numbers being 120^o. Therefore the design range of θ_a for various M'_{ua} can be determined as plotted in Fig (35), which is eqivalent the range confined by the

asymptode and the curve of $\theta_a = 120^\circ$, in Fig (34). It is denoted as the useful design range. The asymptode in Fig (34) and the useful range thus considered are also transformed into the M'_{ua} vs. $(\zeta)_{min}$ diagram in Fig (19).

It has to be noted that the reason thus $(\theta_a)_{min}$ is defined is not only because of the mass flow will decrease for further decreasing θ_a at the same M'_{ua}, but also because further decrease of θ_a gives no gain in compression ratio and thermal efficiency. This is because the Mach Number of flow entering stator M_2, increases with decreasing θ_a. Therefore there is no point to consider designs with θ_a smaller than the limit set by $(\theta_a)_{min}$.

Next problem is to make a survey of the useful design range now outlined to determine the most desirable design points within the range at various tip compressor Mach Numbers M'_{ua}. It is known now that the design points given by the asymptode in Fig(34) will undoubtly give the maximum mass flow rates. But from the analysis of chapter III, it is known that the Mach Number of flow entering stator M_{2a} at tip radius is at its lowest for designs with $\theta_a = 120^\circ$, therefore results in high compression ratio and thermal efficiency. But

from the analysis of maximum blade height, it was concluded that the blade height of designs with large θ_a is larger than that of designs with smaller θ_a, for the same tip compressor Mach Number M'_{ua}. Since the Mach Number M_2, of flow entering stator increases as the radius decreases, it is very possible that at hub radius the Mach Number M_2 for designs with $(\theta_a) = (\theta_a)_{min}$ will be smaller than that for designs with $(\theta_a) = 120^\circ$. Hence the average thermal efficiency and compression ratio of designs with $(\theta_a) = (\theta_a)_{min}$ will likely be able to match that of designs with $(\theta_a) = 120^\circ$, and may be even better. Futhermore, due to the difference in blade height, the efficiency drop from tip radius to hub in the former will possibly be less than in the later designs for the same tip compressor Mach Numbers M'_{ua}. The choice of the most desirable design points of the useful design range remains among those on the curve of $(\theta_a) = (\theta_a)_{min}$ and the curve of $(\theta_a) = 120^\circ$ in Fig (35). Performances of design points on both curves at $M'_{ua} = 1.055; 0.926; 0.840; 0.770$, are calculated as follows to give comparison:

M_{1a}	1.055*	1.055	0.926*	0.926	0.840*	0.840	0.770*	0.770
θ_a°	102.6*	120.0	90.00*	120.0	79.60*	120.0	71.00*	120.0
ς_{min}	0.905	0.890	0.878	0.848	0.860	0.814	0.844	0.783
M_{1tip}	0.714	0.632	0.686	0.553	0.686	0.498	0.696	0.453
M_{1hub}	0.760	0.700	0.740	0.640	0.740	0.595	0.745	0.555
M_{2tip}	1.725	1.675	1.535	1.465	1.420	1.320	1.345	1.200
M_{2hub}	2.000	2.020	1.830	1.850	1.728	1.755	1.640	1.670
R_{tip}	3.070	3.140	2.578	2.640	2.270	2.325	2.041	2.090
R_{hub}	2.620	2.582	2.257	2.220	2.010	1.985	1.851	1.827
η_{tip}	0.851	0.867	0.909	0.933	0.937	0.965	0.955	0.989
η_{hub}	0.713	0.701	0.763	0.746	0.787	0.767	0.812	0.792
$R_{av.}$	2.845	2.861	2.417	2.430	2.140	2.155	1.946	1.958
$\eta_{av.}$	0.782	0.784	0.836	0.839	0.862	0.866	0.883	0.890
$\eta_{\substack{drop \\ tip-hub}}$	13.8%	16.6%	14.7%	18.7%	15.0%	19.8%	14.3%	19.7%
$\frac{W\sqrt{T_{1a}}}{\pi r_{1a}^2 \cdot p_{1a}}$	.0550	.0475	.0762	.0588	.0950	.0654	.1145	.0697
$(\alpha_1/\beta_1/\beta_2)^\circ_{tip}$	38.70	30.00	45.00	30.00	50.20	30.00	54.50	30.00
$\alpha^\circ_{1\,hub}$	35.80	27.35	41.20	26.15	45.93	25.20	49.80	24.36
$\beta^\circ_{1\,hub}$	48.60	41.50	58.30	48.35	65.08	55.50	70.22	63.40
$\beta^\circ_{2\,hub}$	28.00	19.95	30.80	17.40	34.00	15.65	37.00	14.30
$\alpha^\circ_{2\,tip}$	14.93	10.90	18.40	10.90	21.80	10.90	25.00	10.90
$\alpha^\circ_{2\,hub}$	13.50	9.50	16.20	9.15	19.00	8.80	21.50	8.59

* Marks the design points taken on the Design Curve in Fig(35).

The results of the survey show that the design points on the curve of $(\theta_a) = (\theta_a)_{min}$ are better than that on the curve of $\theta_a = 120^0$. Hence the former is designated as the Design Curve of compressors. The survey shows that at same tip compressor Mach Numbers M'_{ua}, the design points on the Design Curve are better than those on the curve of $\theta_a=120^\circ$ due to following reasons:

(1) high rate of mass flow, in fact the design points on the Design Curve give the maximum mass flow rates obtainable.

(2) small blade height, hence less cost in manufacturing and better dynamic strength of blades can be expected.

(3) less efficiency drop from tip to hub radius, hence favorable in radial equilibrium considerations of flow in stator. It has to be noted that the efficiency drop in both cases does not diverge. For $(\theta_a) = (\theta_a)_{min}$ the maximum efficiency drop is around 15% when M'_{ua} is around 0.840. For $\theta_a = 120^\circ$ the maximum efficiency drop is also around $M'_{ua} = 0.840$ but at 20% . The reason of it is because of the fact, thermal efficiency of normal compression shock increases at decreasing Mach Numbers. At high M'_{ua} , although Mach Numbers M_2 both at tip and hub radius are high

but the blade height is small, the difference of M_2 hence is also small from tip to hub radius, therefore the efficiency drop is small. At low M'_{ua}, although the difference of M_2 is increased due to large blade height, but the M_2 at tip and hub radius are both small, hence it also results in small efficiency drop. That is why the maximum radial efficiency drop is found at M'_{ua} around 0.840.

(4) the disadvantage of high flow Mach Number M_2 entering stator at tip radius is compensated by the advantage of low Mach Number at hub due to small blade height, hence the average efficiency and compression ratio are about the same as designs with $\theta_a = 120^o$.

(5) the disadvantage of high flow Mach Number entering rotor is compensated by the advantage of small angle of turn in rotor.

(6) large stagger of stator, consequently less construction difficulty of stator. Furthermore, the problem of subsonic diffusion and turning the flow into the axial direction of compressor will be earsier to handle without causing too much trouble to the stator design.

The Design Curve is also plotted in the $(\zeta)_{min}$ vs. M'_{ua} and (θ_a) vs. M'_{ua} diagrams in Fig (19) and Fig (35) respectively.

7. The Effective Design Points

The results of the calculations of the performances at various design points of the Design Curve are plotted in Fig(38), which will be referred to later as the Design Charts.

It can be seen from the Design Charts, that for design points with tip compressor Mach Numbers M'_{ua} less than say around 0.8, the average compression ratio will be less than 2. By considering compression ratio less than 2 as dissatisfactory, the design points on the Design Curve with M'_{ua} less than 0.8 are ruled out, thus the lowest design point in the sence of operating speed and compression ratio is determined.

As the operating speed or the tip compressor Mach Number M'_{ua} increases, the compression ratio is increased, but the rate of mass flow decreases sharply. To visualize the fact, let us assume a sea level operating condition: 520° Fabs. and 14.7 lbs/in^2, and assume that the tip diameter in consideration is 2ft. It follows:

M'_{ua}	1.055	0.926	0.840	0.770
$\frac{W\sqrt{\theta_0}}{\pi r_t^2 \cdot p_0}$	.0550	.0762	.0950	.1145
W (lbs/sec)	16.10	22.30	27.75	33.42

The conventional axial flow compressor of the same tip diameter at sea level operating condition can produce an output of around 75 lbs/sec. Consider that a minmum rate of mass flow of one forth of the amount as acceptable in practice, the design points with M'_{ua} higher than 1.0 are thus ruled out owing to the impractical low mass flow rates. Hence the highest design point in the sense of operating speed is limited to $M'_{ua} = 1.0$.

The conclusion can be drawn that the effective design points are confined within the following limits:

$$0.8 \leq (M'_{ua}) \leq 1.0$$

$$75^{\circ} \leq (\theta_a) \leq 97.5^{\circ}$$

$$0.851 \leq (\eta)_{min} \leq 0.893$$

The performance and design at the effective design points are plotted in the Design Charts, Fig(38).

8. Summary and Discussion

A non-dimensional analysis of compressor performances along the radial direction is presented. The analysis is based on the following premises:

(1) flow being two-dimensional, steady, adiabatic and reversible except at the normal compression shock.

(2) normal compression shock formed at the entrance of outlet stator being the only cause of energy losses involved.

(3) perfect gas flow, $k = 1.4$, its initial stagnation conditions being the same at all radii.

(4) constant circulation at all radii.

Pure impulse type rotor profile is adapted for the design at tip radius in order to avoid deceleration of flow at large angle of turning in rotor. Therefore the velocity diagrams at tip radius coincide with those being dicussed in chapter II.

Blade angles along radial direction are determined by the considerations of constant circulation of all radii and the turning angle θ_a at tip radius in rotor. It is shown that as the radius decreases; the blade angles at guide fan outlet and entrance of outlet stator decrease, at the rotor blades the inlet angle

increases and the outlet angle decreases.

Pressure before and after the rotor are found to decreases as the radius decreases. Also the pressure drop across rotor increases. Therfore with radius decreasing, flow is increasingly accelerated through rotor passage. This results in limit of blade height, namely the root radius of blade will be determined by the condition when flow at rotor exit reaches its local velocity of sound. This consideration is necessary since further decrease in radius or increase in blade height will cause flow choking and large losses and seperation of flow at hub will result. The maximum limit of blade height design is found to decrease rapidly with increasing operating speed for the same designed θ_a, and for the same operating speeds M_{ua}' , it decreases with decreasing θ_a , as shown in Fig (19).

The calculations of performances at various radii show that as the radius decreases, the compression ratio and thermal efficiency drop, as shown in Fig (20), (21) and (22). It is due to the increasing Mach Number M_2 of flow entering stator, hence the increasing losses in normal compression shock, as shown in Fig (16), (17) and (18).

The rate of mass flow is found as a function of θ_a , M_{ua}' and $(\varsigma)_{min}$. Since that $(\varsigma)_{min}$ is a function

of M'_{ua} and θ_a , therfore the rate of mass flow is only a function of M'_{ua} and θ_a . For θ_a = constant, it decreases as M'_{ua} increases, the rate of change depends greatly on the value of θ_a, as can be seen in Fig (34). The asymptode of the cuves of mass flow rate for various θ_a gives the maximum flow curve as a function of M'_{ua}. Also the corresponding design of θ_a, limiting blade height $(\zeta)_{min}$, at the maximum flow conditions are thus found as plotted in Fig(35) and Fig(19) as functions of M'_{ua} only. The value of θ_a thus determined togeather with $\theta_a = 120^\circ$ gives the useful design range of various M'_{ua}. A survey of this range disclosed that the design points determined by the asymptode in Fig(34) are more desirable than the design points on the curve $\theta_a = 120^\circ$, therefore the asymptode is designated as the Design Curve.

The significance of the Design Curve is that the design of compressor is entirely determined once an operating speed is chosen. It has become a function of M'_{ua} only. Hence each value of M'_{ua} represents a design point, and the only one design point.

By considering a minimum average compression ratio equal to 2, the lowest design point on the design curve is determined at $M'_{ua} = 0.8$. The consideration of minimum mass flow rate ruled out the design points

at M'_{ua} higher than 1.0. Thus the effective design points are outlined. The corresponding design and performance at various effective design points are plotted in the Design Charts in Fig(38). The performance and design at the limiting design points are listed below:

	$(M'_{ua})_{min}$	$(M'_{ua})_{max}$
	0.800	1.000
(θ_a)	75°	97.5°
$(\varsigma)_{min}$	0.851	0.893
$R_{av.}$	2.000	2.650
$\eta_{av.}$	0.875	0.806
$\frac{W\sqrt{T_{10}}}{\pi r_t^2 \cdot p_{10}}$	0.106	0.063
$\eta_{\text{drop tip-hub}}$	14.5%	14.1%

The thermal efficiency, rate of mass flow, blade height all decrease with increasing tip compressor Mach Number or speed. The compression ratio and the turning angle in rotor at tip radius decreases with increasing operating speed. The radial drop of thermal efficiency from tip to hub radius is at its maximum value of 15% at the design point $M'_{ua} = 0.84$.

V OUTLET STATOR

1. Introduction

The results of the analysis in Chapter II concluded that at same operating speeds(also same initial stagnation conditions of flow), compressor with large angle of turning θ in rotor gives higher compression ratio and thermal efficiency than compressors designed with small turning angle θ in rotor. Since that at same operating speeds, work done will be the same for all designs, and the only loss considered in the analysis was that due to normal compression shocks at entrance of outlet stator, it is obvious that the intensity of normal compression shock increases as the turning angle θ in rotor decreases. This can be explained from Fig (3); along a line of constant Mach Number of compressor M_4 , the magnitude of Mach Number M_2 of flow entering outlet stator increases as the turning angle θ in rotor decreases. The increasing losses in normal compression shock at increasing high Mach Numbers thus cause the decrease of thermal efficiency and compression ratio at decreasing turning angle θ. Therefore the compression ratio and thermal efficiency at all design points can be greatly improved if flow can be decelerated to lower Mach Number in the stator passage before bringing it to normal

compression shock.

In the analysis of constant circulation stage design in previous chapter, it is shown that Mach Number M_2 of flow entering outlet stator increases as the radius decreases, therefore,for the same reason the compression ratio and thermal efficiency drop as the radius decreases. Properly designed stator to minimize normal shock effects will not only increase overall efficiency and compression ratio of compressor, but also reduce the efficiency drop radially to improve the condition of radial equilibrium in stator.

Also in order to achieve high efficiency, flow should be directed and diffused in the axial direction of compressor in stator passage before it enters collector downstream. Therefore the design of outlet stator should enable the stator to minimize compression shock effects, diffuse and turn the flow into the axial direction of compressor.

2. Limiting Contraction Ratio of Stator Passage

To reduce the Mach Number of incoming flow in the stator passage before bringing it to a normal compression shock means that the passage will have to be contracted. By considering only the flow conditions at design points, theoretically it would be possible to contract the passage to the corresponding critical area ratio of incoming flow, so that it can be decelerated through the velocity of sound with no loss whatsoever. But this is known impossible, since a slight disturbance downstream will cause choking of flow, as been discussed by Kantrowitz in reference, and a normal compression shock at entrance was concluded as necessary to establish a stable diffusion. The limiting contraction of supersonic diffuser was thus derived. The establishment of supersonic flow in the stator passages at design points is similar to that in Kantrowitz's analysis, therfore the same analysis can be be applied. Although full detail can be obtained from the reference on the subject, it is thought best to go over the analysis briefly.

Consider flow condition at design point; the cross sectional area of flow entering stator passage at Mach Number M_2 is,

$$A_2 = A_0 \cdot \sin \alpha_2 \qquad (66)$$

where A_0 is the area of flow inlet in the direction of compressor axis, Fig(1).

Denoting p_{20} and T_{20} as the stagnation pressure and temperature of flow entering stator, the rate of mass flow entering the stator passage follows,

$$\overline{W} = A_2^* \sqrt{\frac{2g}{R}\cdot\frac{K}{K-1}} \cdot \frac{p_{20}}{\sqrt{T_{20}}} \cdot \left(\frac{p^*}{p_{20}}\right)^{\frac{1}{K}} \cdot \sqrt{1-\left(\frac{p^*}{p_{20}}\right)^{\frac{K-1}{K}}} \qquad (67)$$

where A_2^* is the critical area, at which $M = 1$.

Assuming a normal compression shock is formed at the entrance, M_2 is the Mach Number of flow immediately upstream of the normal shock and the stagnation pressure and temperature downstream are denoted by p_{30} and T_{20}, then the equation of flow follows,

$$\overline{W} = A_3^* \sqrt{\frac{2g}{R}\cdot\frac{K}{K-1}} \cdot \frac{p_{30}}{\sqrt{T_{20}}} \cdot \left(\frac{p^*}{p_{30}}\right)^{\frac{1}{K}} \cdot \sqrt{1-\left(\frac{p^*}{p_{30}}\right)^{\frac{K-1}{K}}} \qquad (68)$$

where similarily A_3^* is the critical area, referring to the stagnation states after the shock, which at the same time is the limiting cross sectional area to permit flow to pass. Hence $A_3^* = A_{min}$, equations (67) and (68) give,

$$\frac{A_{MIN}}{A_2^*} = \frac{p_{20}}{p_{30}} \qquad (69)$$

or,

$$\frac{A_{MIN}}{A_2} = \frac{p_{20}}{p_{30}} \cdot \frac{A_2^*}{A_2} \tag{70}$$

since

$$\frac{p_{20}}{p_{30}} = \frac{\left(\frac{2}{k-1} + M_2^2\right)\left(\frac{2k}{k-1} M_2^2 - 1\right)^{\frac{1}{k-1}}}{M_2^{\frac{2k}{k-1}} \cdot \left(\frac{k+1}{k-1}\right)^{\left(\frac{k+1}{k-1}\right)}} ,$$

$$\frac{A^*}{A_2} = \frac{M_2}{\left(\frac{2}{k+1} + \frac{k-1}{k+1} M_2^2\right)^{\frac{k+1}{2(k-1)}}}$$

therefore

$$\frac{A_{MIN}}{A_2} = f(M_2) \tag{71}$$

the limiting contraction ratio of stator passage can be determined according to the Mach Number of flow entering the stator. The limiting contration ratios thus determined for approaching Mach Numbers from 1 to 4 , are tabulated in Table (XIV) and plotted in Fig(23).

Optimum total pressure recovery or efficiency will be obtained if normal compression shock is controlled at the minimum cross sectional area A_{min}, of the stator passage. The Mach Number of flow at this optimum operating condition immediately upstream of the normal shock $(M)_{A_{min}}$, can be determined by M_2 and the corresponding limiting contraction ratio through the equation of isentropic flow. Hence

the optimum total pressure recovery (p'_{3o}/p_{2o}) can also be calculated. Results are tabulated in Table (XIV). Also in the same table, the total pressure recovery in the case of straight stator passage (p_{3o}/p_{2o}), assuming deceleration through a normal compression shock at stator entrance, is also tabulated. Comparison of total pressure recoveries of both cases at same initial Mach Numbers M_2, is shown through (p'_{3o}/p_{3o}) also in the same table.

3. Non-Dimensional Calculations of Optimum Performances at Various Design Points

The calculation of compressor performances at various design points so far has based on the assumption that normal compression shock takes place right at the entrance of stator, that only straight stator passage has been taken into consideration.

Consider now that the stator passage at all radii at all design points is contracted with the limiting contraction ratio (A_{min}/A_2), according to the Mach Number M_2 of flow entering stator, and that the normal compression shock is controlled by back pressure adjustment at the minimum cross sectional area (A_{min}), then the optimum performance of compressor at various design points can be calculated.

The optimum performances at various design points considered in the primary investigation at one radius, in chapter II, are thus calculated and plotted in Fig (23), (24) and (25). The results show that considerable improvment in thermal efficiency and compression ratio at all design points could be obtained. Take the design point $\theta = 120^{\circ}$; $M_1 = 1.318$ for example, the optimum performance thus calculated follows:

$$R' = 4.880$$

$$\eta' = 0.835$$

compared with the performance calculated previously:

$$R = 4.145$$

$$\eta = 0.732$$

it shows 10.5% increase in thermal efficiency and 17.75% increase in compression ratio.

Similarily, the calculation of optimum performances for the design points from the Design Curve, investigated in the analysis of constant circulation stage, follows:

M'_{ua}	1.055	0.926	0.840	0.770
R'_{tip}	3.345	2.712	2.357	2.090
R'_{hub}	3.020	2.520	2.200	1.995
η'_{tip}	0.920	0.963	0.985	0.991
η'_{hub}	0.840	0.882	0.896	0.920
$R'_{av.}$	3.183	2.616	2.279	2.043
$\eta'_{av.}$	0.880	0.923	0.941	0.955
$\eta_{drop\ tip-hub}$	8%	8.1%	8.9%	7.1%

comparing with the previously calculated results, it can be seen that not only the average compression ratio and thermal efficiency are greatly improved, but also the efficiency drop from tip to hub radius has greatly reduced to less than 9% ! This has the significance in predicting that with contracted stator passage design, the Effective

Design Points of constant circulation compressors presented previously will have acceptable radial equilibrium conditions in the stator. Results calculated are also plotted in the Design Charts in Fig (38).

4. Supersonic Cascades for Stator Design

With the contraction ratios of stator passages at various design points been determined, the next problem is the design of proper entrance region of cascades so that all wave patterns originating from the blade leading edges can be confined within the cascades and losses can be reduced to a minimum. This is done as illustrated in Fig(27),in the cascade design for an entering Mach Number equal to 2 at zero angle of attack. The stagger angle of 10.9° corresponds to the design of turning angle in rotor $\theta = 120^{\circ}$. The flow condition corresponds to the design point with a Compressor Mach Number $M_u' = 1.24$.

Before explaining the construction of cascade design illustrated in Fig(27), it is thought best to write down the equations of the well known isentropic flow around a corner and the symbols used in explaining the design.

Fig$(27)_a$ shown a stream line of supersonic flow around corner denoted by 0, where r is the distance from any point on the stream line to the corner 0. At $r = r^*$, the Mach Number of stream there is equal to the local velocity of sound. α_m is the Mach angle, γ_m is the angle of turning of the super-

sonic stream from M = 1 to M, all are functions of Mach Number M;

$$\alpha_m = \sin^{-1}\left(\frac{1}{M}\right)$$

$$\gamma_m = \sqrt{\frac{K+1}{K-1}}\,\tan^{-1}\sqrt{\frac{K-1}{K+1}(M^2-1)} - \tan^{-1}\sqrt{M^2-1}$$

the angle ω_m can be calculated from the relation;

$$\omega_m = \frac{\pi}{2} + \gamma_m - \alpha_m$$

the ratio of (r/r*) can be determined from the relation,

$$\frac{r}{r^*} = \left[\cos\left(\sqrt{\frac{K-1}{K+1}}\,\omega_m\right)\right]^{-\frac{K+1}{K-1}}$$

thus the stream lines of flow around a corner between any two given Mach Numbers can be constructed by choosing a certain reference scale of r*. If the difference of the two given Mach Numbers are relatively small then the same flow pattern reversed can be used in the case of compression as a close approximation.

The construction of cascade design in Fig(27) begins with drawing parallel lines from blade tips point 1 and 1' with a stagger angle $\alpha_2 = 10.9^\circ$ ($\overline{11'}$ chosen equal to 2.5"). Referring to them as stagger lines, the distance between them thus represents A_2 for unit thickness of flow. From point 1' draw line $\overline{10}$ making

an angle with the stagger line equal to the Mach angle of the entering flow Mach Number, so it is 30° for $M_2 = 2$. Point 0 is chosen such that $\overline{01'} > \overline{01''}$, so that the point of infinite pressure gradient will not be included in the flow passage. A reference scale of $r^* = 0.5''$ is chosen to fix the point 0.

For $M_2 = 2$, the limiting contraction ratio calculated is $A_{min}/A_2 = 0.822$, which gives $M = 1.75$ at the minimum cross sectional area. Referring to the flow pattern of isentropic expansion around corner, for:

$M = 1.75$; $r/r^* = 2.42$, $\gamma_m = 19.27°$, $\alpha_m = 34.85°$, $\omega_m = 74.42°$

$M = 2.00$; $r/r^* = 3.28$, $\gamma_m = 26.38°$, $\alpha_m = 30.00°$, $\omega_m = 86.38°$

and assume isentropic compression from $M = 2$ to 1.75, the boundaries of passage $\overset{\frown}{1'2}$ and $\overset{\frown}{1''2'}$ corresponding the stream lines can be drawn.

Point 3 is determined by drawing a perpendicular from point 2' to the line which makes an angle equal to the Mach angle of $M = 1.75$ with $\overline{20}$; $\measuredangle 322' = 34.85°$. $\overline{2'3}$ thus represents the minimum cross sectional area of flow passage. It is impossible to predict just how long this throat section should be to provide a stable normal shock controlled there by back pressure, theoretically it is not necessary as long as point 3

is determined as described. However, a length of $\overline{34} = \overline{2'3}$ is considered for the throat section.

By assuming a normal compression shock in the throat section, the Mach Number downstream of the compression shock will be 0.628. In order to reduce the velocity of flow before turning, the passage is diverged with angle of 6° from section $\overline{44'}$ to section $\overline{55'}$. The area ratio of $\overline{44'}/\overline{55'}$ equal to 0.862 provides the diffusion of flow from $M = 0.628$ to $M = 0.5$. Flow is then directed at the Mach Number 0.5 to the axial direction of compressor at section $\overline{66'}$. The constant cross sectional area of passage is extended to section $\overline{77'}$ in order to stablize the flow after turning. After section $\overline{77'}$, flow is then diffused in the passage with an diverging angle of 30°.

It has to be noted that the diverging angle of passage beginning at section $\overline{44'}$ and $\overline{77'}$ are best to choose as small as possible in order to obtain high efficiency of diffusion. Also in order to avoid flow seperation, flow should be diffused to low Mach Number before turning it. But that then means considerable increase of dimensions of cascade profiles both in length and width will have to be necessary.

The construction of stator for the constant circulation compressors studied in Chapter IV can be

followed by applying the same method from point to point along the radial direction.

5. Summary

The design of supersonic cascades presented has following advantages:

(1) All wave patterns originating from leading edges are confined within the cascades. The energy loss associating with extended wave patterns ahead of cascades in reference (3) is avoided.

(2) The design of entrance region of cascades functions:

a. confining all wave pattern originating from leading edges of cascades within the passage.

b. contraction of passage (A_{min}/A_2), minimizing shock effects.

c. directing flow through a small angle of turning towards compressor axis and permitting finite thickness of blades to resist the force resulted from normal compression shocks on both sides.

(3) By controlling normal compression shocks in throat sections, optimum compression ratio and thermal efficiency can be obtained. Drop in thermal efficiency and compression ratio from tip radius to hub can be reduced. The result is higher overall performance at all design points than calculated by assuming straight stator passages.

Elimination of boundary layers to prevent flow seperation in the compression shock can be accomplished by installation of suction slits in the shroud and hub of stator. This method has been used successfully by Weise[1].

VI EXPERIMENTAL FIELD ON THE SUPERSONIC CASCADE

1. Introduction

The purpose of the study in this chapter is to investigate the possibilities of the supersonic stator dicussed in the previous chapter, through experimental tests of two-dimensional cascades. Due to lacking of facilities to make supersonic wind tunnel test, it was decided to make an approach to the problem through the means of hydraulic analogy. Water channel in M.I.T. was used to conduct the experiment.

The fundamental theory of hydraulic analogy, normal hydraulic jump etc.,have been presented by Preiswerk in reference (4). A brief review of his work was thought necessary to introduce the hydraulic resemblance of limiting contraction ratio of supersonic diffuser, the analogy of flow area and the design of experimental cascade presented in this chapter.

2. Theory of Hydraulic Analogy

Consider water flows through an open channel of horizontal bottom symmetrical to the x - axis as shown in Fig$(28)_a$. At x = 0, flow is considered at rest, assuming the width of channel there is infinite and the height of water from free surface to the bottom is l_0. Assume that there is no energy loss, no rotational motion in the flow and that water is incompressible.

Consider a flow filament which passes through the point $(0, y_0, z_0)$: The Bernoulli equation along this filament states,

$$p + \frac{\rho V^2}{2} + \rho g z = p_0 + \rho g z_0 \qquad (1)$$

assuming that the vertical acceleration of water flow is negligible compared with the acceleration of gravity, then the static pressure at a point of flow depends linearly om the vertical distance under the free surface at that point, that is,

$$\begin{aligned} p_0 - p_s &= \rho g (l_0 - z_0) \\ p - p_s &= \rho g (l - z) \end{aligned} \qquad (2)$$

where p_s denotes the static pressure at surface.

substituting equation (2) into equation (1) it follows,

$$V^2 = 2g(l_o - l) = 2g\Delta l \qquad (3)$$

the energy equation (3) holds for all flow filaments passing through y-z plane at x = 0.

Since all the flow filaments that lie one above another, have the same l_o and at rest at x = 0, since equation (3) does not contain the coordinate z , hence the velocity V at x is constant over the entire depth and width, and is given only by the difference in height Δl between the initial stagnation height and free surface. Δl being,at most equal to l_o, the maximum obtainable velocity therefore is,

$$V_{max} = \sqrt{2gl_o} \qquad (4)$$

equation (3) can thus be written,

$$\left(\frac{V}{V_{max}}\right)^2 = \frac{V^2}{2gl_o} = \frac{\Delta l}{l_o} \qquad (5)$$

In a flow of perfect gas the ratio of local velocity to maximum velocity is,

$$\left(\frac{V}{V_{max}}\right)^2 = \frac{T_o - T}{T_o} = \frac{\Delta T}{T_o} \qquad (6)$$

from equation (5) and (6) it can be seen that the ratio

of (V/V_{max}) will be the same in gas and water flow if,

$$\frac{l_o - l}{l_o} = \frac{T_o - T}{T_o}$$

or,

$$\frac{l}{l_o} = \frac{T}{T_o}$$

therfore with respect to the velocity there exists an analogy between the two flows, if the depth ratio l/l_o of water flow is compared with the temperature ratio T/T_o of gas flow.

Consider next a small fluid prism at (x,y) Fig(28)$_a$ with edge dx and dy and height l as shown in Fig(28)$_b$. Let u,v, be the horizontal components and w the vertical component of the velocity V in the direction of the coordinate axis x,y, and z.

Assuming that the vertical acceleration of the water is negligible compared with the acceleration of gravity, from equation (2),

$$\frac{\partial p}{\partial x} = \rho g \frac{\partial l}{\partial x}$$
$$\frac{\partial p}{\partial y} = \rho g \frac{\partial l}{\partial y} \qquad (7)$$

the right side of the above equations are independent of z, therefore the horizontal accelerations for all points along a vertical are independent of z also. Hence

the horizontal velocity components u and v are constant over the entire depth since they were so at the initial state at x = 0.

The continuity condition for the stationary flow of an incompressible fluid requires that the volume flow going into the prism per unit time must be equal to that coming out of the prism,

$$d q_{in} = d q_{out}$$

and

$$d q_{in} = u \cdot l \cdot dy + v \cdot l \cdot dx$$

$$d q_{out} = \left(u + \frac{\partial u}{\partial x} dx\right)\left(l + \frac{\partial l}{\partial x} dx\right) dy + \left(v + \frac{\partial v}{\partial y} dy\right)\left(l + \frac{\partial l}{\partial y} dy\right) dx$$

it follows,

$$\frac{\partial (l \cdot u)}{\partial x} + \frac{\partial (l \cdot v)}{\partial y} = 0 \qquad (8)$$

by comparing this equation with the continuity equation for a two-dimensional compressible flow,

$$\frac{\partial (\varrho u)}{\partial x} + \frac{\partial (\varrho v)}{\partial y} = 0 \qquad (9)$$

it shows that similar to the energy equations the equations of continuity for the two flows bear the same form. This gives a further condition for the analogy that the specific mass ϱ of gas flow corresponds to the water depth l . The change of specific mass

from point to point of the gas flow can be explained as the change of water depth from point to point in the analogy. But since from the energy equations of the two flows the water depth was simultaneously also the analogeous magnitude for the gas temperature T, therefore from the isentropic relation,

$$\frac{\rho}{\rho_0} = \left(\frac{T}{T_0}\right)^{\frac{1}{k-1}}$$

the analogy requires that

$$k = 2 \tag{10}$$

Hence the flow of water in horizontal open channel without energy losses is analogeous to the two-dimensional isentropic gas flow with a fictitious gas constant of $k = c_p/c_v = 2$.

With the assumption of irrotational motion,

$$\frac{\partial v}{\partial x} - \frac{\partial u}{\partial y} = 0 \tag{11}$$

there exists a velocity potential $\phi(x,y)$ and,

$$\frac{\partial \phi}{\partial x} = u \quad , \quad \frac{\partial \phi}{\partial y} = v \tag{12}$$

from the energy equation,

$$l = l_0 - \frac{V^2}{2g}$$

it follows

$$\frac{\partial l}{\partial x} = -\frac{1}{2g}\frac{\partial (V^2)}{\partial x}, \quad \frac{\partial l}{\partial y} = -\frac{1}{2g}\frac{\partial (V^2)}{\partial y}$$

where $$V^2 = u^2 + v^2 + w^2$$

since u , v and V are constant over a vertical, so is w also a constant, and since w = 0 at the bottom, it may be neglected in comparison with the components u and v. With this assumption,

$$V^2 = u^2 + v^2$$

and

$$\frac{\partial l}{\partial x} = \frac{1}{g}\left(u\frac{\partial u}{\partial x} + v\frac{\partial v}{\partial x}\right)$$

$$\frac{\partial l}{\partial y} = \frac{1}{g}\left(u\frac{\partial u}{\partial y} + v\frac{\partial v}{\partial y}\right) \qquad (13)$$

substituted into the equation of continuity (8) it follows,

$$\frac{\partial u}{\partial x}\left(1 - \frac{u^2}{gl}\right) + \frac{\partial v}{\partial y}\left(1 - \frac{v^2}{gl}\right) - \left(\frac{\partial u}{\partial y} + \frac{\partial v}{\partial x}\right)\frac{uv}{gl} = 0$$

or

$$\phi_{xx}\left(1 - \frac{\phi_x^2}{gl}\right) + \phi_{yy}\left(1 - \frac{\phi_y^2}{gl}\right) - 2\phi_{xy}\frac{\phi_x\phi_y}{gl} = 0 \qquad (14)$$

It is seen that the differential equation for the velocity potential of the ideal free surface water flow over a horizontal bottom shows similarity

with the differential equation for the velocity potential of a two dimensional compressible flow,

$$\Phi_{xx}\left(1-\frac{\Phi_x^2}{c^2}\right)+\Phi_{yy}\left(1-\frac{\Phi_y^2}{c^2}\right)-2\Phi_{xy}\frac{\Phi_x\Phi_y}{c^2}=0 \qquad (15)$$

therefore equations (14) and (15) are identical if $g\ell/2g\ell_o$ is replaced by $c^2/2gh_o$. Hence $\sqrt{g\ell}$, which is the basic wave velocity in shallow water, corresponds to the local velocity of sound in the gas flow.

It can be concluded from the analysis that the ideal free surface water flow over a horizontal bottom holds analogy with the two-dimensional isentropic compressible flow with a fictitious gas constant equal to 2. Hence all relationships of properties in water flow can be directly derived from the corresponding known expressions for isentropic compressible flow by simply substituting with $k = 2$, as long as there is no energy loss involved.

By substituting $k = 2$ into the equations for the case of perfect gas flow around a corner, it follows,

$$\begin{aligned}
&\alpha_m = \sin^{-1}\frac{1}{M} \quad , \quad M = \frac{V}{\sqrt{g\ell}} \quad , \\
&\gamma_m = \sqrt{3}\,\tan^{-1}\sqrt{\frac{M^2-1}{3}} - \tan^{-1}\sqrt{M^2-1} \\
&\omega_m = \frac{\pi}{2} + \gamma_m - \alpha_m \\
&\frac{r}{r^*} = \frac{1}{\left[\cos\left(\frac{\omega_m}{\sqrt{3}}\right)\right]^3}
\end{aligned} \qquad (16)$$

3. Resemblance of Normal Hydraulic Jump to the Normal Compression Shock

Assuming ideal water flow over a horizontal bottom in an open channel is decelerated from a velocity $V_x > \sqrt{g l_x}$ through a normal hydraulic jump to a velocity $V_y < \sqrt{g l_y}$. Denote l_x as the depth of water flow upstream of the normal hydraulic jump and l_y as the depth of water downstream, as shown in Fig(28)$_c$.

The equation of continuity states,

$$l_x \cdot V_x = l_y \cdot V_y \tag{17}$$

if the width of channel is b, the momentum equation for the direction normal to the jump states that the change in momentum is equal to the force,

$$(\rho \cdot V_y \cdot l_y \cdot b) V_y - (\rho \cdot V_x \cdot l_x \cdot b) V_x = b \cdot l_x \left(g \cdot \frac{\rho \cdot l_x}{2}\right) - b \cdot l_y \left(g \cdot \frac{\rho \cdot l_y}{2}\right)$$

rearranged,

$$l_y \cdot V_y^2 + g \cdot \frac{l_y^2}{2} = l_x V_x^2 + g \cdot \frac{l_x^2}{2} \tag{18}$$

from equation (17),

$$l_x^2 \cdot V_x^2 = l_y^2 \cdot V_y^2$$

or

$$\frac{V_x^2}{g l_x} \cdot l_x^3 = \frac{V_y^2}{g l_y} \cdot l_y^3$$

it follows,

$$M_x^2 \cdot l_x^3 = M_y^2 \cdot l_y^3 \qquad (19)$$

similarily, equation (18) can be rearranged to,

$$l_x^2 (1 + 2 M_x^2) = l_y^2 (1 + 2 M_y^2) \qquad (20)$$

define

$$n = \frac{l_y}{l_x} \qquad (21)$$

as the ratio of water depth after the normal hydraulic jump to that before the jump, equations (19) and (20) can thus be written;

$$n^3 = \frac{M_x^2}{M_y^2} \qquad (22)$$

and

$$n^2 = \frac{1 + 2 M_x^2}{1 + 2 M_y^2} \qquad (23)$$

by eliminating M_y from the above equations it follows,

$$M_x^2 = \frac{1}{2} (n^2 + n) \qquad (24)$$

similarily by eliminating M_x it gives,

$$M_y^2 = \frac{1}{2} \left(\frac{n+1}{n^2} \right) \qquad (25)$$

Equations (24) and (25), with n as a parameter can be solved for M_x and M_y. Numerical values of M_y are calculated for M_x from 1 to 4 in table (XVI) and plotted in Fig (29).

If l_{x_0} is the depth of water at stagnation state before the normal hydraulic jump and l_{y_0} is that after the jump, then the energy loss per unit mass flow due to the hydraulic jump is simply the difference of its potential energy at the two stagnation states;

$$\Delta E = g\frac{l_{x_0}}{2} - g\frac{l_{y_0}}{2} \tag{26}$$

the recovery of total energy per unit mass flow after the hydraulic jump then is,

$$\frac{E_y}{E_x} = \frac{l_{y_0}}{l_{x_0}} \tag{27}$$

from the energy equations;

$$l_{x_0} = l_x \left(1 + \frac{M_x^2}{2}\right)$$

and

$$l_{y_0} = l_y \left(1 + \frac{M_y^2}{2}\right)$$

it follows,

$$\frac{E_y}{E_x} = n \cdot \frac{2 + M_y^2}{2 + M_x^2} \tag{28}$$

Numerical values of E_y/E_x for M_x from

1 to 4 are calculated in Table (XVI) and plotted in Fig (29). It can be seen that the energy loss in normal hydraulic jump increases quickly with the increasing value of M_x, even at $M_x = 2$ it amounts to about ten per cent of the original total energy.

It has to be noted that unlike the case of normal compression shock of perfect gas flow where no energy loss is assumed, the case of normal hydraulic jump results in energy loss transferred into heat. Since the depth of water flow corresponds to the absolute temperature or enthalpy of perfect gas flow with k = 2 in the analogy, it is obvious that the hydraulic jump does not hold strict analogy to the normal compression shock in gas flow of k = 2. Hence the equations for normal compression shock in gas flow cannot be applied to the normal hydraulic jump. However it bears close qulitative resemblance.

4. Analogy in Water Channel Width and Area of Compressible Flow Passage

Consider water flowing through an open channel with horizontal bottom, its width changes, as shown in Fig $(28)_d$. Assuming at section (1) the width of channel is b_1, the velocity and depth of water there being V_1 and ℓ_1 respectively. At channel section (2), width of channel is b_2, and the velocity and depth of water there are V_2 and ℓ_2 respectively.

Assume that there is no energy loss, then the energy equation gives,

$$\ell_0 = \ell_1 + \frac{V_1^2}{2g} = \ell_2 + \frac{V_2^2}{2g} \tag{29}$$

and from the equation of continuity,

$$\ell_1 \cdot b_1 \cdot V_1 = \ell_2 \cdot b_2 \cdot V_2 \tag{30}$$

with $M = V/\sqrt{g\ell}$, equations (29) and (30) can be rearranged to,

$$\left(\frac{\ell_2}{\ell_1}\right) = \frac{2 + M_1^2}{2 + M_2^2} \tag{29}'$$

and

$$M_1^2 = M_2^2 \cdot \left(\frac{\ell_2}{\ell_1}\right)^3 \cdot \left(\frac{b_2}{b_1}\right)^2 \tag{30}'$$

by eliminating the term ℓ_2/ℓ_1 from above equations, it follows,

$$\left(\frac{b_2}{b_1}\right)^2 = \frac{M_1^2}{M_2^2}\left(\frac{2+M_2^2}{2+M_1^2}\right)^3 \qquad (31)$$

Equation (31) gives the relation of channel width in the application of hydraulic analogy. It is more convenient to use in the case of isentropic flow, since the ratio of channel width is much more easy to measure than the depth of water flow,futhermore since the width of channel can be measured much more accurately than depth of water flow,hence better results can be obtained.

Consider next that at section (2), the water flow reaches its local velocity of wave propagation, $M_2 = 1$, and denote the width of channel there by b^*, from equation (31), it follows,

$$\frac{b^*}{b_1} = M_1\left(\frac{3}{2+M_1^2}\right)^{3/2} \qquad (32)$$

It can be seen that the right side of the equation becomes identical with the expression for critical area ratio in an isentropic gas flow with $k = 2$;

$$\left(\frac{A^*}{A}\right) = \sqrt{\left(\frac{k+1}{2}\right)^{\frac{k+1}{k-1}}} \; \frac{M}{\left(1+\frac{k-1}{2}M^2\right)^{\frac{k+1}{2(k-1)}}}$$

Thus in the case of ideal free surface water flow over a horizontal bottom with no energy loss, the width of channel is analogeous to the area of flow passage in an isentropic compressible flow with k = 2.

Numerical calculations of equation (32) for M_1 from 0 to 4 are tabulated in Table (XVII) and plotted in Fig (30).

5. Resemblance in Limiting Contraction Ratio and Experimental Tests

a. Theory

From discussions in paragraph 3, it is obvious that the limiting contraction ratio of supersonic diffusers for the design conditions, in the case of water flow, can not be directly obtained by substituting $k = 2$ into the expressions derived in paragraph 2 of the previous chapter. The premises of the limiting contraction ratio for the design condition assumed that the establishment of supersonic flow in the diffuser is preceded by a normal compression shock at the diffuser entrance, which then moves downstream and can be controlled at the minimum cross sectional area by back pressure adjustments. The limiting contraction ratio of the design condition of diffusers was then determined by the continuity condition of flow. Assume that the establishment of flow in water diffusers is similarily preceded by a normal hydraulic jump at diffuser entrance, then the limiting contraction ratio can be determined as follows: Assume that the Mach Number of flow approaching the diffuser entrance b_2 at the design condition is M_2, and

$$M_2 > \sqrt{gl_2}$$

assume that a normal hydraulic jump is formed at the entrance, then the Mach Number of flow after the jump, M_{2s} can be calculated from equations (24) and (25) or read from Fig (29). The limiting contraction ratio can thus be determined from equation (32), it follows:

$$\frac{b_{min}}{b_2} = M_{2s}\left(\frac{3}{2 + M_{2s}^2}\right)^{3/2} \qquad (33)$$

Numerical calculations of equation (33) are calculated for design Mach Numbers from 1 to 4, and tabulated and plotted in Table(XVII) and Fig(31) respectively. The Mach Number at b_{min} for the design condition can be calculated from equation (31).

b. Experimental Tests

Experimental tests on the limiting contraction ratio are conducted in the M.I.T. water channel.

Fig(32) and (33) show the diffusers designed to operate at Mach Numbers equal to 2 and 3 respectively. The diffusers made, are shown in picture (A).

The width of the openings of diffusers are all made equal to 1 inch. The contraction ratios of diffusers (1_a) and (2_a) are made equal to the critical contraction ratios (b*/b), calculated from equation(32), thus the dimensions of diffusers tips $(1)_a$ and $(2)_a$ are listed as follows:

Diffuser Tip	Opening	Design Mach Number	Throat
$(1)_a$	1"	2	0.707"
$(2)_a$	1"	3	0.428"

The contraction ratios of diffuser tips $(1)_b$ and $(2)_b$ are made according to the limiting contraction ratios (b_{min}/b),calculated from equation (33) for approaching Mach Numbers equal to 2 and 3 respectively. The dimensions of diffuser tips $(1)_b$ and $(2)_b$ are:

Diffuser Tip	Opening	Design Mach Number	Throat
$(1)_b$	1"	2	0.814"
$(2)_b$	1"	3	0.663"

All diffusers are made of 1 inch wide hard brass and glued in exact dimensions on thick transparent cellulose plates in order to assure their positions. Diffuser walls are used to help stabilize flow downstream of diffuser tips.

Parallel lights are directed from below perpendicularly to the horizontal glass bottom of water channel. A double flashed glass plate was placed on top of the diffusers so that pictures taken are all shadowgraphs.

Diffuser tip in the picture with no diffuser walls attachen are diffusers $(1)_a$ and $(2)_a$ and those with diffuser walls attached are diffuser tips $(1)_b$ and $(2)_b$.

In all the pictures taken, two diffusers were lined up in a straight line perpendicular to the direction of the uniform approaching flow, so that the inlet conditions of flow for both diffusers were the same. The approaching flow Mach Number is indicated by the protractor showing the Mach angle on the right side of the pictures.

Pictures No.1 and No.2 were taken when the approaching flow was accelerated to Mach Number 2, which corresponds to the design condition of the diffusers. Diffuser $(1)_a$ at this stationary design condition showed 'Spill'of flow as can be seen in both pictures. Diffuser $(1)_b$ showed 'supersonic' speed throughout the passage.

Picture No. 4 shows the moment when the flow was being accelerated to Mach Number 2. An unstable normal hydraulic jump can be seen formed inside of the diffuser $(1)_a$, which was soon pushed out. After that diffuser $(1)_a$ showed Spill condition as shown in pictures No. 1 and No. 2. In diffuser $(1)_b$, there was also seen a normal hydraulic jump ,, which also was very unstable. When flow was being accelerated but before it reached Mach Number 2, this normal hydraulic jump frequently formed in-

side of the diffuser before its throat section and then pushed out right afterwards, then diffuser $(1)_b$ also showed Spill condition. The phenomena observed at both diffusers were fundamentally identical. The difference came when flow Mach Number reached 2, the pulsation hydraulic jump observed in diffuser $(1)_b$ previously, moved quickly downstream passing the throat section and clear, stable 'supersonic' flow pattern followed in the entire diffuser. Whereas in the diffuser $(1)_a$, when flow stopped accelerating, the pulsation normal hydraulic jump disappeared, and the Spill took place and stayed at the diffuser entrance.

The results observed seems to support fully the limiting contraction ratio for water differs derived.

The pulsation normal hydraulic jump observed in the diffusers was probably originated at the diffuser entrance and then moved downstream, but hard to see. It moved only so far downstream when the Mach Number of flow immediately upstream of the jump and the width of passage there caused 'sonic' velocity at throat section. When this position was reached, it would be impossible for the jump to move further towards the throat, since then it would require a larger throat section due to the change of normal hydraulic jump to narrower section of diffuser , and hence the decreasing Mach Number

of flow upstream of the normal hydraulic jump. A slight disturbance of flow downstream of the throat was probably the cause of pushing it back out of the diffuser, then Spill condition followed. The irregularity of flow at Spill condition at diffuser entrance was probably the the cause of such establishment of the normal hydraulic jump, because it would be impossible if the flow Mach Number at diffuser entrance were entirely uniform, as the free stream. The same reasoning can be applied to prédict the possibility of pulsation normal compression shocks in real supersonic diffusers at starting conditions. Hence the conclusion can be drawn : the supersonic diffusers with limiting contraction ratio will be able to establish supersonic flow in the diffusers when they are operated at their design conditions. A normal compression shock formed at diffuser entrance moving downstream through the throat section will serve as a mechanism of such establishment. Discontinuity of performance of such diffuser in the form of Spill condtion and pulsation compression shocks will probably offer a serious problem to its starting condition, that is before the flow upstream is accelerated to its design Mach Number.

Picture No. 3 was taken when the flow was slowing down to Mach Number 2 . In diffuser $(1)_a$, a normal hydraulic jump pushing out of the the diffuser can be seen.

No normal hydraulic jump formed at throat section of diffuser $(1)_b$, until the flow was slowed down further. The normal hydraulic jump in diffuser $(1)_a$ observed,was of entirely different nature than that observed during acceleration of flow. It was formed at the throat section and moved steadyly upstream and finally out of the diffuser as flow slowed down. No Spill condition of flow at entrance of diffuser was observed either after that. This phenomenon is very easy to explain: When the Mach Number of flow upstream was higher than the design Mach Number 2, and higher than the minimum Mach Number which will permit the establishment of'supersonic' flow in diffuser $(1)_a$, the flow conditions in both diffusers $(1)_a$ and $(1)_b$ had been already'supersonic'. Following the decreasing Mach Number of flow upstream, the Mach Numbers of flow at throat sections in both diffusers also decreases. When the Mach Number upstream reached 2, the Mach Number of flow at throat section of diffuser $(1)_a$ reached its local velocity of 'sound'. Further decrease of Mach Number upstream made it impossible for flow to pass the throat isentropically, hence the flow adjusted itself by means of the normal compression shock at the throat section and moved upstream to wider sections of diffuser with decreasing flow Mach Number upstream. By stopping the decrease of flow Mach Number upstream

however, after picture No. 3 was taken, the same flow condition identical with picture No.1 and No. 2 was observed, as it had been expected.

Similar tests were made with diffusers $(2)_a$ and $(2)_b$ and same results were obtained.

Picture No. 5 and No.6 show the diffusers when flow upstream was being acclerated to Mach Number 3. Pulsation normal hydraulic jump was observed in diffuser $(2)_b$ during the flow acceleration,altered with Spill conditions similar to the previous tests. But no pulsation normal hydraulic jump was observed in diffuser $(2)_a$, it was in Spill condition since the Spill started. This is probably due the strong contraction ratio and the rapid contraction of the diffuser passage towards the throat, so that pulsation hydraulic jump was impossible. Establishment of 'supersonic' flow preceded by a normal hydraulic jump at entrance was also observed in diffuser $(2)_b$.

Picture No.7 was taken when the flow upstream was slowed down to Mach Number at 3,after'supersomic' flow had been established in diffuser $(2)_a$, and a normal hydraulic jump just formed at the throat section of diffuser $(2)_a$ can be seen in the picture. It is similar to picture No.3.

Howerer, the hydraulic jump in diffuser did

not move out steadily as observed previously with diffuser $(1)_a$, it pushed suddenly out of the diffuser followed by the spill condition at entrance of diffuser $(2)_a$, while Mach Number of flow upstream was being slowed down gradually. It is shown in picture No.8, the Mach Number of flow upstream was slowed down below 3, as can be seen from the Mach angle on the protractor. The flow in diffuser $(2)_b$ was still 'supersonic'. The sudden push of the normal hydraulic jump out of diffuser $(2)_a$ and hence caused the spill condition was probably due to the same reason that no pulsation jumps occured during flow accleration mentioned previously.

c. Conclusions

The results of the experimental tests let formulate the following conclusions:

(1) The establishment of 'supersonic' flow in water diffusers is preceded by a normal hydraulic jump at diffuser entrance. The limiting contraction ratio for water diffusers derived from this assumption has also been fully supported by the experimental tests.

(2) The establishment of 'supersonic' flow in water diffusers is found similar to the real supersonic diffusers as presented by Kantrowitz[8].

(3) The limiting contraction ratio for water diffusers derived, bears both qualitative and quantitative resemblance to that of real supersonic diffusers. As a matter of fact it is even better than by assuming strict hydraulic analogy in limiting contraction ratio with k = 2. It can be seen from following:

Limiting contraction ratio,

	k = 1.4	Water	k = 2
M = 2	0.822	0.814	0.885
M = 3	0.720	0.663	0.827

(4) When flow is accelerated before reaching the design Mach Number of the supersonic diffuser with the corresponding contraction ratio, discontinuity of performance will likely be caused by Spill conditions or altered with pulsation compression shocks between the diffuser entrance and throat section, no supersonic flow condition ~~downstream~~ upstream of the throat can be reached. At these operating conditions the diffuser has no function.

(5) The establishment of supersonic flow in the diffuser and hence the function of the diffuser starts when the flow upstream reaches its design Mach Number. Control of normal compression shock by means of back pressure adjustments to fix it in the diverging part of the diffuser can also be visualized in water

diffuser tests as will be presented later in the cascade tests.

6. Design of Experimental Supersonic Cascade

The construction of the experimental supersonic cascade in Fig(36) follows the same procedure as was described in the previous chapter, except the dimensions are different, since it is designed for water channel test. The design condition of the cascade assumes an entering flow with $M = 2$ at zero angle of attack. The stagger angle 10.9° corresponds the design with a turning angle θ equal to 120° in rotor. The flow condition of design corresponds the design point with compressor Mach Number $M_u' = 1.24$.

Since the subsonic turning and diffusion of flow is not the object of the present study, hence straight diverging passage of flow after the throat section is adopted for design. This consideration also reduces the manufacturing cost a great deal.

Using the same notations in Fig (27), the design of cascade in Fig (36) is stated as follows:

By assuming $A_2=0.5"$, it follows that $\overline{11'} = 2.641"$. The limiting contraction ratio for $M_2 = 2$, $b_{min}/b_2 = 0.814$ determines the Mach Number at throat section at $M = 1.555$. It follows from equation (16) that for,

$M = 2.00$: $r/r^* = 2.830, \nu_m = 18^{\circ}, \alpha_m = 30^{\circ}, \omega_m = 78^{\circ}$

$M \cong 1.555$: $r/r^* = 1.788$, $\nu_m = 9.9^\circ$, $\alpha_m = 40^\circ$, $\omega_m = 59.9^\circ$

choosing $r/r^* = 3/4"$, the curves $\overset{\frown}{1'2}$ and $\overset{\frown}{1"2'}$ were drawn according to the streamlines determined by step to step calculations. The length of the throat section was chosen equal to half of the width. After the throat section, passage was diverged with an angle at 6°.

Profile of the cascade thus designed is dimensioned in Fig(37). Four stainless steel blades of 1 inch width were made as per drawing for experimental tests.

7. Experimental Results on the Supersonic Cascade Tests in Water Channel

Picture (B) shows the set-up position of the experimental cascade designed. Flow approaches the cascade from the left hand side of the picture.(from the position looking into the picture) Methods used in taking the pictures presented are classified and described as follows:

1. Shadow-graph Method: parallel lighting is directed from below perpendicularly towards the horizontal glass bottom of the water channel, a double-flashed glass plate is placed on top of the cascade, so that pictures taken with this method show wave patterns projected on the flashed glass plate in shadow form. Pictures taken with this method are distinguishable from the others by having protractor in them. Protractors placed on top of the double-flashed glass plate are used to measure the flow Mach Number through the wave angle indicated.

2. Direct-Lighting Method: source of lighting and camera are on the same side of the channel bottom. Pictures are taken with direct lighting on the flow patterm. This method is used only to take close-up pictures of the part of the flow pattern interested in. This method has proved being able to show the flow pattern in more details than the shadow-graph method permits. But the later seems

to be the only effective method in taking pictures to show the general flow pattern of the entire cascade.

3. Powder-Method: fine grained light powder spread continuously over the surface of water upstream of the cascade is found as an effective method to detect streamlines of flow. Hence it is used to place the cascade in the right positions with respect to the direction of free stream as desired. Also it is used to judge whether there is 'spill' of flow at cascade. Direct lighting system is used for picture taking.

Beside the photograghic methods described, depth-measurement method is also used to help the investigation of flow patterns at various test conditions.

The experimental tests conducted are aimed at the following problems of the cascade:

1. the starting conditions
2. the design condition and normal shock control.

The results are presented as follows:

Picture No.1 to No.12 show the cascade at various approaching flow Mach Numbers with zero angle of attack to the cascade. The Mach angle or the Mach Number of approaching flow is measured from the protractor and marked in each picture. The

pictures were taken in sequence during the continuous acceleration of flow upstream by control valve adjustment, in order to catch the pulsation shocks in the diffuser tips which were lined up with the first blade of the cascade. The diffuser tips shown in the pictures were from left to right: diffuser tip $(1)_a$ and $(1)_b$, which had been used previously in limiting contraction ratio tests. They were both designed for flow Mach Number of 2, diffuser tip $(1)_a$ has the contraction ratio; $0.707 = A^*/A$ and the contraction ratio of diffuser $(1)_b$ is the same as that of the cascade; $0.814 = A_{min}/A$. The purpose of such arrangement was to compare the starting condition of cascade to that of the diffuser with the same limiting contraction ratio.

The cascade at starting condition showed being entirely different from that of the diffuser $(1)_b$, despite of the fact that their contraction ratio were the same. The unstable flow pattern observed previously with the diffusers,when flow upstream was being accelerated towards the design Mach Number, repeated itself. The camera caught the moments when the pulsation normal hydraulic jumps were in action. But no pulsation hydraulic jumps or spill condition showed with the cascade. The flow pattern was observed being extremely stable during the entire process. It can be seen in the pictures. That the conclusion of no Spill condition with the cascade

during start condition can be proved from No.31, No.32 and No.33.

Pictures No.31, No.32 and No.33 were taken with the powder method at different flow Mach Numbers upstream. The flow Mach Number in picture No.31 can be judged from the visible attached bow wave shown at the tip of the third blade, it probably coincides with that in picture No.1, around 1.052. It has to be noted that the reason that only bow wave at third blade can be seen in the picture is only because of the position of light source (shown as a round white spot at lower left). Actually wave patterns at each blade were identical, except the first one which had no other blade preceding it, hence it was to be expected so. Picture No.32 showed clear Mach wave at the third blade of the cascade, the camera position during taking these three pictures, was placed directly above the third blade, hence the pictures should show the flow pattern around the third blade true to scale. The Mach angle was measured at 40°, which gives the flow Mach Number at 1.555, hence coincides with the flow condition ~~when~~ of picture No.9. Picture No.33 was taken when the flow Mach Number upstream reached the design condition of the cascade, M = 2. It also can be seen from the Mach angle shown at the tip of the third blade. In all the pictures taken, the streamlines made

visible by the powders spread upstream, show very clearly that no Spill took place at the cascade. Picture No.31 represents the transonic condition, picture No.32 represents the flow Mach Number upstream of the cascade below its design Mach Number and picture No. 33 shows the design condition. Therefore it can be concluded that, from the flow patterns shown by picture No.1 to No.12 and the detection of streamlines shown by picture No.31 to No.33, the cascade does not choke or 'spill' during its start. The phenomenen of the starting condition of the cascade, which showed entire difference from the diffuser with the same contraction ratio, will be explained later in the next paragraph.

By examining the flow patterns shown in pictures No.1 to No.12, it can be seen that the flow patterns in all the cascade passages are identical, also by measuring the Mach Angles at each blade, the Mach waves are proved being parallel to each other. Therefore the results coincides with what had been expected with the cascade design: at zero angle of attack each cascade passage can be treated as isolated, same flow condition approaches all cascade blades, all compression waves are confined within the cascade passages, no possibility of extended wave patterns ahead of cascade.

The cascade operating at the design condition

are shown in picture No.11 and No.12. The control of normal hydraulic jump in the diverging passage at the design condition by back pressure adjustments are illustrated in picture No.34 and No.35.

The back pressure adjustments was carried out by placing a straight cascade at various positions downstream. Picture No.34 shows the position of the axiliary cascade downstream, it consists of four straight blades made of 1 inch wide copper. Due to position of the auxiliary cascade, it is evident that the back pressure of the first cascade passage is the least and it increases at the second and still more at the last passage. It can be seen that there is no normal hydraulic jump in the first passage. The position of the normal hydraulic jump in the last passage is much nearer to the throat section then it is in the second passage. The normal hydraulic jump in both passages showed being very stable in position.

Picture No.35 shows that only back pressure control to the last passage was applied, and only in the last passage the normal hydraulic jump appeared.

Hence it can be concluded that the normal compression shock in the diverging part of the supersonic cascade is stable, its position can be controlled by adjustment of pressure downstream. Increase in back pressure causes the normal shock to move upstream .

Picture No. 20 to No.25 show the cascade in the position making an angle of attack of -5^{o} with the flow direction upstream, at various free stream Mach Numbers. The pictures show that the condition of flow entering cascade is entirely controlled by the first blade. Through the first blade,flow is directed entering the cascade with zero angle of attack. The identical flow patterns, the parallel Mach waves originating from the following blades leaves no doubt in this conclusion. It coincides with the theoretical analysis: after flow passed the first blade,it is accelerated through a 5 degree turning into the direction of zero angle of attack to the cascade, the expansion waves originating from the tip of the first blade, which govern the flow condition downstream,follow the isentropic flow around a corner pattern. In the case of supersonic stator of compressor, it is hard to see how the same situation could happen. There is no first blade to begin with at the stator. Presumably it is more logical to assume that an isentropic uniform expansion of flow takes place so that it enters the stator with zero angle of attack and increased Mach Number due to enlarged flow area.

Picture No. 26 to No.28 show the position of the cascade making an angle of attack of $+5^{o}$ with the free stream. The pictures show that an oblique compression

wave takes place at the leading edge of the first blade, the wave originating from the blades following are all parallel. There seems no doubt that the flow condition entering cascade is entirely controlled by the first blade. The flow conditions follow the oblique shock relation where the wedge angle is equal to the angle of attack. The results observed coincides with the theoretical analysis for the designed cascade. But it is difficult to apply the phenomenen to the stator ,since there is no first stator to begin. However, an assumption that flow is deflected uniformly with zero angle of attack entering stator associated with an energy loss equivalent to that of an oblique shock at the same wedge angle , seems to be logical.

Apply the conclusions reached to the analysis of flow characteristics in chapter III, it may be concluded that the flow characteristic at mass flow rates below the design condition will probably follow the results as analyzed. At flow rates exceeded the design condition, an assumption of energy loss of flow as described may be made in calculating the characteristic.

8. Starting Conditions

The flow patterns observed during starting conditions of the cascade were different from that of diffusers. There was no 'spill' of flow.

Bow wave system attached to the cascade was observed when flow upstream reached transonic region. The bow waves extended themselves as the flow velocity upstream was increased. But they were always attached to the cascade, once formed.

Picture No. 13 shows the bow wave system developed to a large arc attached to the cascade tip. The velocity upstream was a little above the velocity of sound.

When the velocity of free stream was further increased, the bow wave leg on the free stream side of the cascade tips disappeared. The bow wave leg on the cascade side extended itself near the wall of the adjacent blade. It is shown in Picture No.14.

The bow wave system thus observed seemes to serve as a starting mechanism of the cascade at transonic region so that no 'spill' of flow occured. The phenomenen may be explained as follows:

As the flow velocity upstream reached the transonic region, flow velocity at throat of cascade had reached sonic velocity. The fact that mass flow per unit area there reached its maximum caused the bow wave system

at cascade tips. Flow became subsonic after the bow waves, hence the flow condition approaching the projection area was partially supersonic and subsonic as illustrated in Fig(41). But became entirely subsonic after passing all bow waves. Hence the cascade acted as a laval nozzle; subsonic velocity upstream of the throat, sonic throat, and supersonic stream after the throat. This also helps to explain why the bow waves were always attached to the cascade. Namely the throat of cascade was always sonic once bow waves were formed, hence the flow condition downstream of the throat was always supersonic. For this reason disturbance downstream could not effect the flow conditions upstream, unless the back pressure downstream is increased so high that can force a normal compression shock to form downstream and push it passing the throat. Therefore as long as the flow conditions upstream will permit the bow wave system to pass the mass flow through the throat, it remains attached to the cascade.

In the case of an isolated body, bow wave is caused by the same reason. A convex point on the boundary of the isolated boby and a free stream form a temperary sonic throat. But this temperary laval nozzle is very unstable, since that a slight disturbace from free stream will destroy its existence, as shown in Fig(40). Hence the bow wave can be pushed indefinitely ahead the body.

Due to asymmetry of the cascade tips, the bow wave legs cannot be symmetrical. Also the bow wave leg on the curved tip side exists longer than on the flat side as the flow upstream is accelerated. Picture No.14 shows very clearly that on the flat side the bow wave disappeared, a Mach wave took place. The bow wave on the curved tip side extended reaching the wall. The flow conditions near the wall there were probably close to that of acrossing a normal compression shock, as illustrated in Fig (42). Further increase of flow Mach Number ended the bow wave system. It cannot exist to fulfill the mechanism between the upstream condition and the sonic throat condition downstream, excess fluid began to accumulate on the flat wall due to pressure gradient,as shown in pictures No.15 to No.18. It was first suspected as 'spill' of flow, and powder method was used to detect the streamlines of flow. The pictures show that all streamlines went through the cascade, which proved that no 'spill' of flow happened.

To explain the flow patterns, a fork shock system is illustrated in Fig(43). Following that bow wave reached the wall, excess fluid begin to be pushed back and accumulate on the flat wall due to the fact that throat already reached sonic velocity. Hence the dead fluid there cause formation of the fork shock. Since that pressure ratio across the fork shock must be the same everywhere

along the fork shock, hence it will probanly take curved form due to curvature of blade entrance. For the same reason the branch point of the fork must be at the blade tip. The first branch of the fork shock is a weak oblique shock due to angle of dead fluid at the wall, the second branch is a strong oblique shock, hence flow downstream is subsonic. Flow then is accelerated to sonic velocity at the throat. Similar to the bow wave system the fork shock system is also controlled by the flow conditions upstream and sonic condition at throat. Or in other words the fork shock system adjusts itself according to the supersonic condition of free stream and the sonic condition downstream at the cascade throat.

Detailed analysis of fork shock itself is beyond the scope of this study. However useful informations may be found from the studies done by Weise[5] and Eggink[6].

Although that fork shock system was not observed clearly at diffuser experiments, it is conceivable that fork shocks at blade tips could happen. At transonic region bow waves attached to the blade tips extend themselves as the Mach Number of flow upstream is increased. When both bow waves reach each onther, the flow pattern in the middle of the diffuser resembles a normal compression shock. It then branches into two fork shocks near

the diffuser walls. Similar as the cascade, the throat of diffuser had reached sonic velocity condition and remained so ever since the begin of bow waves. Further increase of flow Mach Number upstream causes fluid to come out of the diffuser. But unlike the cascade, since there is no place to let the dead fluid accumulate to continue fork shock mechanism, the diffuser 'spills'.

The flow pattern of fork shock system at the cascade disappeared as flow upstream was accelerated to the design condition of the cascade. Supersonic flow entering cascade through the throat was immediately established after that. The process was too quick to be observed during the experiment, but there is little doubt that the establishment of supersonic flow was following a normal compression shock formed at entrance and then moved passing the throat.

Hence summarized, the starting mechanism of the cascade at transonic condition is established by attached bow wave system, Before the flow is accelerated to the design condition, the starting mechanism is established by fork shock system. When flow velocity reaches the design condition, supersonic flow in the entire cascade is established after formation of a normal compression shock at cascade entrance. The flow conditions at cascade throat are always sonic before flow upstream

of the cascade is accelerated from transonic region to the design condition. During that period flow conditions from entrance region to the throat are always subsonic, and flow conditions downstream of the throat supersonic.

Depth measurements were also made to examine the starting mechanisms. The depth measurements made at transonic conditions were later proved unreliable, hence they are not presented. But the results obtained at Mach Number of undisturbed flow equal to 1.56 showed good agreement with the theory.

Fig(39) shows the points where depth measurements were made. The results at upstream Mach Number M = 1.56 are presented in Table(XIX) and plotted in Fig(44). The stagnation water height of undisturbed flow was measured by a pitot-tube. Sinee that the stagnation height decreases after any kind of hydraulic jump, hence the critical water depth of the undisturbed flow serves as a measure to judge the 'subsonic' conditions.

The 'sonic' condition at throat,station(10), is judged by the 'subsonic' condition upstream and the decreasing water height downstream.

The gradual increase of water height before the cascade entrance, station(6), indicates a weak oblique hydraulic jump. The height of water across any hydraulic

jump does not increase suddenly as it is supposed to theoretically. The slope of hydraulic jump only increases as the intensity of hydraulic jump increases, but it never reaches 90^{o} even at normal hydraulic jumps at high Mach Numbers.

The high water depth between stations (6) and (7) indicates that flow there passed a strong hydraulic jump and became 'subsonic'. It corresponds to the strong oblique shock assumed in Fig(43).

The continuity of flow was also detected by the results of depth measurements. By assuming constant stagnation water height, the mass flow calculated showed that it increases towards the cascade entrance. This is of cause not possible. But on the other hand it proved that the stagnation water height decreases towards the entrance and that a hydraulic jump existed. Also it is possible that mass flow remained constant. The latter was positively proved by the powder method experiments.

At the design condition, flow pattern at cascade entrance region follows almost exactly as it had been expected in design. Picture No.19 shows the close up picture of taken with direct lighting method. Except that the intercepting lines caused by boundary layer on the wall which were not considered in design, the pattern of compression waves coincides exactly with the design.

The wave angle of the first compression wave measures at exactly 30 degree and that of the last compression wave is measured at 40 degree.

The control of normal hydraulic jump at various positions downstream of the throat by back pressure adjustments was already mentioned. It concludes that normal compression shock can also be controlled similarily.

Depth measurements of flow at the design condition with a controlled normal hydraulic jump downstream of throat are presented in Table (xx) and plotted in Fig(45). It shows good agreement with theory.

9. Summary and Conclusions

The interpretations of the hydraulic experimental results bring about following theories about supersonic diffusers and the proposed supersonic cascade for stator design:

The capitalized "Curve" and "Flat" will be used to refer to the curved and the flat side of blade tip respectively, and the captalized "Wall" will be used to denote the flat blade part opposite to the tip of the adjacent blade.

a. When flow angle approaching the cascade, measured from plane of rotor, is smaller than the stagger angle of the cascade, flow pattern around the tip of the leading cascade blade follows that of isentropic flow expansion around a corner,which governs the flow entering cascade with zero angle of attack at a higher Mach Number. In the case of compressor stator, the flow assumes uniform isentropic expansion due to increase in flow area. The same flow condition entering stator as in the case of a cascade results.

b. When flow angle approaching the cascade, measured from plane of rotor, is larger than the stagger angle of the cascade, flow pattern at the tip of the leading cascade blade follows that of an oblique shock due to a wedge angle equal to the difference of the

flow angle and the stagger angle of the cascade, which governs the flow entering the cascade at a lower Mach Number at zero angle of attack, but with an energy loss. In the case of compressor stator, flow assumes an uniform compression due to decrease in flow area with an energy loss. It results in the same flow condition entering stator as entering the cascade.

c. Applying the above conclusions to the analysis of flow characteristics in chapter III with straight stator of infinitesimal blade thickness; The flow characteristics at flow rates below the design condition,remain the same as the analysis. The lower limit is set by the stall condition of the subsonic rotor. At flow rates surpassed design condition, flow encounters energy loss before entering stator. Hence the compression ratio and thermal efficiency will probably be lower than calculated,although that the enery loss of normal compression shock assumed at stator entrance will be lower due to lower Mach Number entering stator. The maximum flow condition is determined by the sonic condition at rotor exit, or to be more exact, when the relative velocity leaving rotor reaches local velocity of sound.

d. In a compressor of constant circulation as discussed in chapter IV, assuming straight stator

blades with infinitesimal thickness, the relative velocity of flow leaving rotor at blade root already reaches local velocity of sound at design condition. Therefore at further increase of flow ,choking will start at the blade root. Flow can no more remain radial equilibrium, hence then the assumption of two-dimensional flow is no more valid. Therefore the flow characteristics after flow surpassed the design condition cannot be calculated as in the one-radius analysis. What happens then will be probably sharp drop in both compression ratio and thermal efficiency of compressor until it is completely choked. At flow rate below the design condition the flow characteristics will probably resembleng that in one-radius analysis.

e. From conclusions a. and b., the starting conditions of the supersonic cascade and supersonic compressor can thus be concluded from flow conditions with zero angle of attack to the cascade. The blades in consideration are no more straight or of infinitesimal thickness. They construct converging-diverging passages as designed in chapter V. When the undisturbed flow reaches transonic condition, the mechanism of starting is established by attached bow wave system. Before flow is accelerated to the design Mach Number, the starting mechanism is a fork shock system at entrance. When the

design condition of undisturbed flow is reached, establishment of supersonic flow in stator is preceeded by a normal compression shock at stator entrance. From the beginning of bow wave system till the establishment of supersonic flow in the entire stator, flow conditions upstream of the throat remains subsonic, throat conditions sonic, and supersonic downstream of the throat. Normal compression shock can be controlled downstream near the throat with back pressure adjustments. The contraction of stator passage is determined by the limiting contraction ratio for the design operating condition.

f. The starting mechanism for the diffusers at the transonic region is established by bow waves originating from diffuser tips and attached to the tips. As the Mach Number of undisturbed flow is further increased, the bow wave legs extend and join togeather at middle of the diffuser resembling a normal compression shock. It then branched into fork shocks towards diffuser tips. Further increase of Mach Number of undisturbed flow, results in 'spill' condition of diffusers. It continues until the design condition is reached, then supersonic sonic flow in diffuser is established following a normal compression shock at diffuser entrance.

g. Detached bow waves at flow about an isolated body do not happen to cascade or diffusers. attached bow waves follow the establishment of sonic

velocity of the throat of passage.

h. The flow characteristics of constant circulation compressor with contracted stator design resembles that in discussion of section d.

APPENDIX

I. PHOTOGRAPHS OF THE SUPERSONIC DIFFUSER TIPS AND CASCADE

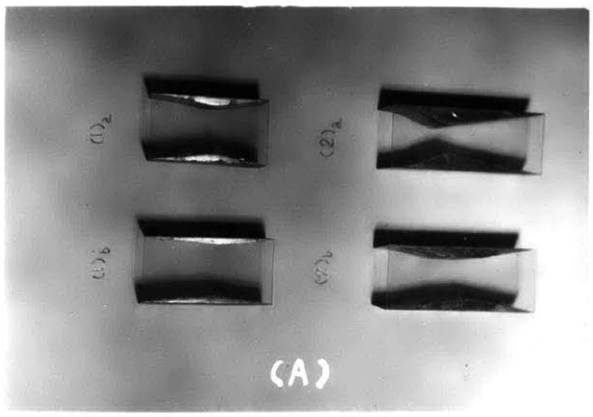
(1)
(2)
(3)
(4)
(A)

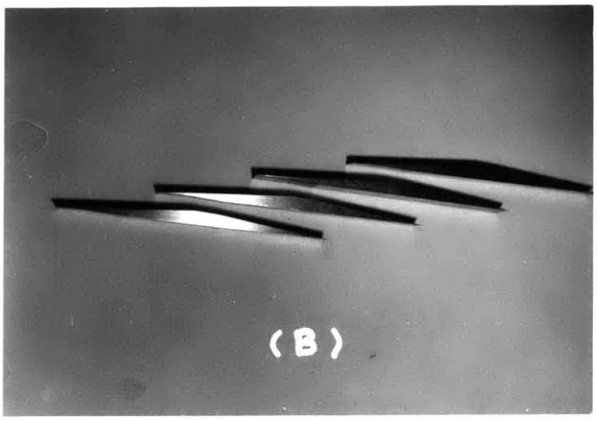
(B)

II. PHOTOGRAPHIC RESULTS OF THE EXPERIMENT ON SUPERSONIC DIFFUSERS

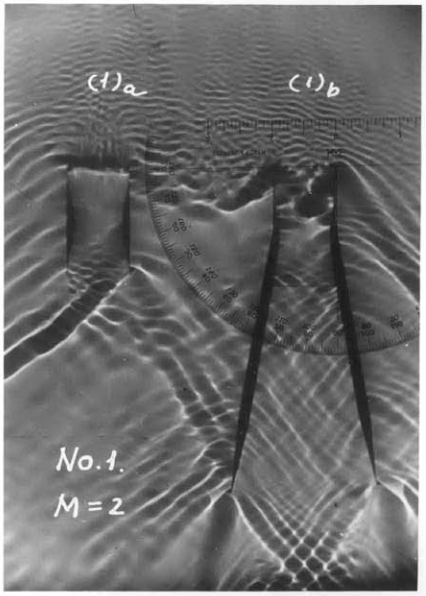
(1)a
(1)b
No.1.
M=2

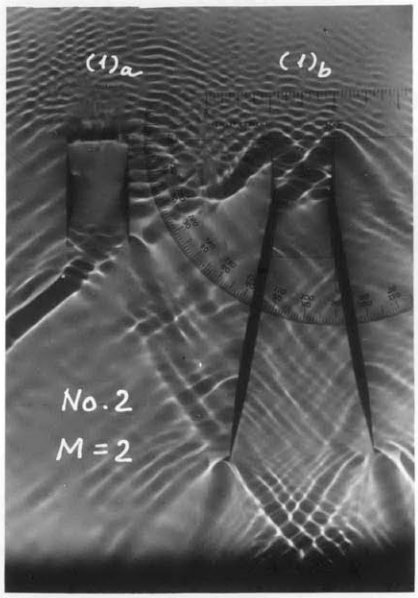
(1)a
(1)b
No.2
M=2

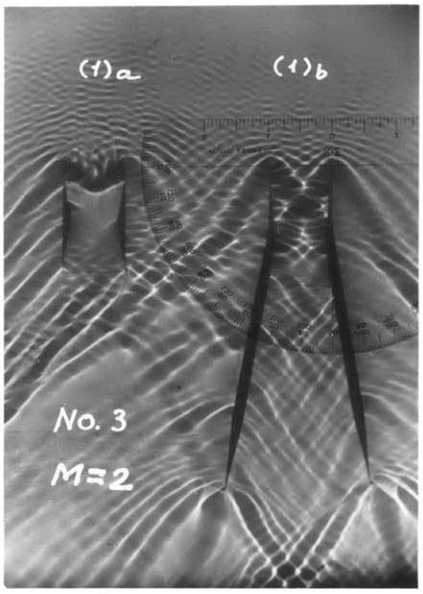
(1)a
(1)b
No. 3
M=2

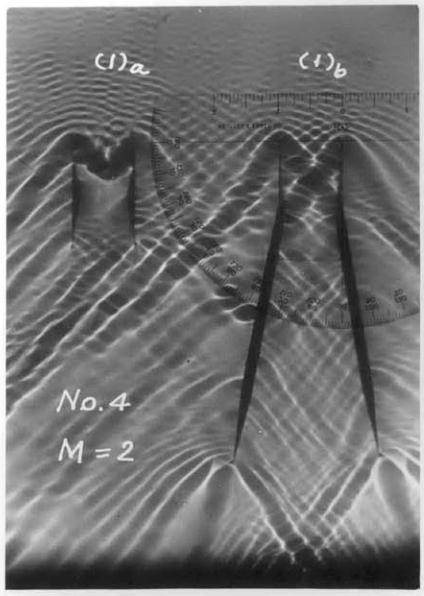
(1)a
(1)b
No.4
M=2

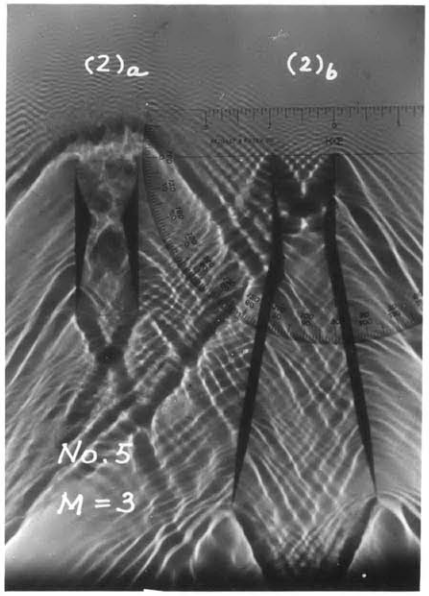
(2)a
(2)b
No.5
M = 3

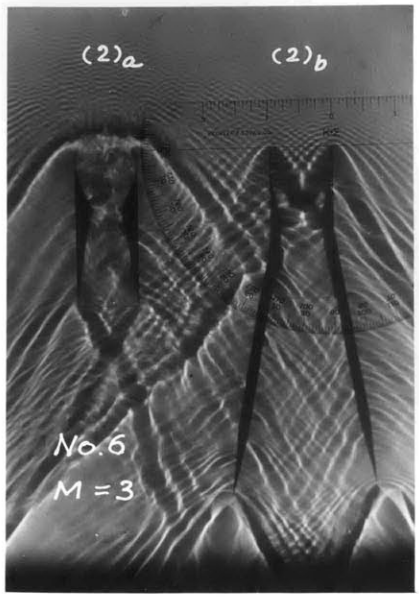
(2)a
(2)b
No.6
M = 3


(2)a
(2)b
No.7
M=3

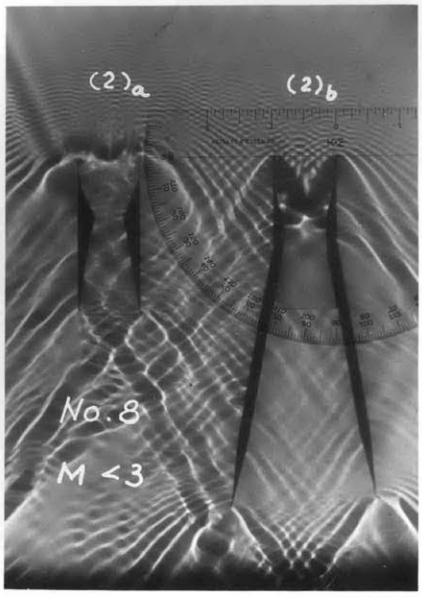
(2)a
(2)b
No.8
M <3

III. PHOTOGRAPHIC RESULTS OF THE EXPERIMENT ON SUPERSONIC CASCADE

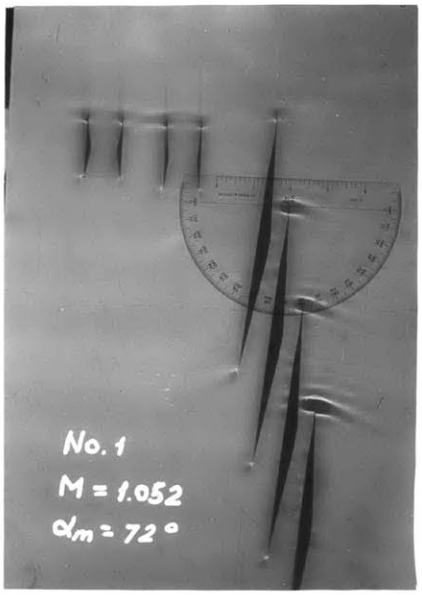
No. 1
M = 1.052
α_m = 72°

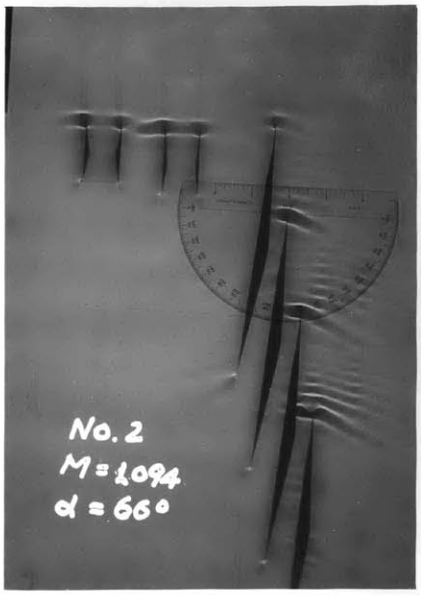
No. 2
M = 1.094
α = 66°

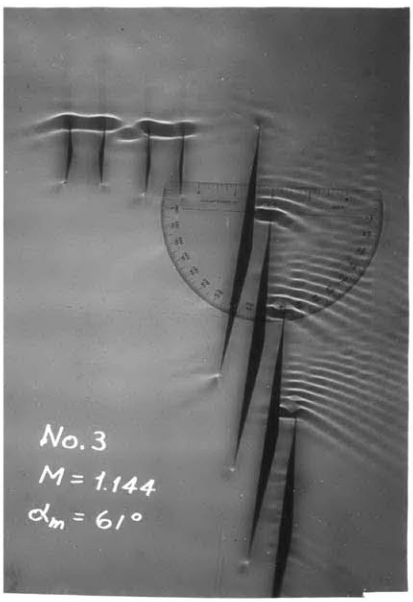
No. 3
M = 1.144
α_m = 61°

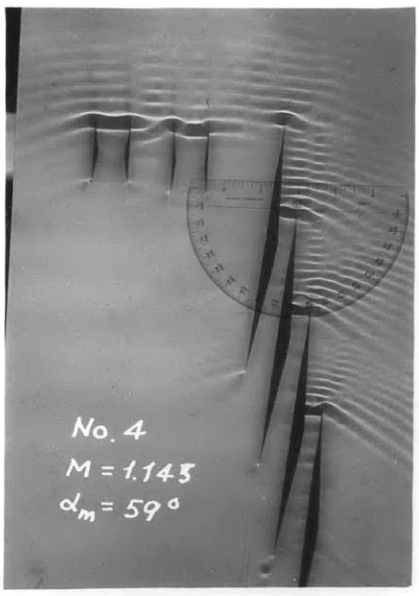
No. 4
M = 1.145
α_m = 59°

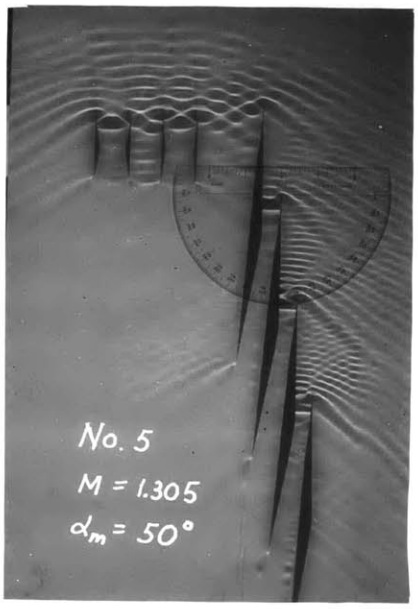
No. 5
M = 1.305
α_m = 50°

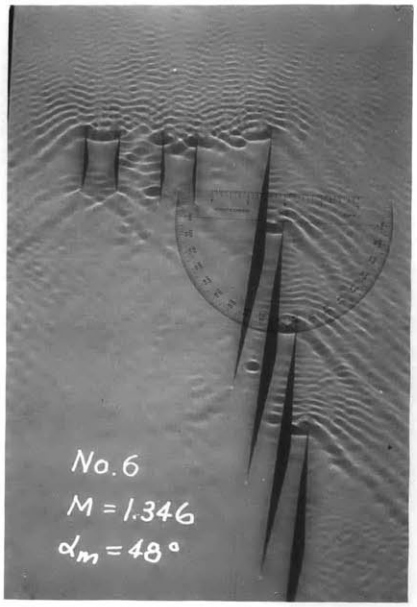
No. 6
M = 1.346
α_m = 48°

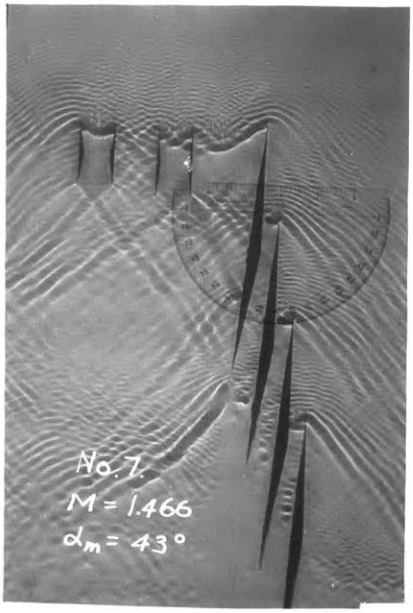
No. 7
M = 1.466
α_m = 43°

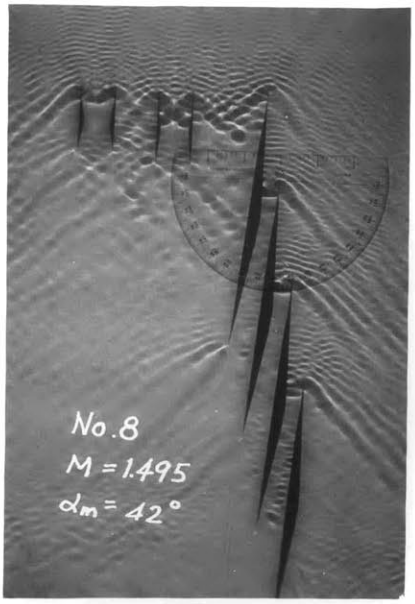
No. 8
M = 1.495
α_m = 42°

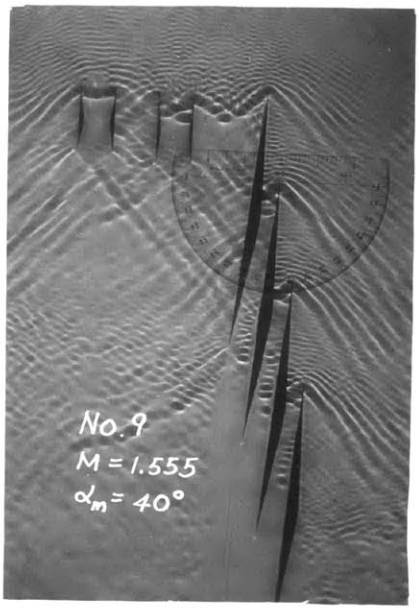
No. 9
M = 1.555
α_m = 40°


No. 10
M = 1.744
α_m = 35°

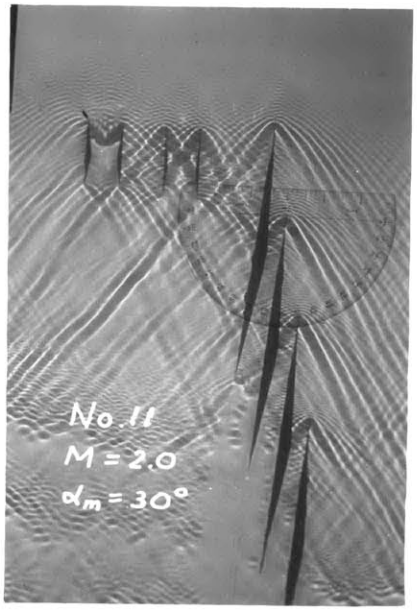
No. 11
M = 2.0
α_m = 30°

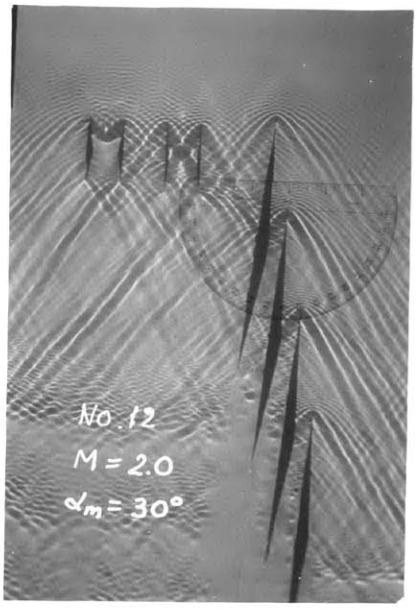
No. 12
M = 2.0
α_m = 30°

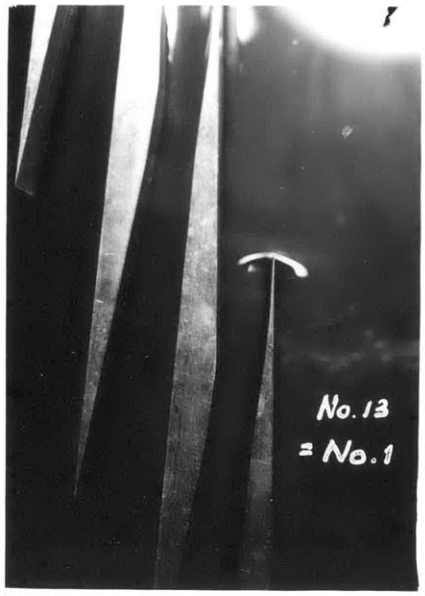
No. 13
= No. 1

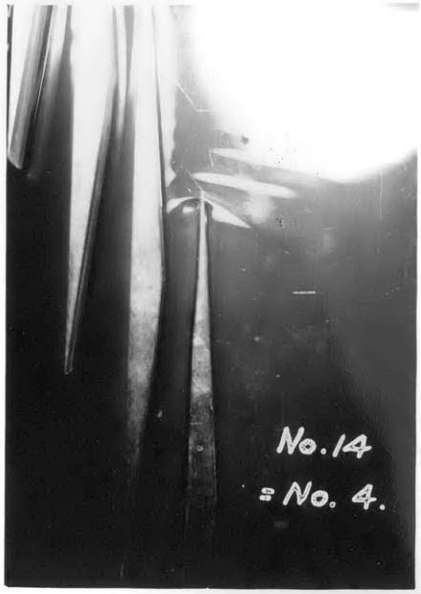
No. 14
= No. 4.


No. 15
= No. 5.


No. 16
= No. 6.


No.17
= No.7


No.18
= No.9

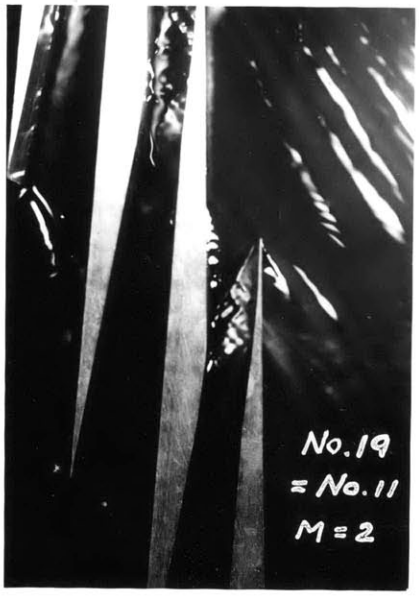
No.19
= No.11
M = 2

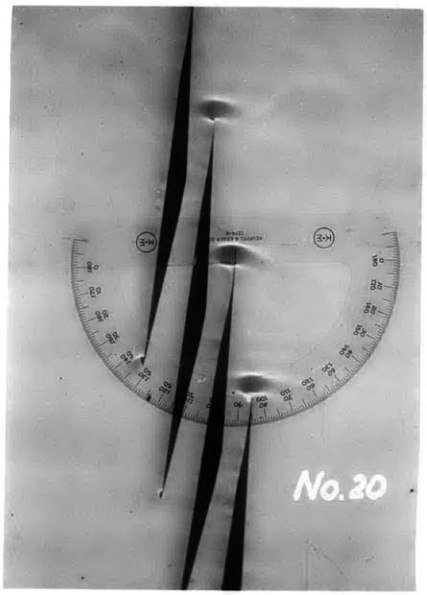
No.20

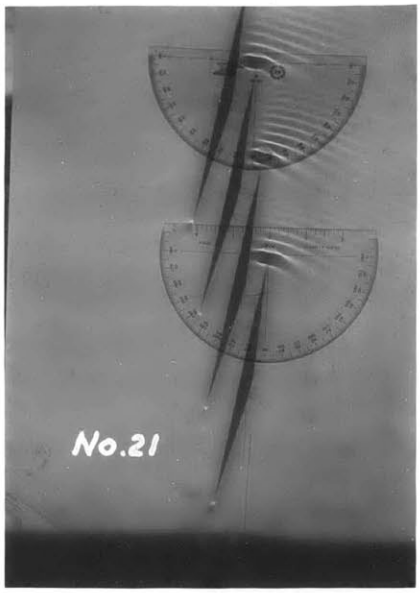
No.21

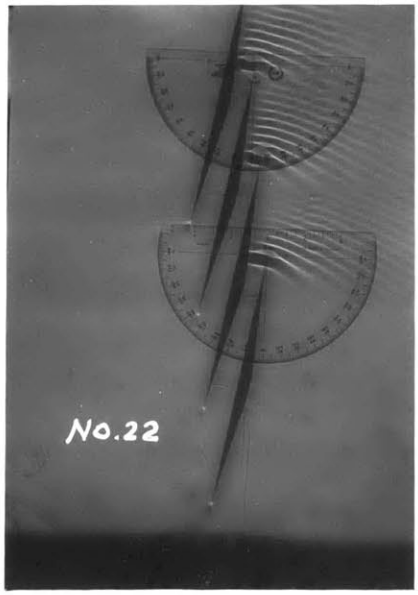
No.22

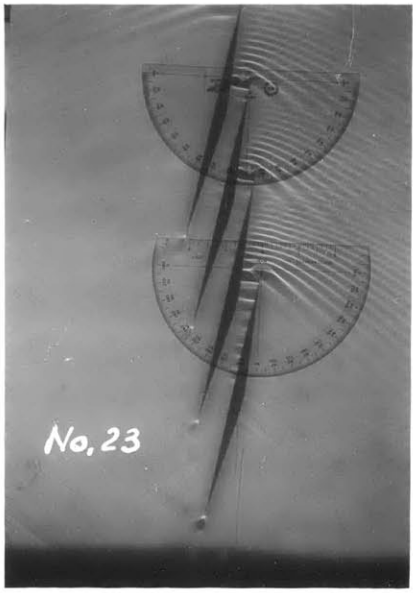
No, 23

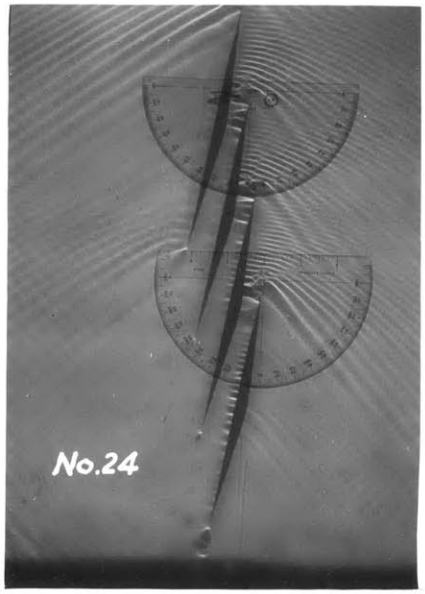
No.24

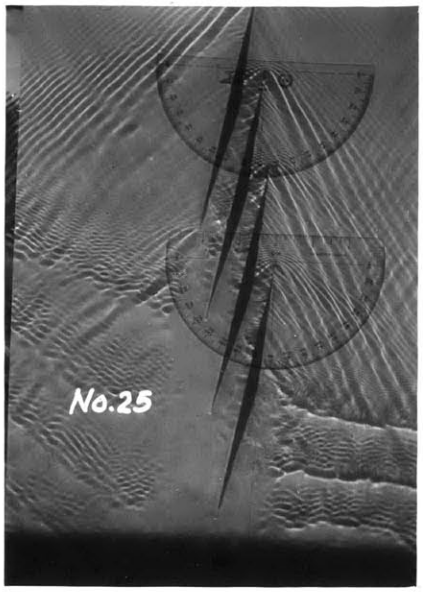
No.25

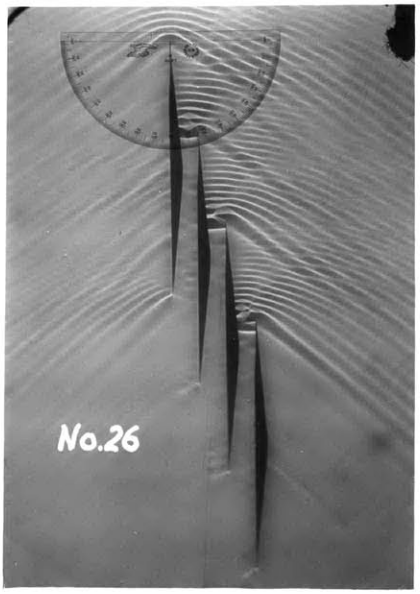
No.26

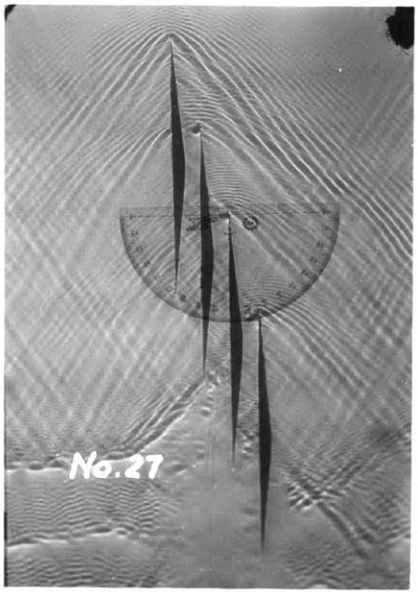
No.27

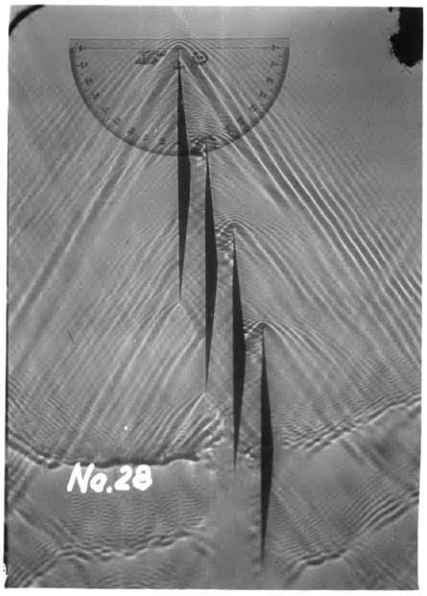
No.28

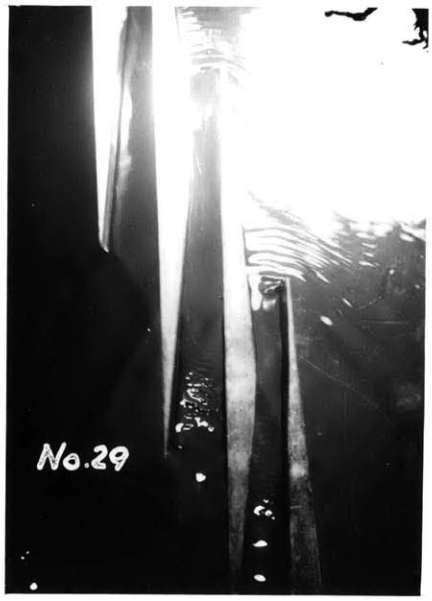
No.29


No.30


No.31


No.32
$\alpha_m = 40°$


No. 33
$\alpha_m = 30°$


No. 34

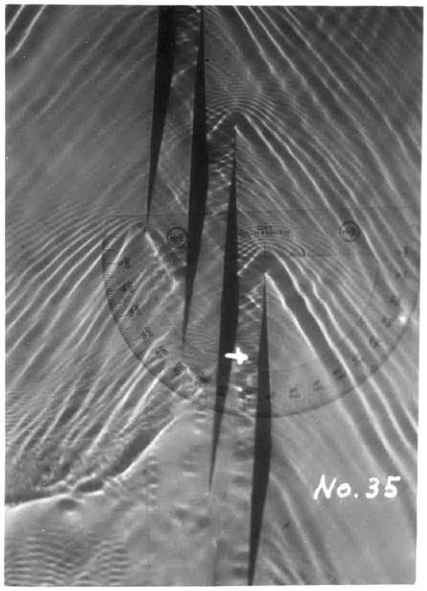
No. 35

IV. FIG(1) TO FIG(45)

Fig (1)

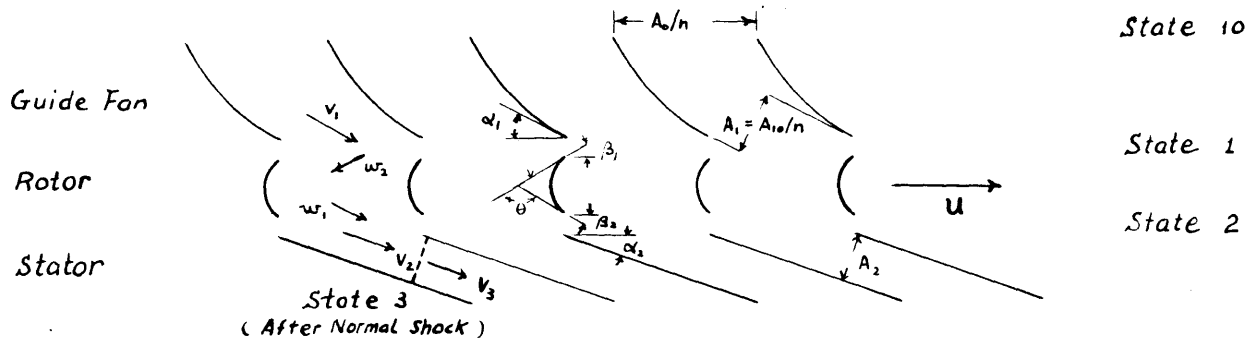

$\angle \alpha_1 = \angle \beta_1 = \angle \beta_2$

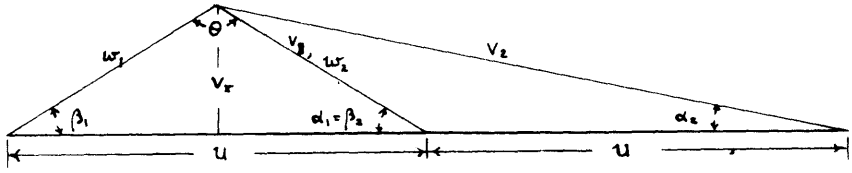

Fig $(1)_a$

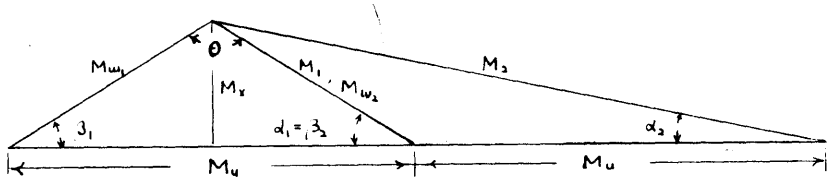

Fig $(1)_b$

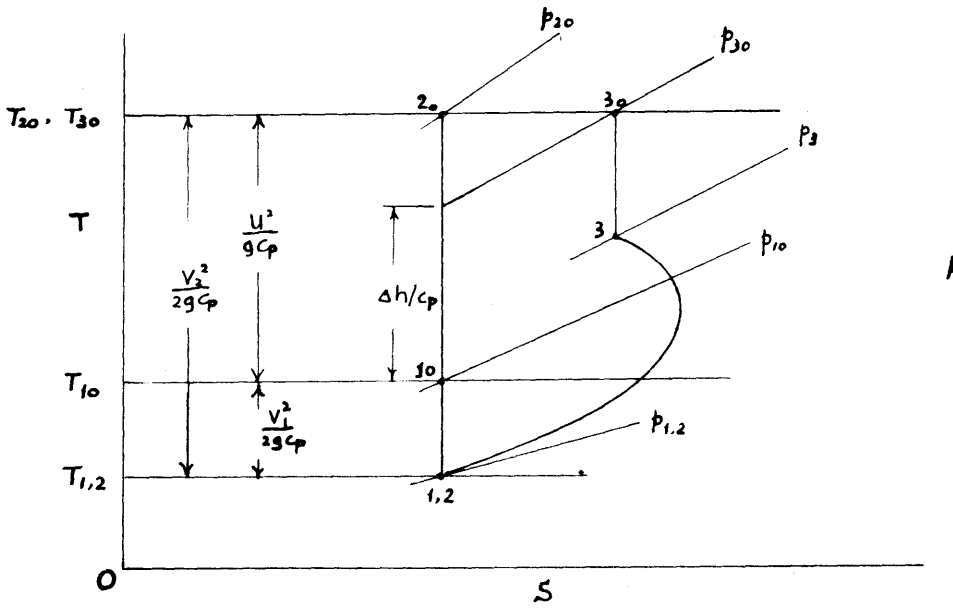

Fig $(1)_c$

Fig (2)

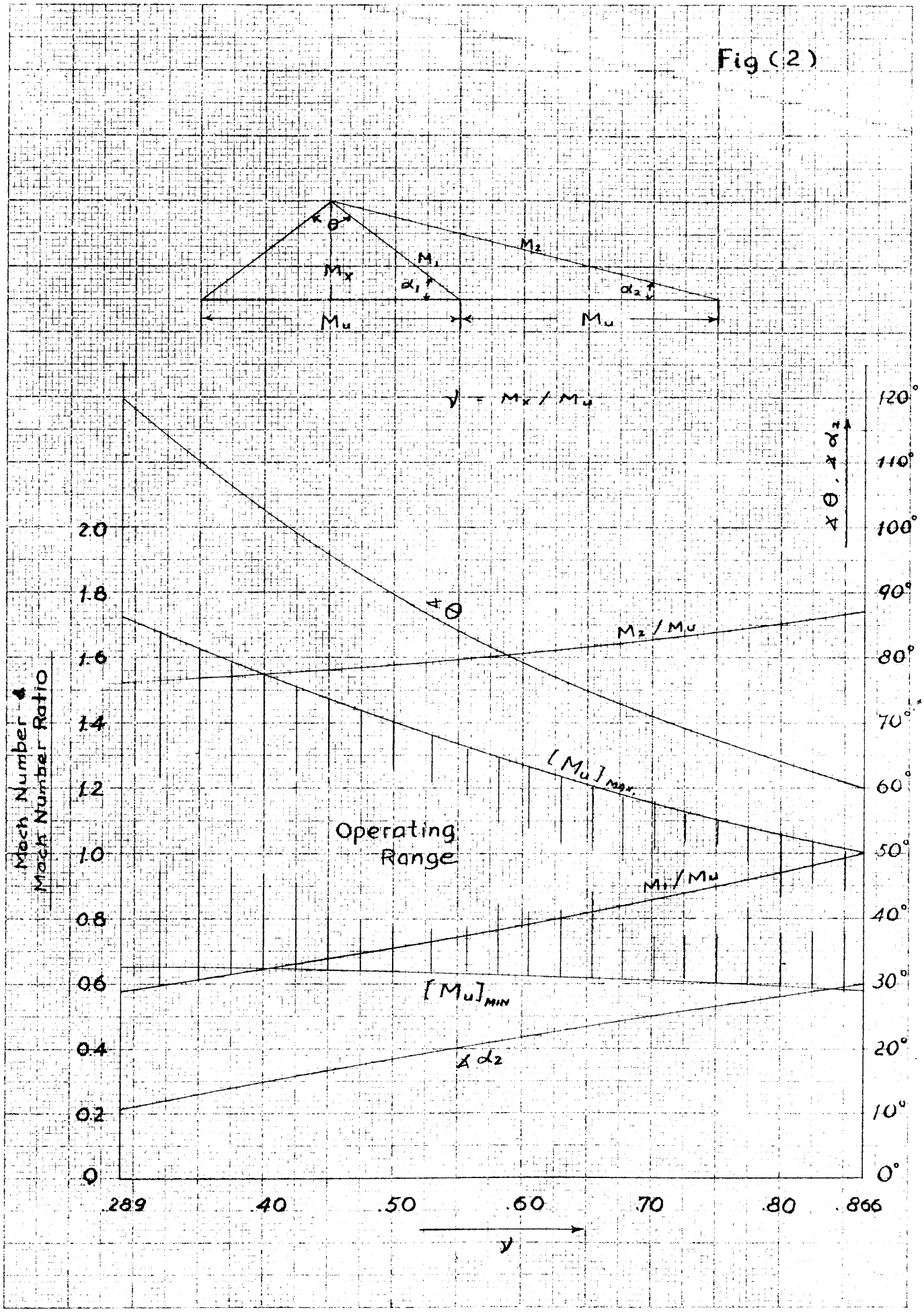
θ
M_x
M_1
M_2
α_1
α_2
M_u
M_u
$\nu = M_x / M_u$
$\angle\theta$
M_2/M_u
$[M_u]_{max.}$
Operating Range
M_1/M_u
$[M_u]_{MIN}$
$\angle\alpha_2$
$\angle\theta + \angle\alpha_2$
Mach Number ÷ Mach Number Ratio
2.0
1.8
1.6
1.4
1.2
1.0
0.8
0.6
0.4
0.2
0
120°
110°
100°
90°
80°
70°
60°
50°
40°
30°
20°
10°
0°
.289
.40
.50
.60
.70
.80
.866
ν

Fig (3)

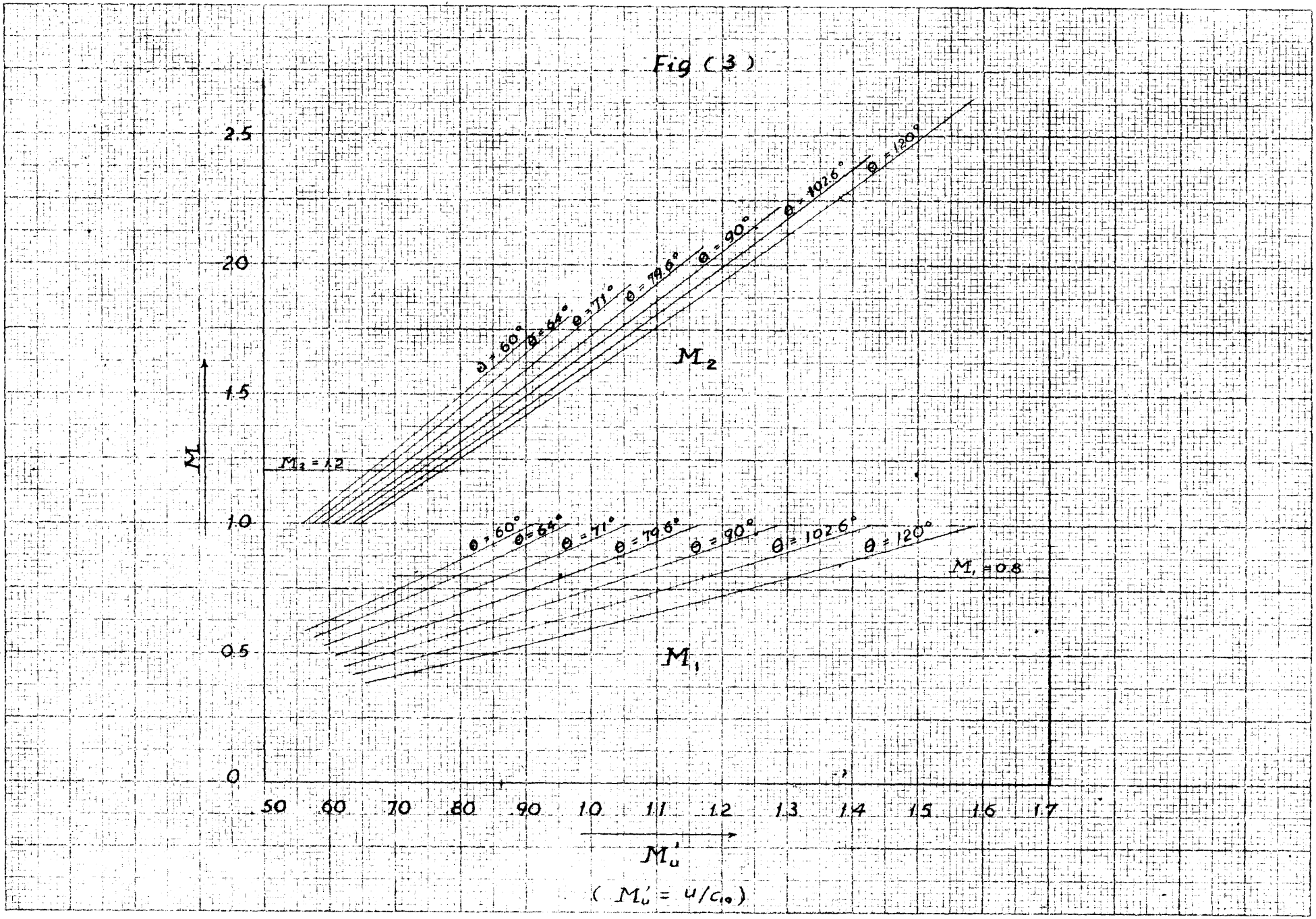
2.5
2.0
1.5
1.0
0.5
0
M
M_2
M_1
$M_2 = 1.2$
$M_1 = 0.8$
θ = 60°
θ = 64°
θ = 71°
θ = 79.6°
θ = 90°
θ = 102.6°
θ = 120°
.50 .60 .70 .80 .90 1.0 1.1 1.2 1.3 1.4 1.5 1.6 1.7
M_u'
($M_u' = u/c_{10}$)

Fig (4)

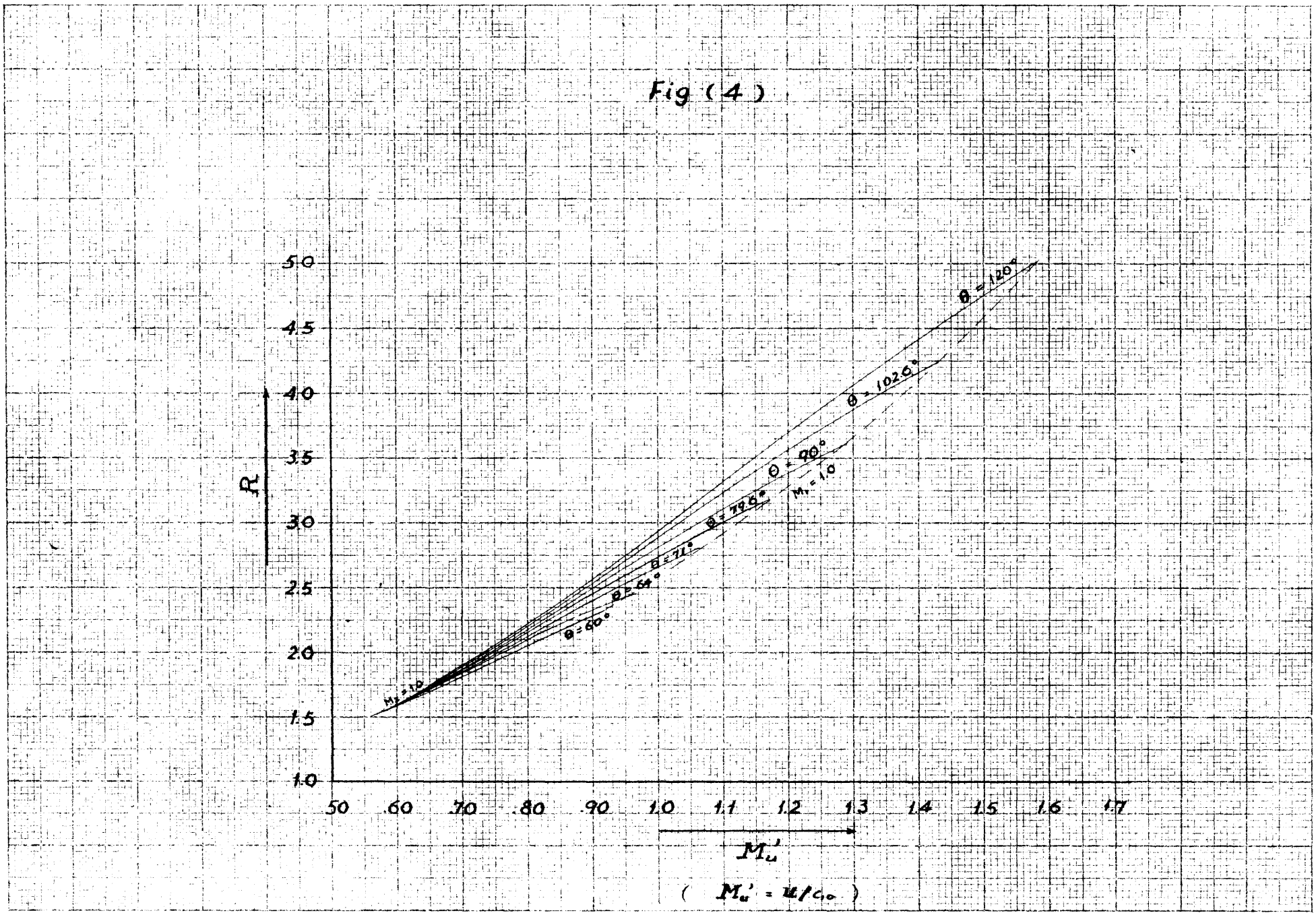
5.0
4.5
4.0
3.5
3.0
2.5
2.0
1.5
1.0
R
.50
.60
.70
.80
.90
1.0
1.1
1.2
1.3
1.4
1.5
1.6
1.7
M_u'
($M_u' = u/c_0$)
$M_1 = 1.0$
$\theta = 120°$
$\theta = 102.6°$
$\theta = 90°$
$\theta = 79.6°$
$\theta = 71°$
$\theta = 64°$
$\theta = 60°$

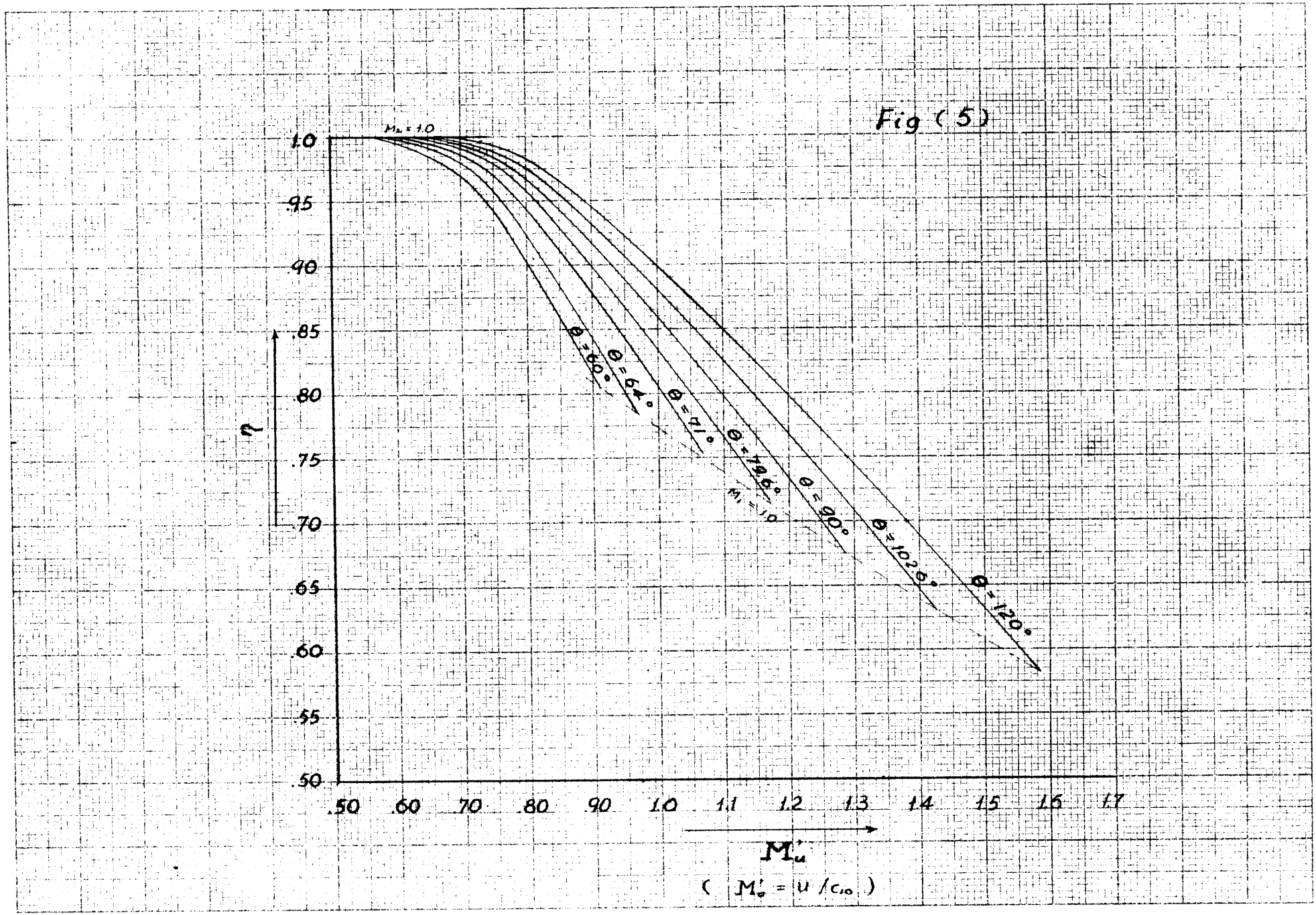
Fig (5)
$M_2 = 1.0$
1.0
.95
.90
.85
.80
.75
.70
.65
.60
.55
.50
η
$\theta = 60°$
$\theta = 64°$
$\theta = 71°$
$\theta = 79.6°$
$M_1 = 1.0$
$\theta = 90°$
$\theta = 102.6°$
$\theta = 120°$
.50 .60 .70 .80 .90 1.0 1.1 1.2 1.3 1.4 1.5 1.6 1.7
M_u'
($M_u' = u / c_{10}$)

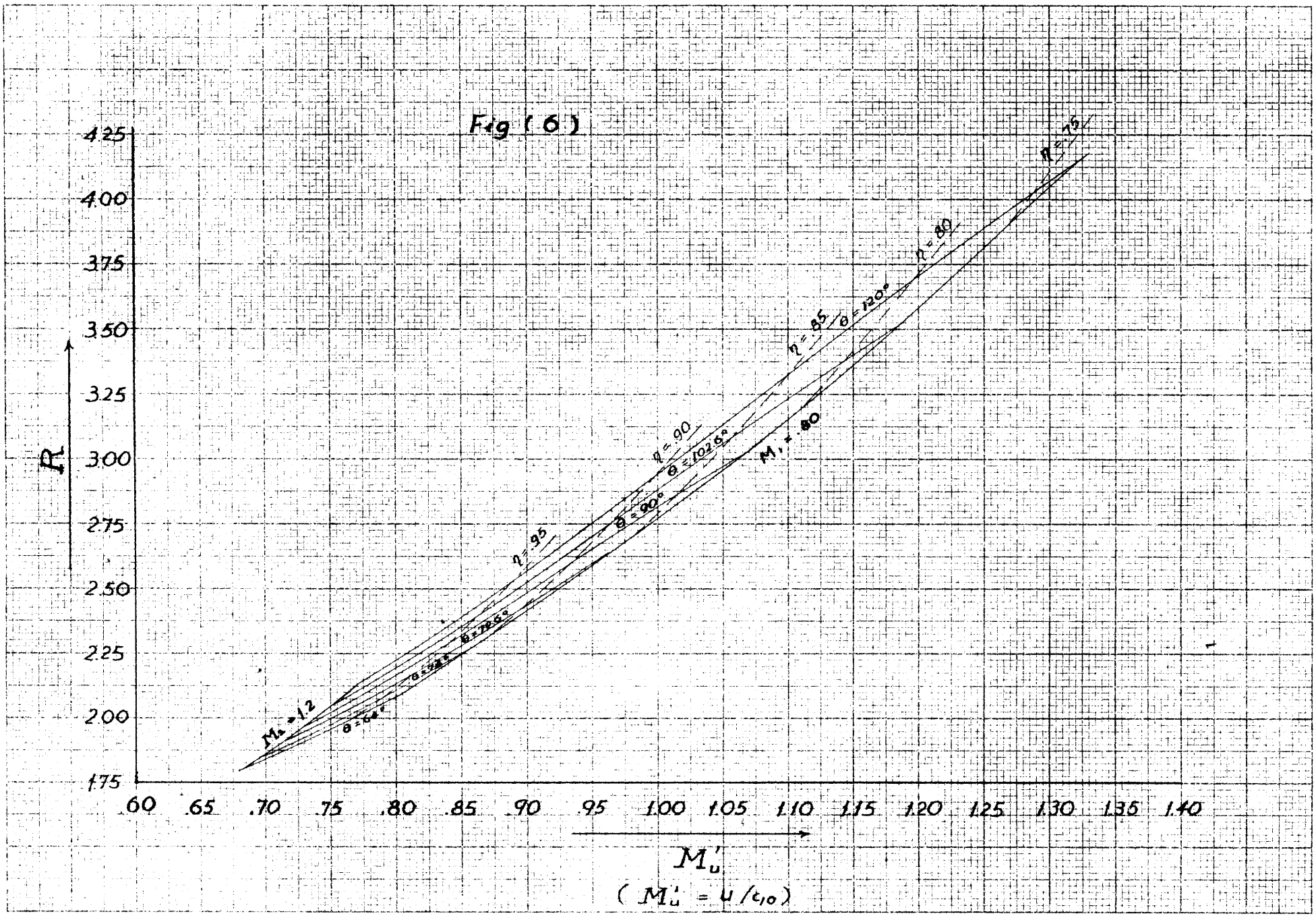
Fig (6)
4.25
4.00
3.75
3.50
3.25
3.00
2.75
2.50
2.25
2.00
1.75
R
.60
.65
.70
.75
.80
.85
.90
.95
1.00
1.05
1.10
1.15
1.20
1.25
1.30
1.35
1.40
M_u'
($M_u' = u/c_{10}$)
$M_1 = 1.2$
$M_1 = 1.50$
$\eta = 90$
$\eta = 95$
$\eta = 80$
$\eta = 85$
$\theta = 64°$
$\theta = 72.5°$
$\theta = 79.5°$
$\theta = 90°$
$\theta = 102.5°$
$\theta = 120°$

Fig (7)

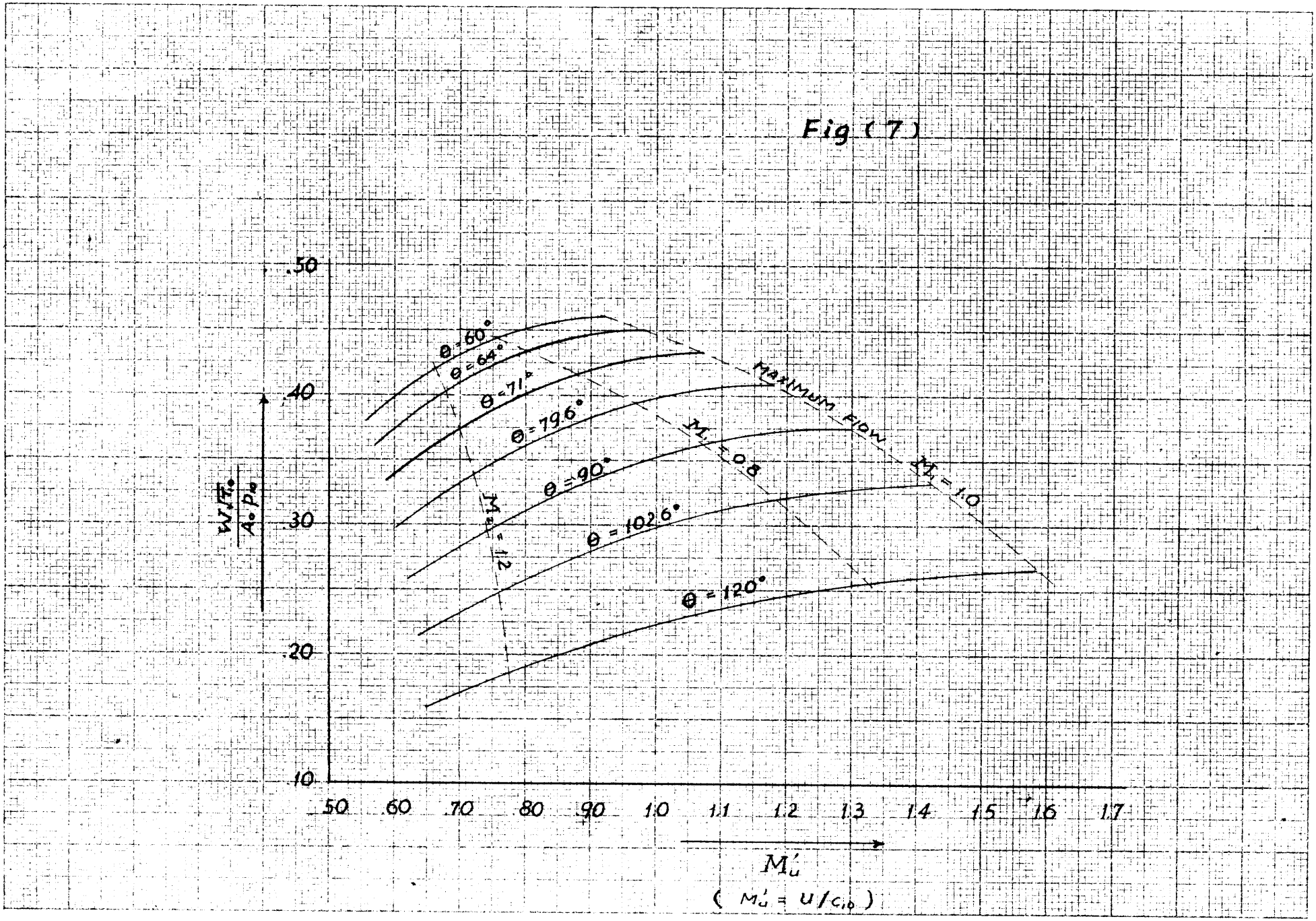
.50
.40
.30
.20
.10
$\frac{W\sqrt{T_0}}{A \cdot P_0}$
θ = 60°
θ = 64°
θ = 71°
θ = 79.6°
θ = 90°
θ = 102.6°
θ = 120°
MAXIMUM FLOW
$M_x = 0.8$
$M_x = 1.0$
$M_{cr} = 1.2$
.50 .60 .70 .80 .90 1.0 1.1 1.2 1.3 1.4 1.5 1.6 1.7
M'_u
($M'_u = U/c_{1_0}$)

Fig (8)

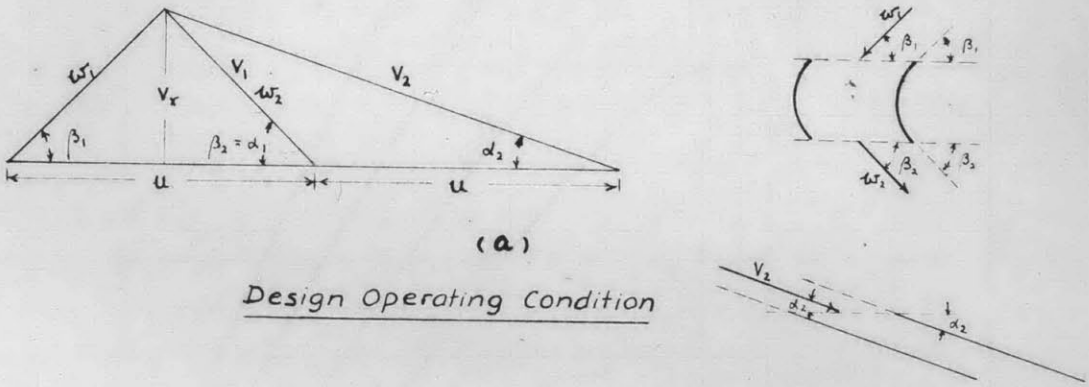

(a)

Design Operating Condition

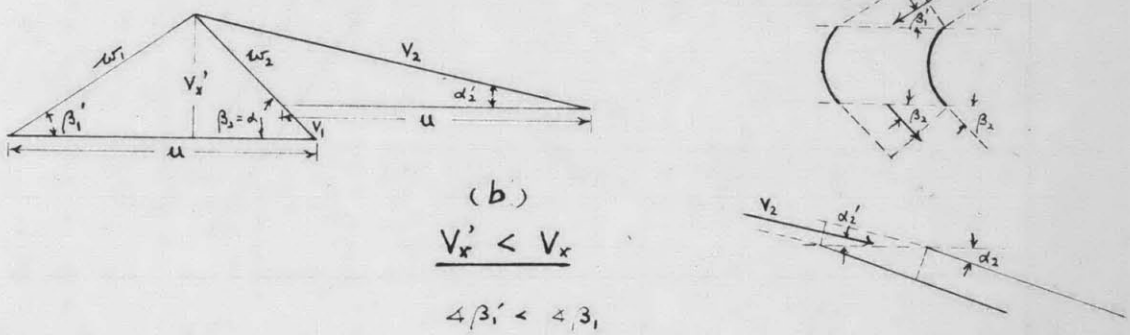

(b)

$V_x' < V_x$

$\angle \beta_1' < \angle \beta_1$

$\angle \alpha_2' < \angle \alpha_2$

u = const.

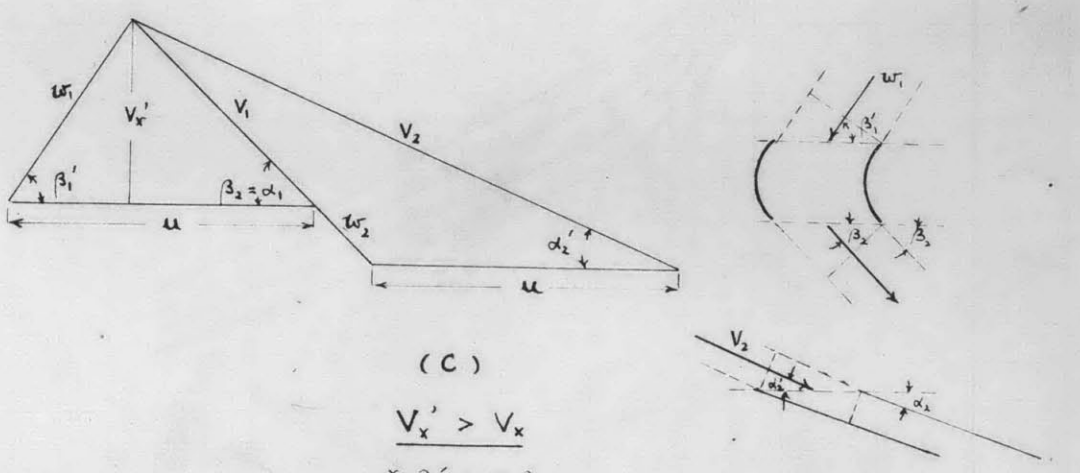

(C)

$V_x' > V_x$

$\angle \beta_1' > \angle \beta_1$

$\angle \alpha_2' > \angle \alpha_2$

u = const.

Fig (9)

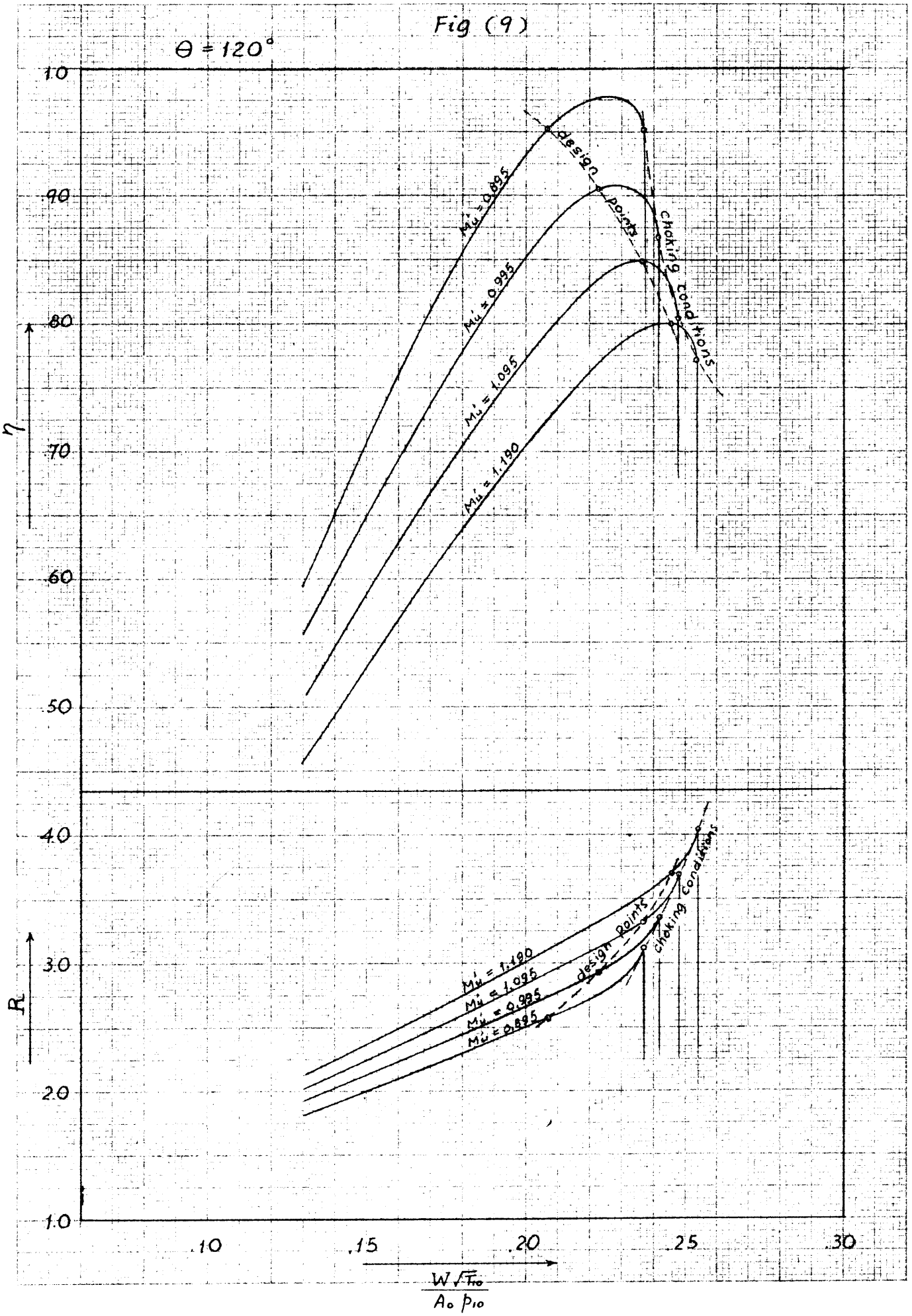
θ = 120°
η
1.0
.90
.80
.70
.60
.50
Design points
choking conditions
Mu' = 0.895
Mu' = 0.995
Mu' = 1.095
Mu' = 1.190
R
4.0
3.0
2.0
1.0
.10
.15
.20
.25
.30
W√T10 / A0 p10

Fig (10)

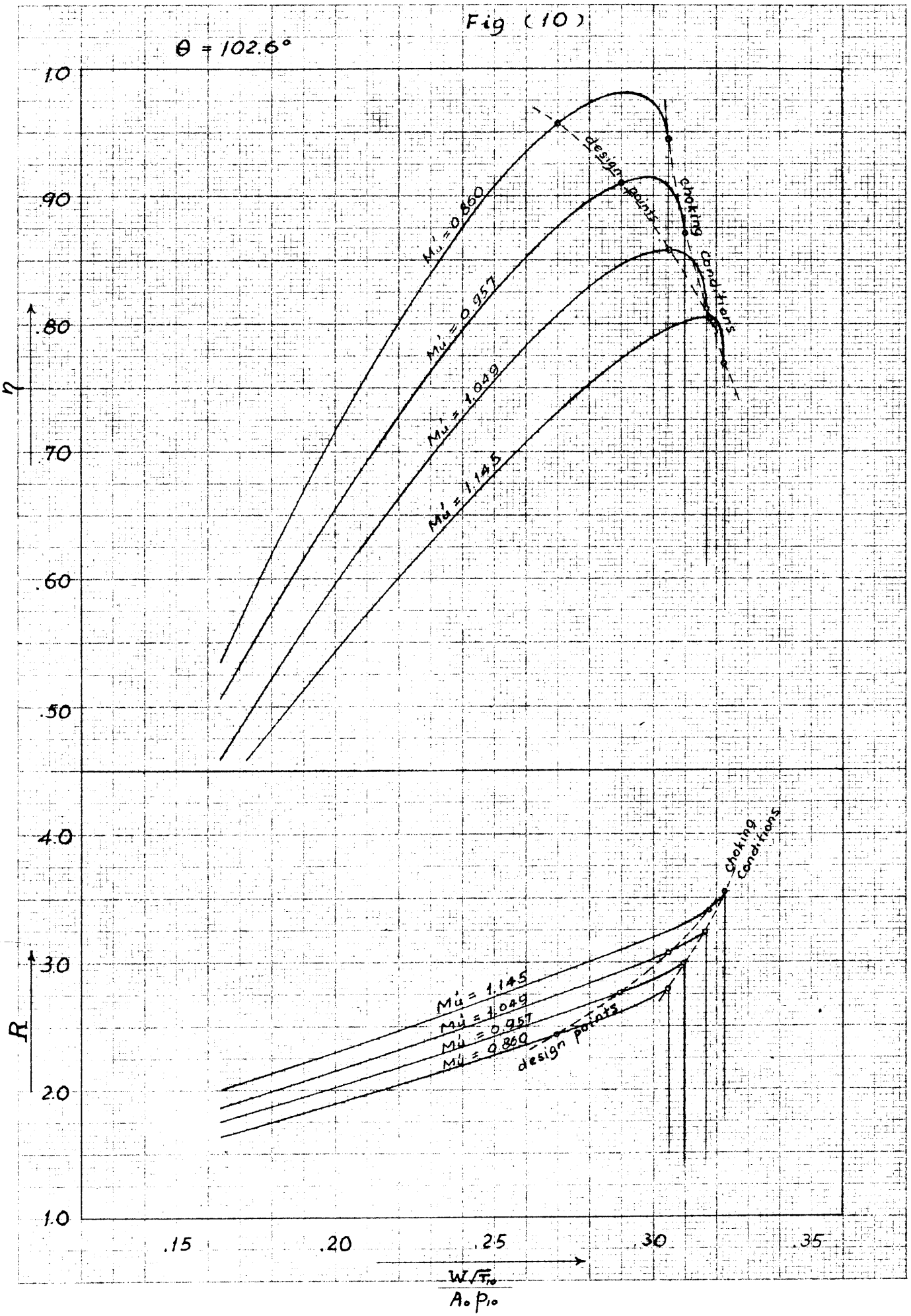
θ = 102.6°
1.0
.90
.80
.70
.60
.50
η
Mu' = 0.860
Mu' = 0.957
Mu' = 1.049
Mu' = 1.145
design points
choking conditions
4.0
3.0
2.0
1.0
R
Mu' = 1.145
Mu' = 1.049
Mu' = 0.957
Mu' = 0.860
design points
choking conditions
.15
.20
.25
.30
.35
W√T₀ / A₀ P₀

Fig (11)

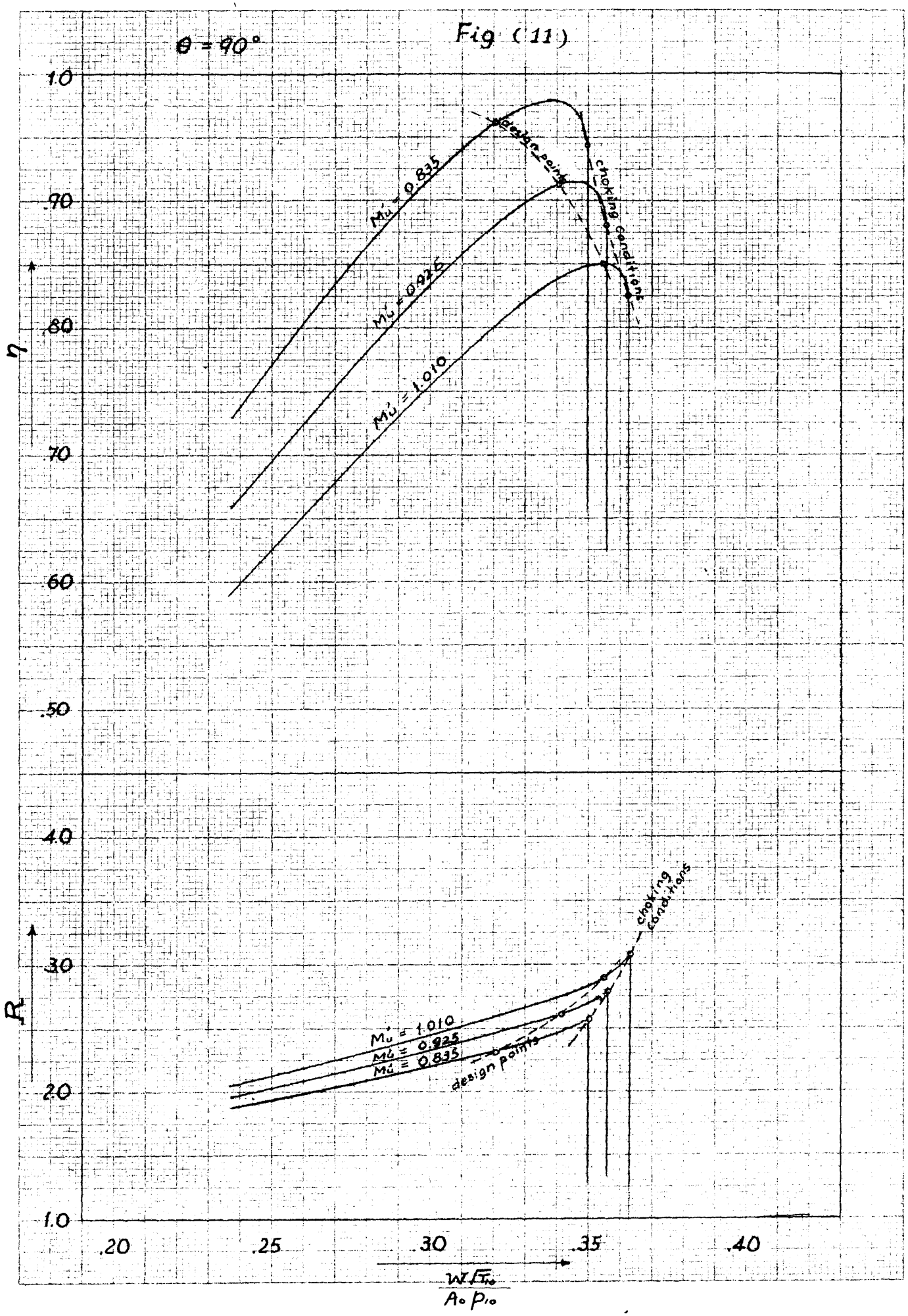
θ = 90°
η
1.0
.90
.80
.70
.60
.50
Mú = 0.835
design points
choking conditions
Mú = 0.925
Mú = 1.010
R
4.0
3.0
2.0
1.0
Mú = 1.010
Mú = 0.925
Mú = 0.835
design points
choking conditions
.20
.25
.30
.35
.40
W√T₀ / A₀ P₀

Fig (12)

Choking Conditions

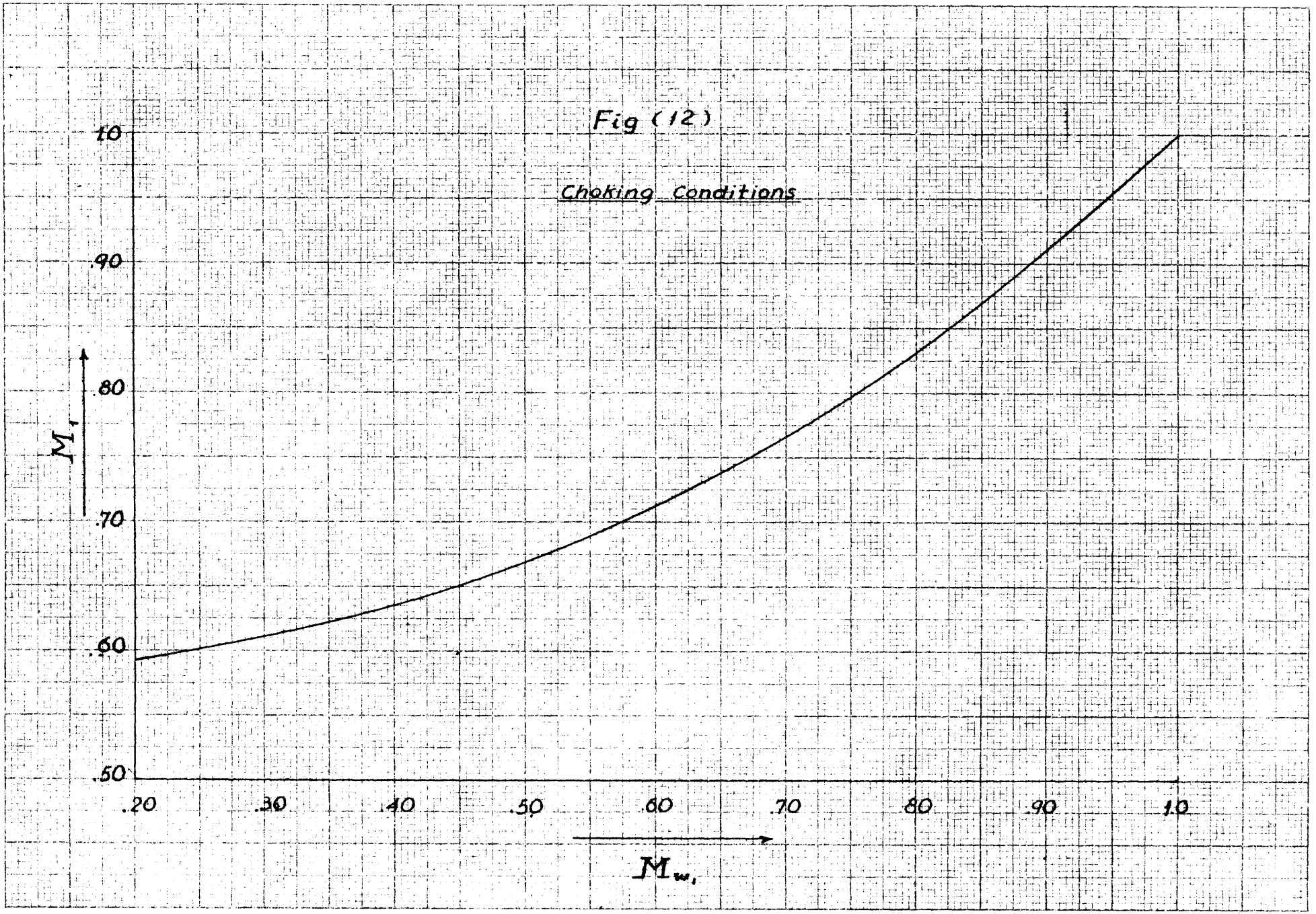

Fig (13)

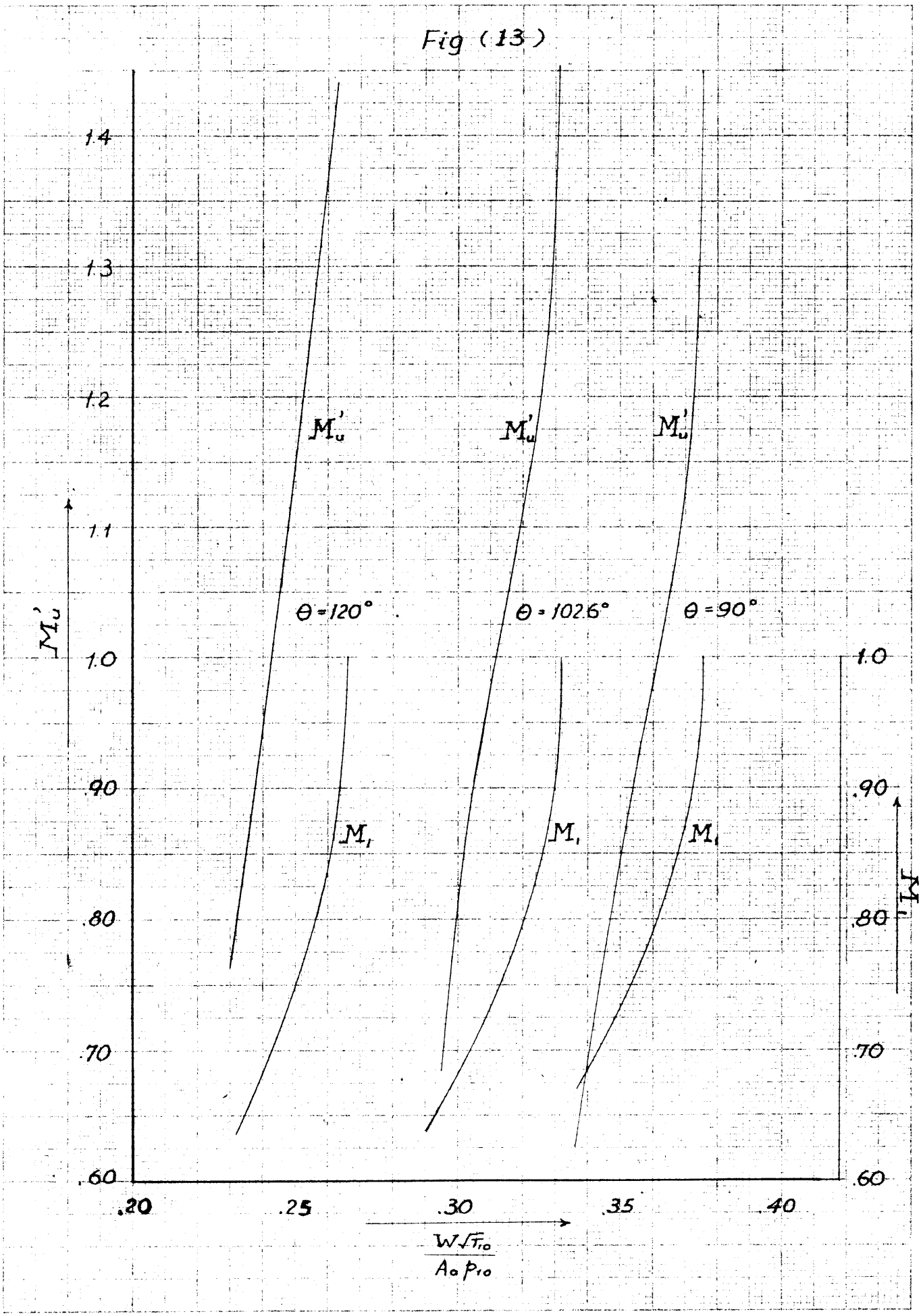
1.4
1.3
1.2
1.1
1.0
.90
.80
.70
.60
M_u'
M_u'
M_u'
$\theta = 120°$
$\theta = 102.6°$
$\theta = 90°$
M_1
M_1
M_1
M_1
.20
.25
.30
.35
.40
$\frac{W\sqrt{T_{10}}}{A_0 P_{10}}$

Fig (14)

$\varsigma = r/r_a$

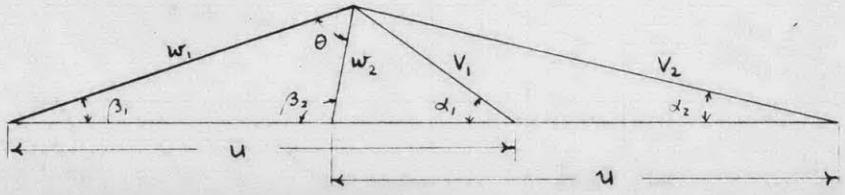

$\varsigma = 1.25$

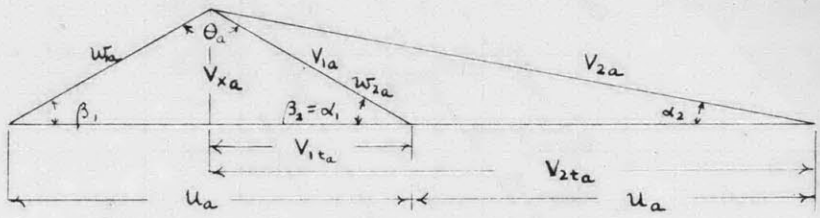

$\varsigma = 1.00$

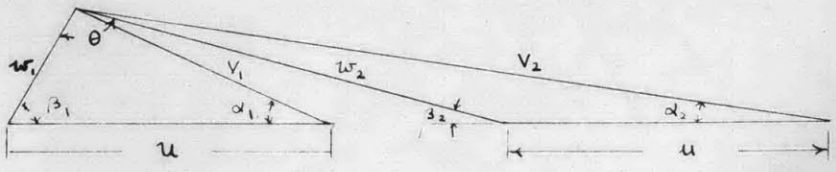

$\varsigma = 0.80$

Fig (15)

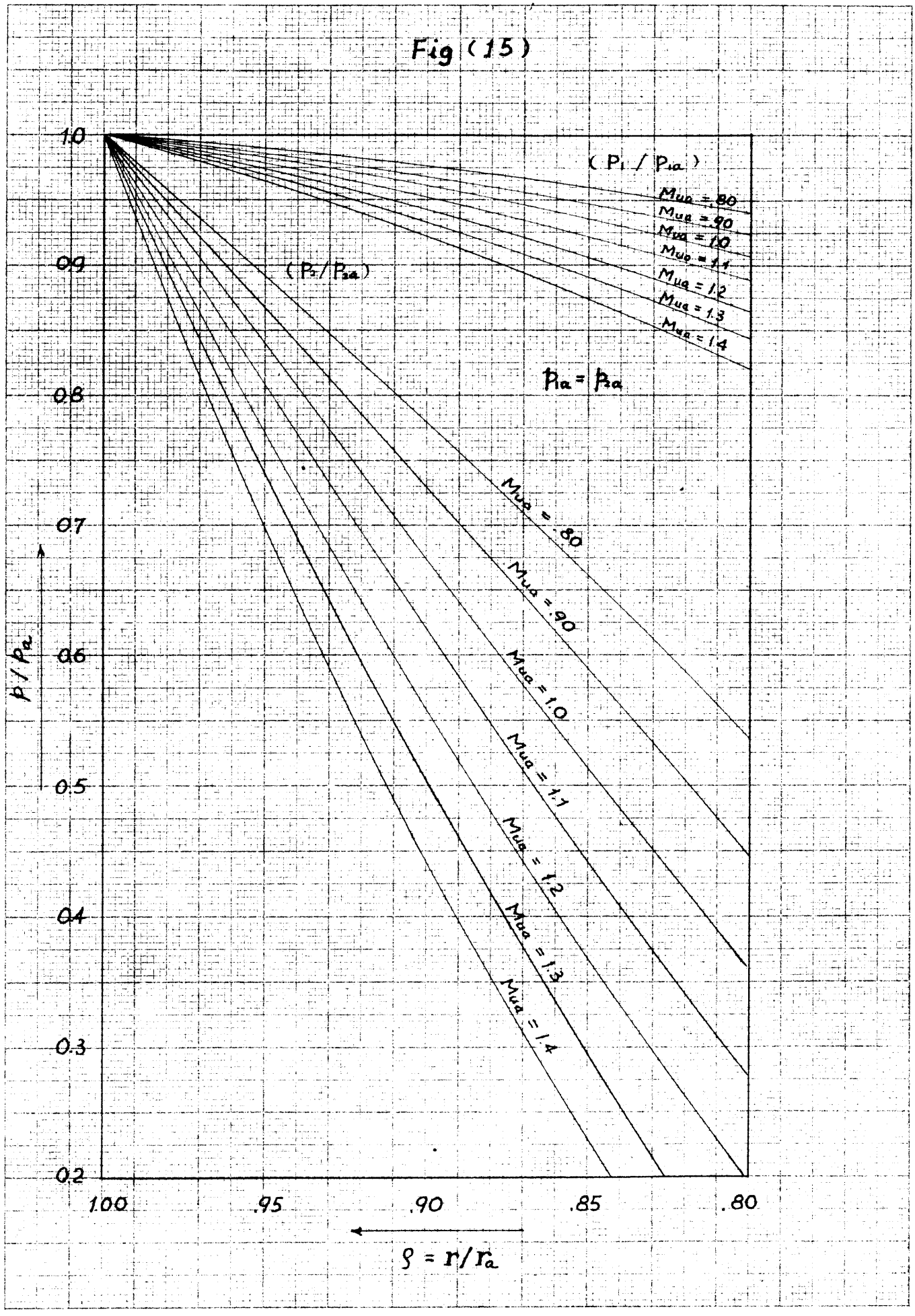
1.0
0.9
0.8
0.7
0.6
0.5
0.4
0.3
0.2
p / pa
(P1 / P1a)
(P2 / P2a)
M1a = .80
M1a = .90
M1a = 1.0
M1a = 1.1
M1a = 1.2
M1a = 1.3
M1a = 1.4
P1a = P2a
M2a = .80
M2a = .90
M2a = 1.0
M2a = 1.1
M2a = 1.2
M2a = 1.3
M2a = 1.4
1.00
.95
.90
.85
.80
ρ = r/ra

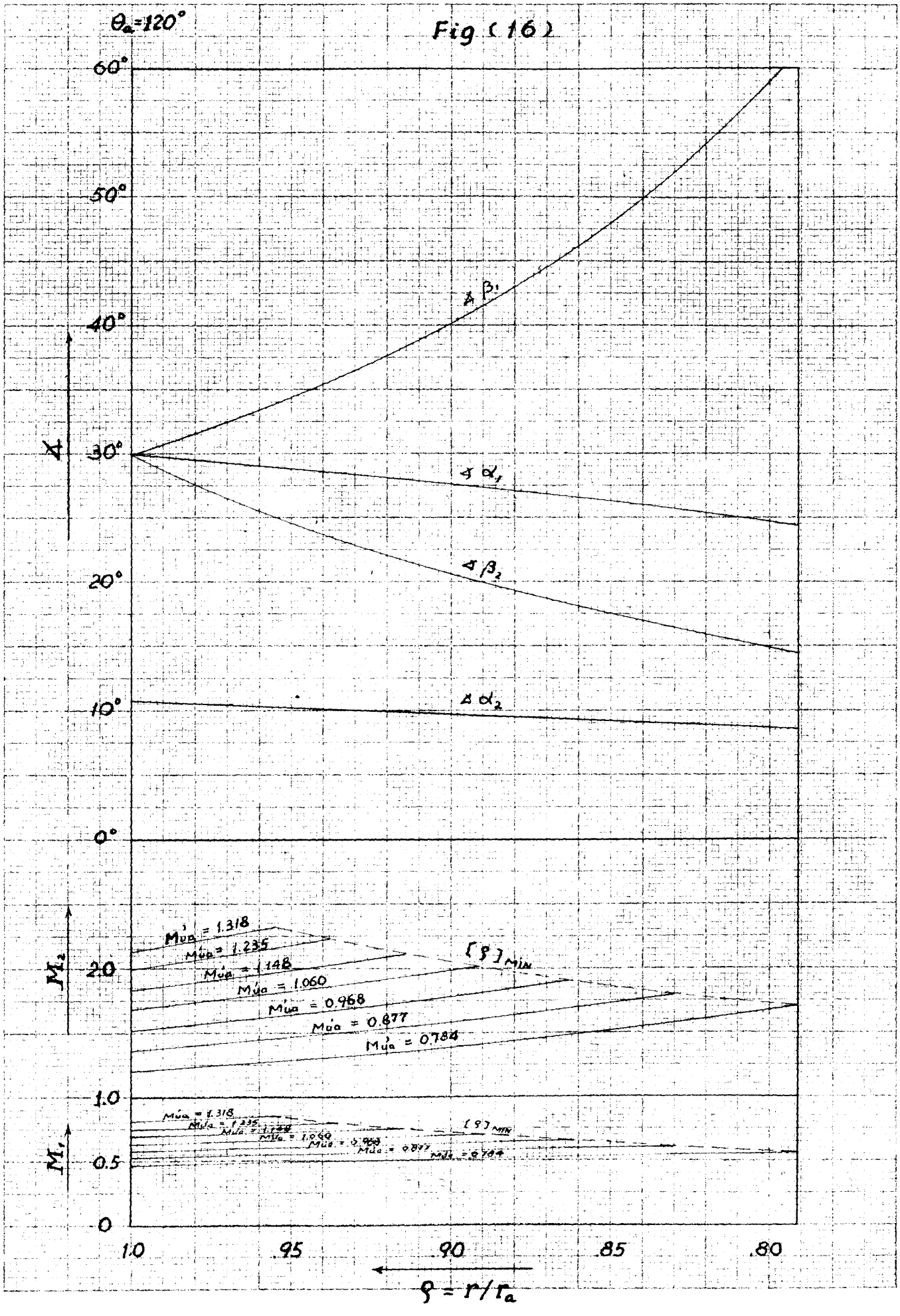
θa=120°
Fig (16)
60°
50°
40°
30°
20°
10°
0°
α
Δ β1
Δ α1
Δ β2
Δ α2
M2
M'ua = 1.318
M'ua = 1.235
M'ua = 1.148
M'ua = 1.060
M'ua = 0.968
M'ua = 0.877
M'ua = 0.784
[ρ]min
2.0
1.0
0.5
0
M1
1.0
.95
.90
.85
.80
ρ = r/ra

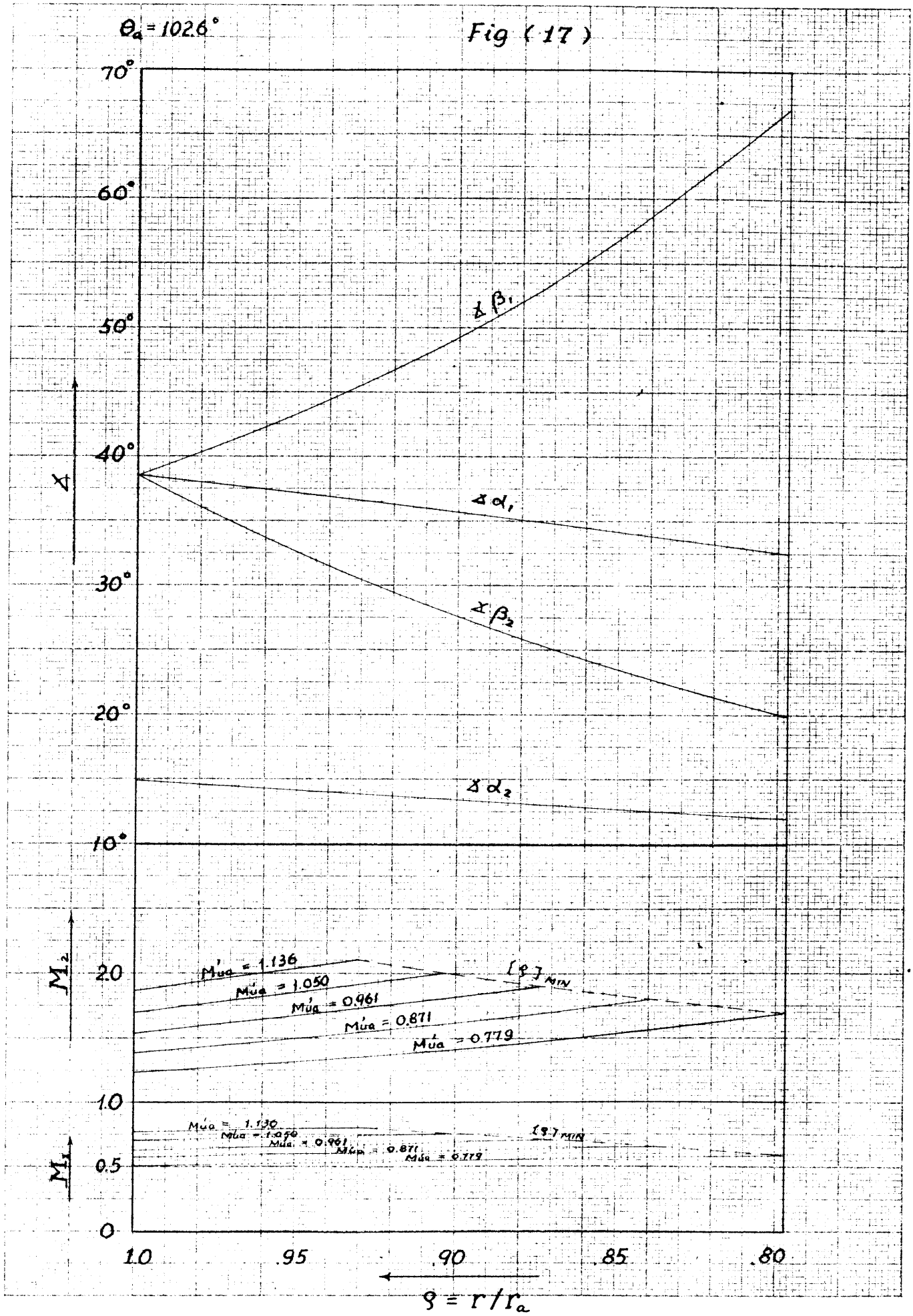
$\theta_a = 102.6°$
Fig (17)
70°
60°
50°
40°
30°
20°
10°
α
$\Delta\beta_1$
$\Delta\alpha_1$
$\Delta\beta_2$
$\Delta\alpha_2$
M_2
2.0
1.0
0.5
0
$M'_{ua} = 1.136$
$M'_{ua} = 1.050$
$M'_{ua} = 0.961$
$M'_{ua} = 0.871$
$M'_{ua} = 0.779$
$[\eta]_{MIN}$
$M_{ua} = 1.130$
$M_{ua} = 1.050$
$M_{ua} = 0.961$
$M_{ua} = 0.871$
$M_{ua} = 0.779$
$[\eta]_{MIN}$
1.0
.95
.90
.85
.80
$\eta = r/r_a$

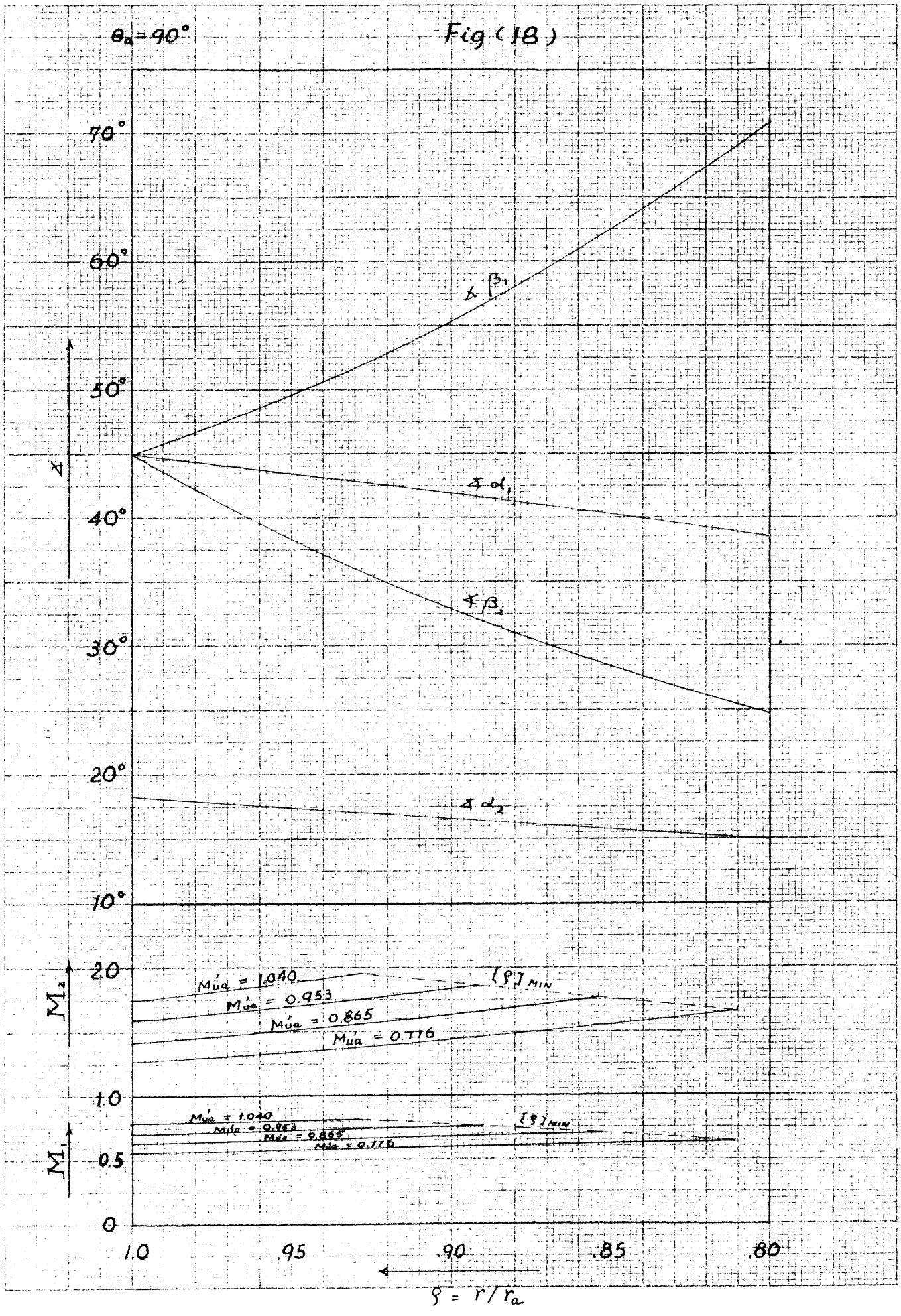
θa = 90°
Fig (18)
70°
60°
50°
40°
30°
20°
10°
α
∠ β1
∠ α1
∠ β2
∠ α2
M2
20
M'ua = 1.040
M'ua = 0.953
M'ua = 0.865
M'ua = 0.776
[ρ]MIN
1.0
M1
0.5
0
1.0
.95
.90
.85
.80
ρ = r/ra

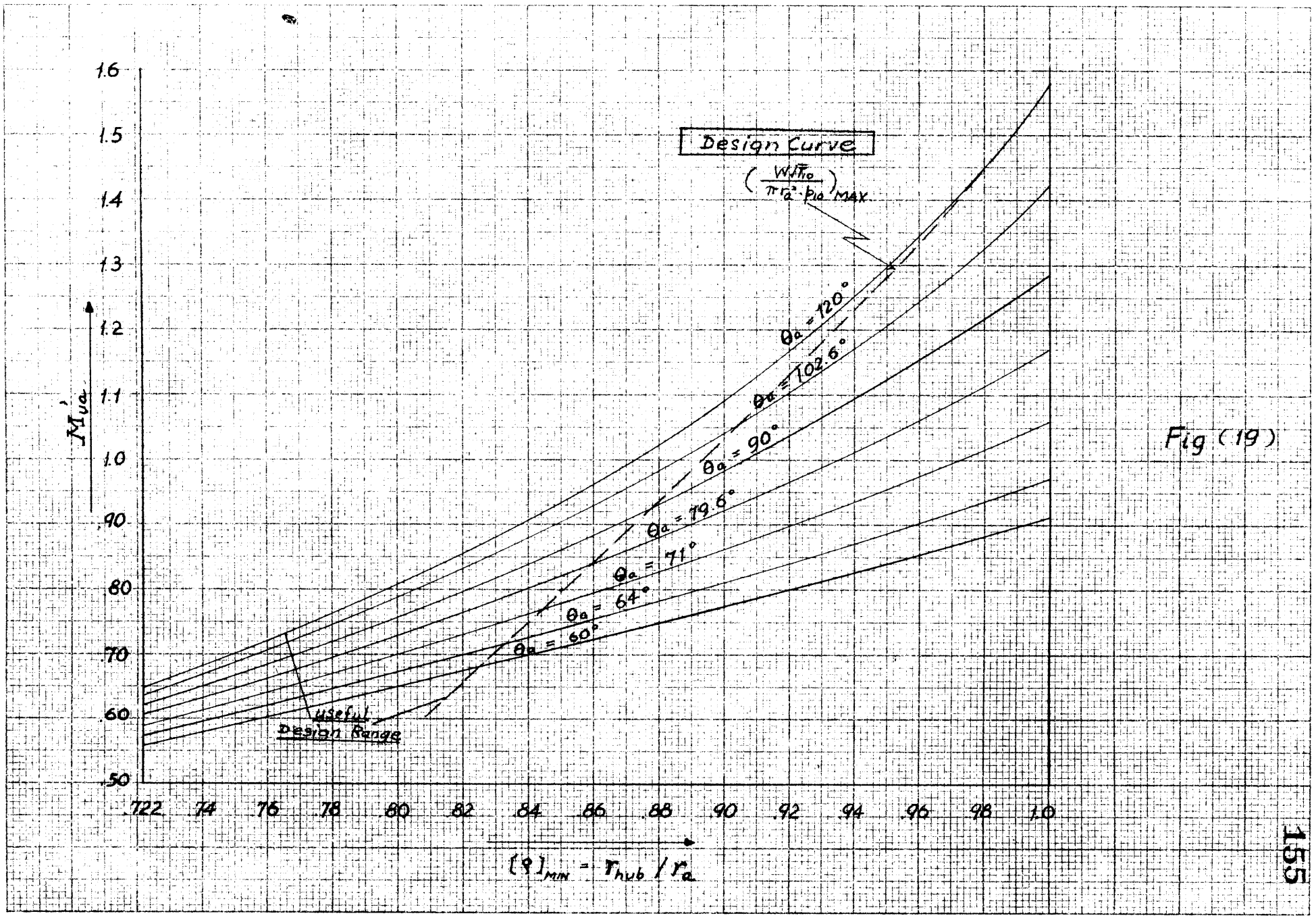
Design Curve
$\left(\frac{W\sqrt{T_{10}}}{\pi r_a^2 \cdot p_{10}}\right)_{MAX}$
$\theta_a = 120°$
$\theta_a = 102.6°$
$\theta_a = 90°$
$\theta_a = 79.6°$
$\theta_a = 71°$
$\theta_a = 64°$
$\theta_a = 60°$
Useful Design Range
M_{ua}
1.6
1.5
1.4
1.3
1.2
1.1
1.0
.90
.80
.70
.60
.50
.72
.74
.76
.78
.80
.82
.84
.86
.88
.90
.92
.94
.96
.98
1.0
$(\varphi)_{MIN} = r_{hub} / r_a$

Fig (19)

Fig (20)

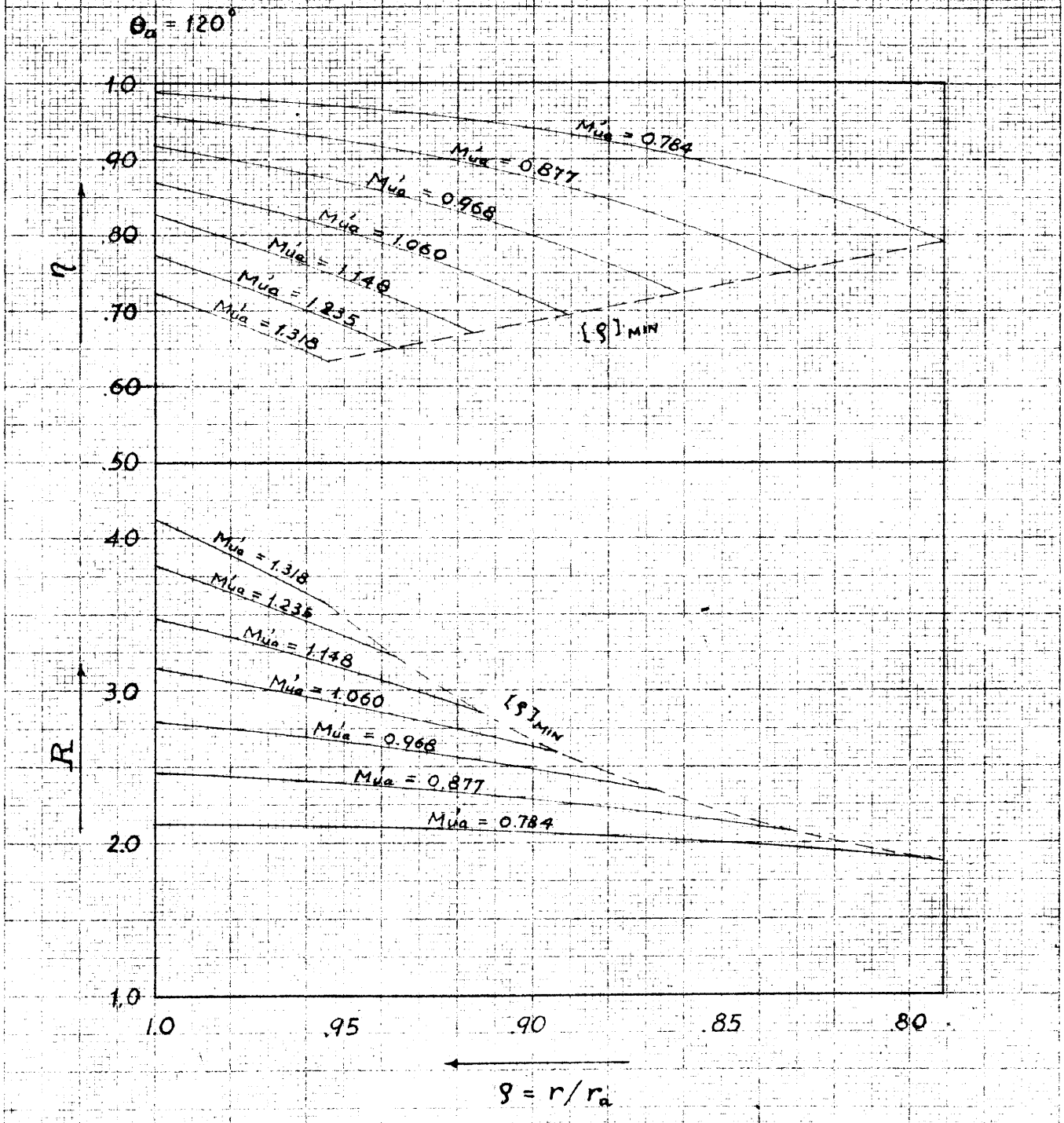
θa = 120°
η
1.0
.90
.80
.70
.60
.50
Múa = 0.784
Múa = 0.877
Múa = 0.968
Múa = 1.060
Múa = 1.148
Múa = 1.235
Múa = 1.318
[ϑ]MIN
R
4.0
3.0
2.0
1.0
Múa = 1.318
Múa = 1.235
Múa = 1.148
Múa = 1.060
Múa = 0.968
Múa = 0.877
Múa = 0.784
[ϑ]MIN
1.0
.95
.90
.85
.80
ϑ = r/ra

Fig (21)

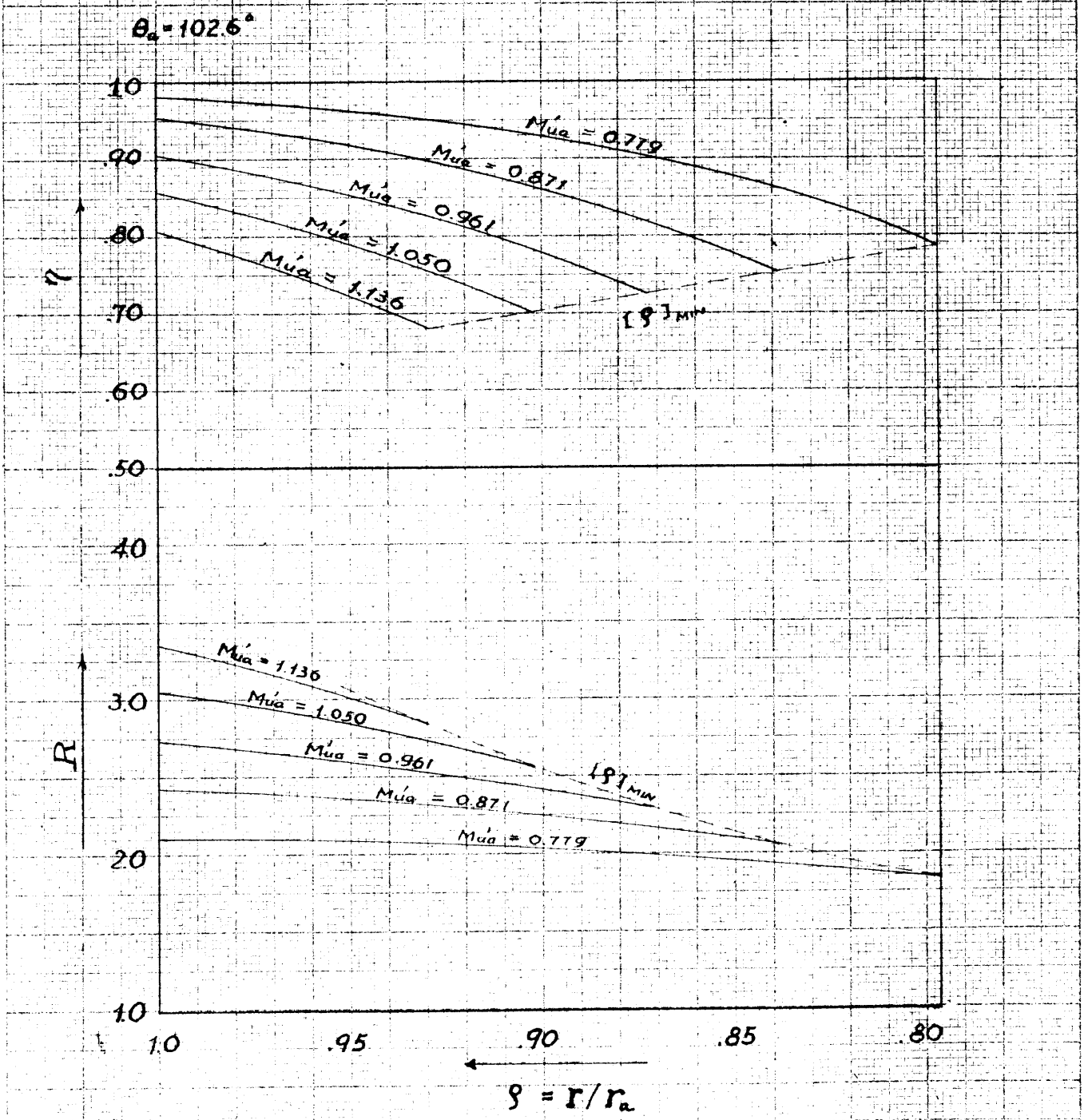
$\theta_a = 102.6°$
1.0
.90
.80
.70
.60
.50
40
η
Múa = 0.779
Múa = 0.871
Múa = 0.961
Múa = 1.050
Múa = 1.136
$[\beta]_{MIN}$
3.0
2.0
1.0
R
Múa = 1.136
Múa = 1.050
Múa = 0.961
Múa = 0.871
Múa = 0.779
$[\beta]_{MIN}$
1.0
.95
.90
.85
.80
$\beta = r/r_a$

Fig (22)

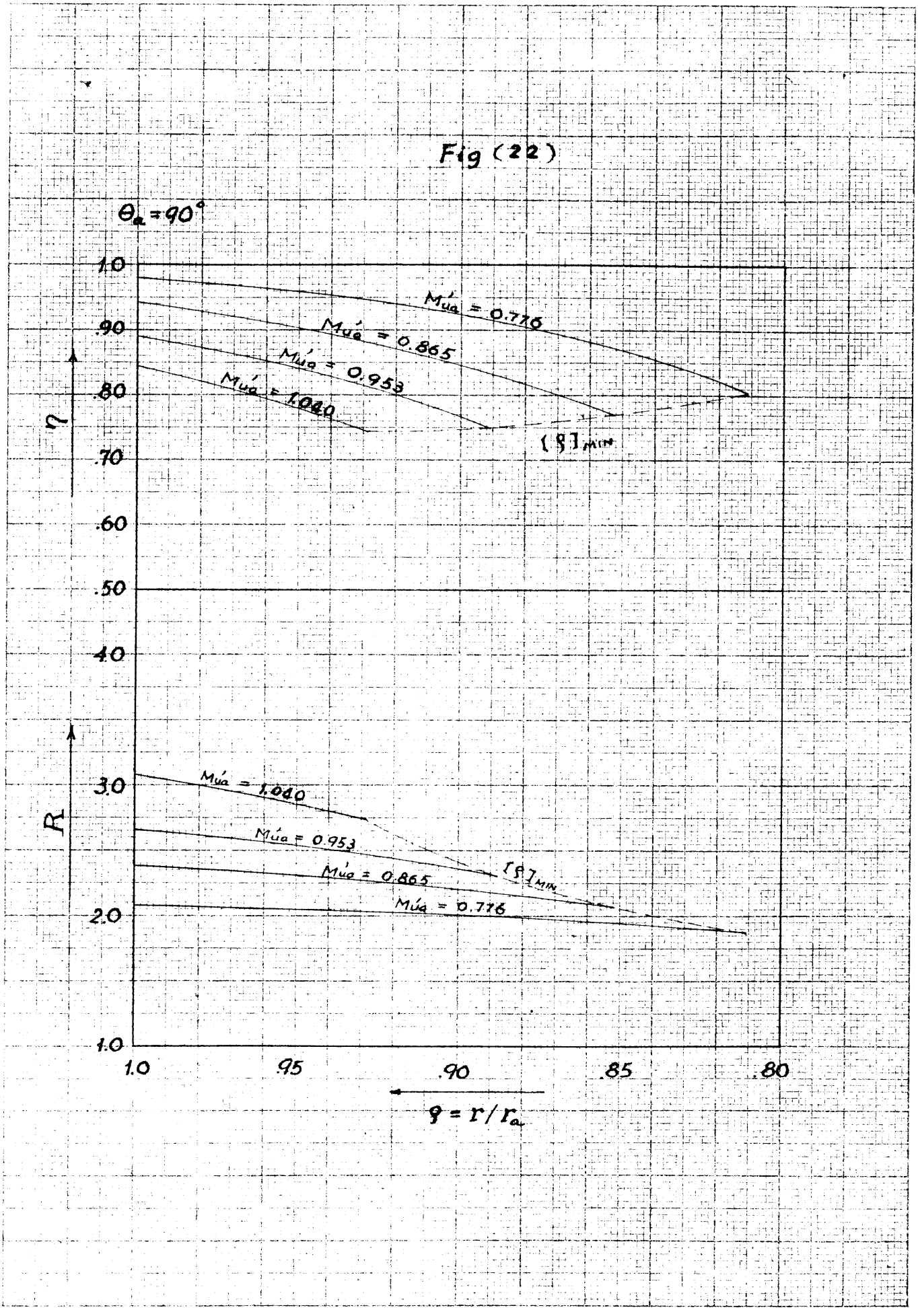
$\theta_a = 90°$
1.0
.90
.80
.70
.60
.50
.40
η
Múa = 0.776
Múa = 0.865
Múa = 0.953
Múa = 1.040
$[\beta]_{MIN}$
3.0
2.0
1.0
R
Múa = 1.040
Múa = 0.953
Múa = 0.865
Múa = 0.776
$[\beta]_{MIN}$
1.0
.95
.90
.85
.80
$\beta = r/r_a$

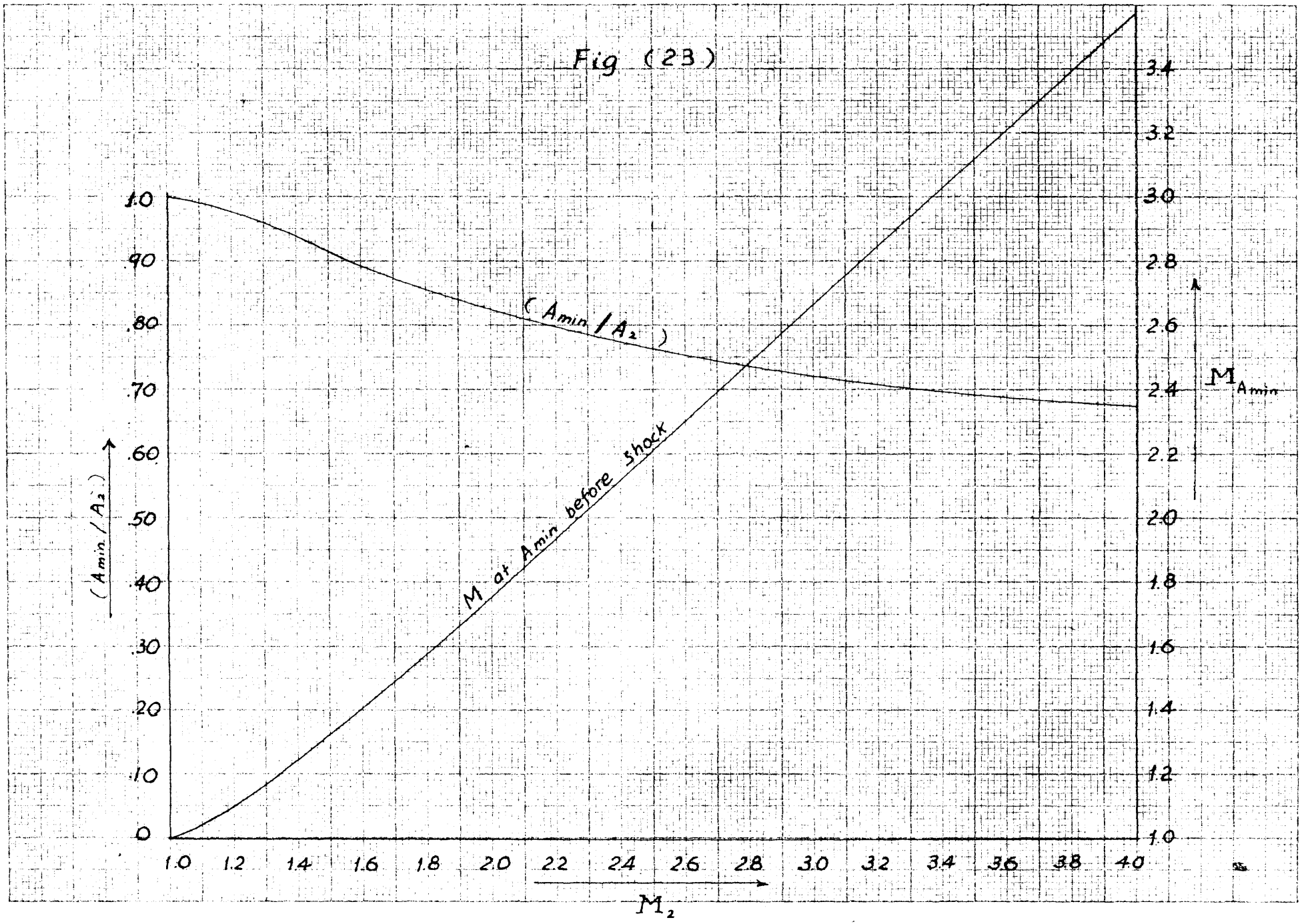
Fig (23)
(Amin / A2)
M at Amin before shock
MAmin
M2
1.0
.90
.80
.70
.60
.50
.40
.30
.20
.10
0
3.4
3.2
3.0
2.8
2.6
2.4
2.2
2.0
1.8
1.6
1.4
1.2
1.0
1.0 1.2 1.4 1.6 1.8 2.0 2.2 2.4 2.6 2.8 3.0 3.2 3.4 3.6 3.8 4.0

Fig (24)

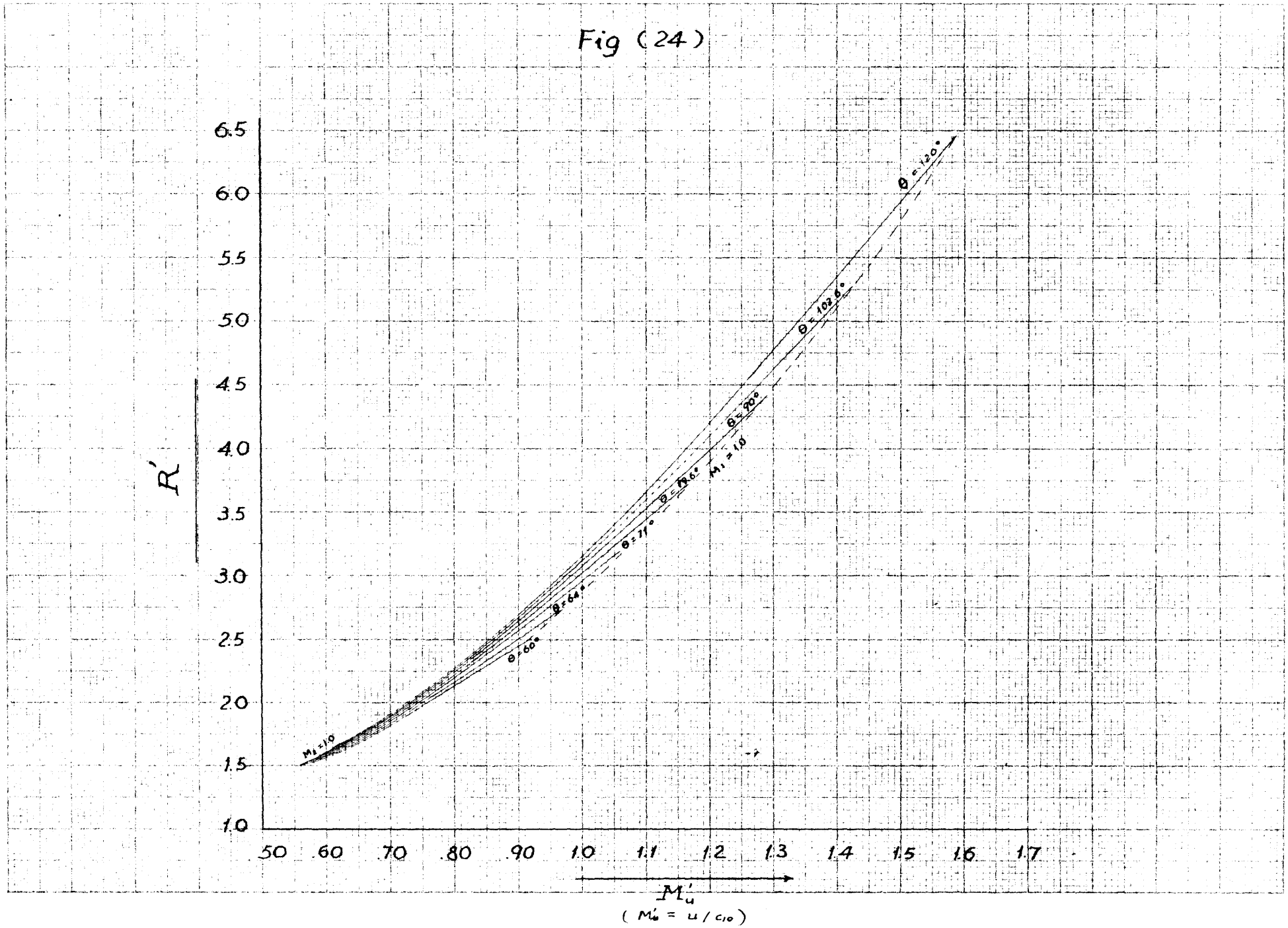
R'
6.5
6.0
5.5
5.0
4.5
4.0
3.5
3.0
2.5
2.0
1.5
1.0
.50
.60
.70
.80
.90
1.0
1.1
1.2
1.3
1.4
1.5
1.6
1.7
M'u
(M'u = u / c10)
θ = 120°
θ = 102.6°
θ = 90°
θ = 76°
θ = 71°
θ = 64°
θ = 60°
M1 = 1.0
M1 = 1.0

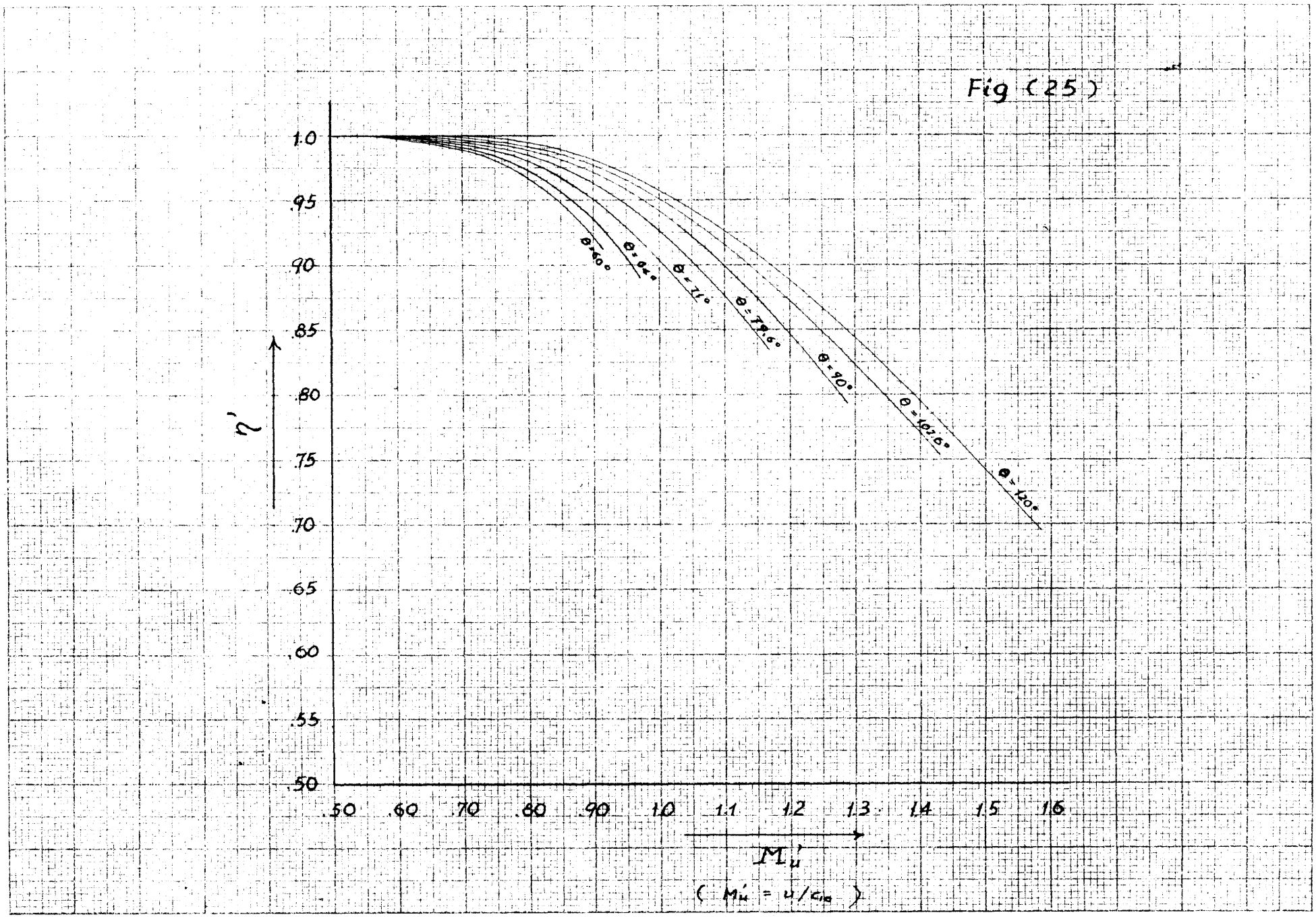
Fig (25)
1.0
.95
.90
.85
.80
.75
.70
.65
.60
.55
.50
η'
θ=60°
θ=64°
θ=71°
θ=79.6°
θ=90°
θ=102.6°
θ=120°
.50
.60
.70
.80
.90
1.0
1.1
1.2
1.3
1.4
1.5
1.6
M_u'
($M_u' = u/c_{th}$)

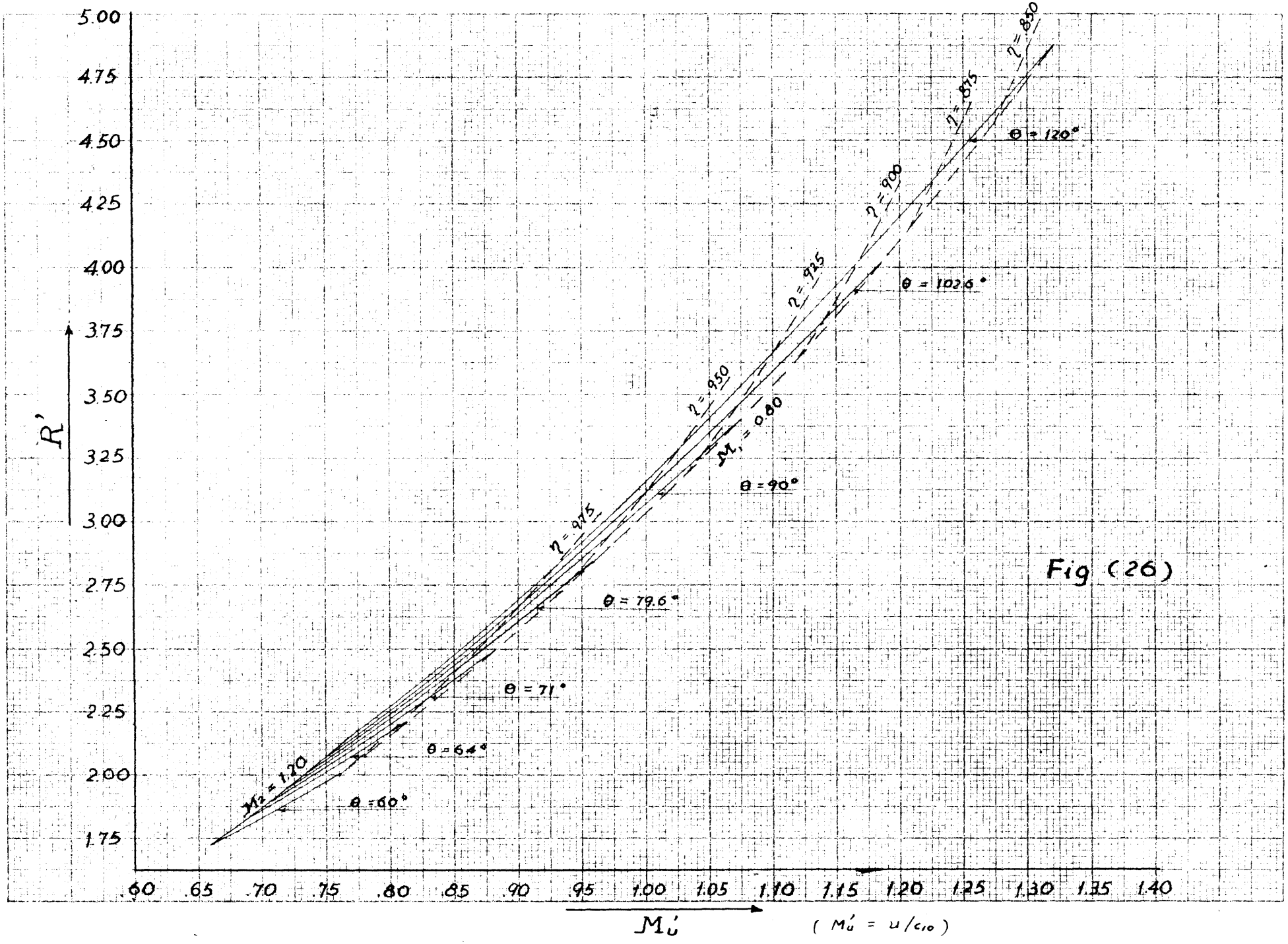
R'
5.00
4.75
4.50
4.25
4.00
3.75
3.50
3.25
3.00
2.75
2.50
2.25
2.00
1.75
.60
.65
.70
.75
.80
.85
.90
.95
1.00
1.05
1.10
1.15
1.20
1.25
1.30
1.35
1.40
M'u
(M'u = u/c10)
η = 850
η = 875
η = 900
η = 925
η = 950
η = 975
M1 = 1.20
M1 = 0.00
θ = 120°
θ = 102.6°
θ = 90°
θ = 79.6°
θ = 71°
θ = 64°
θ = 60°

Fig (26)

Fig (27)

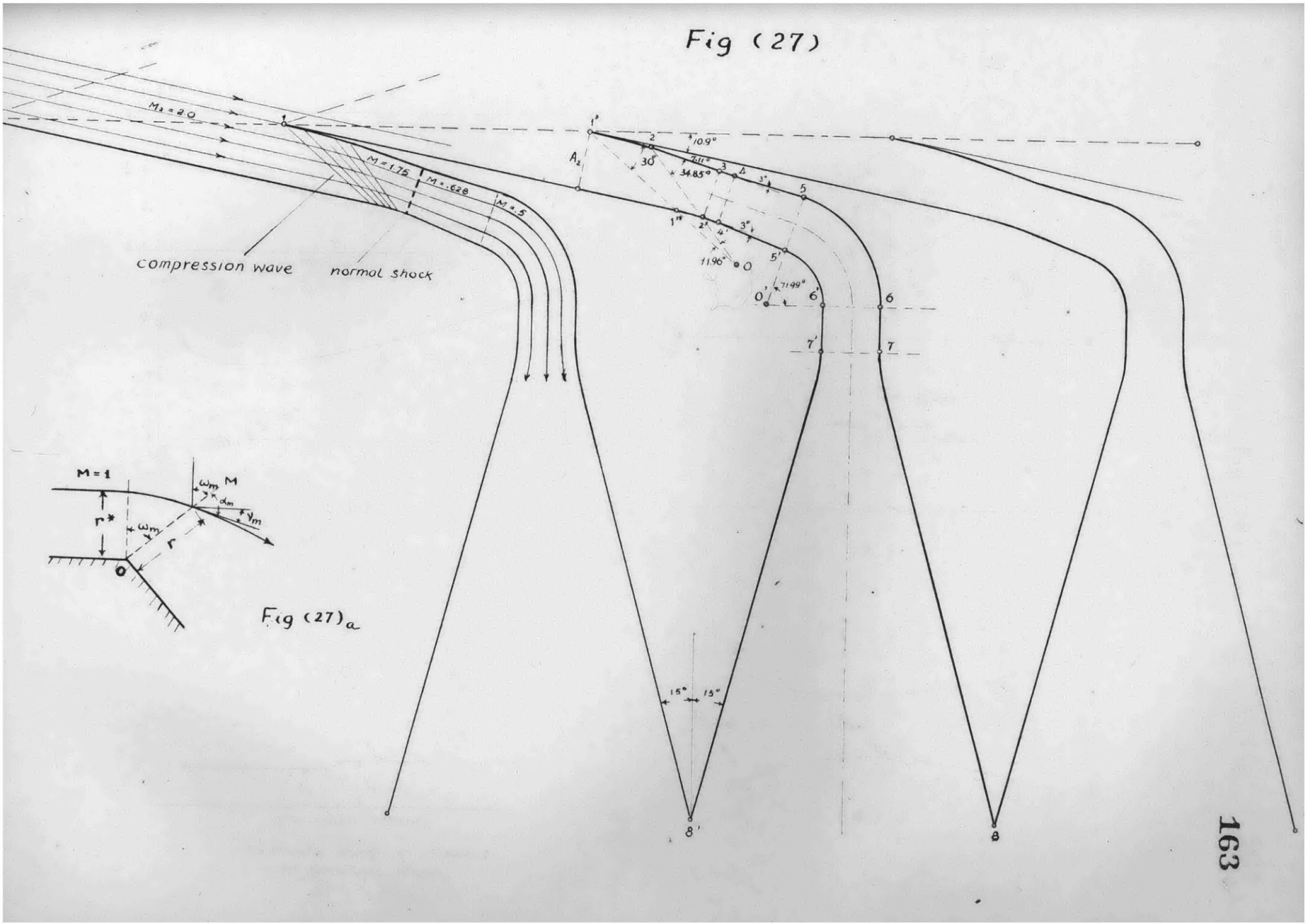

Fig (27)a

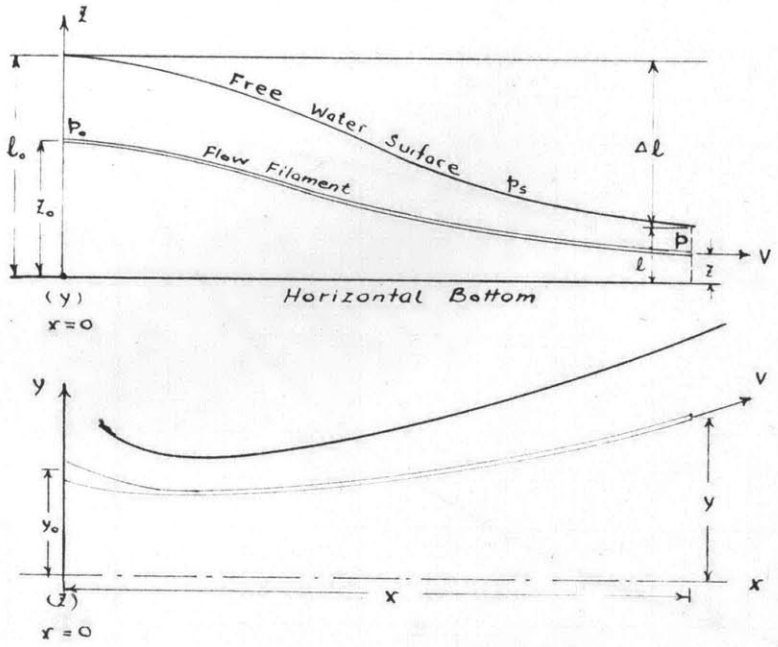

(a)

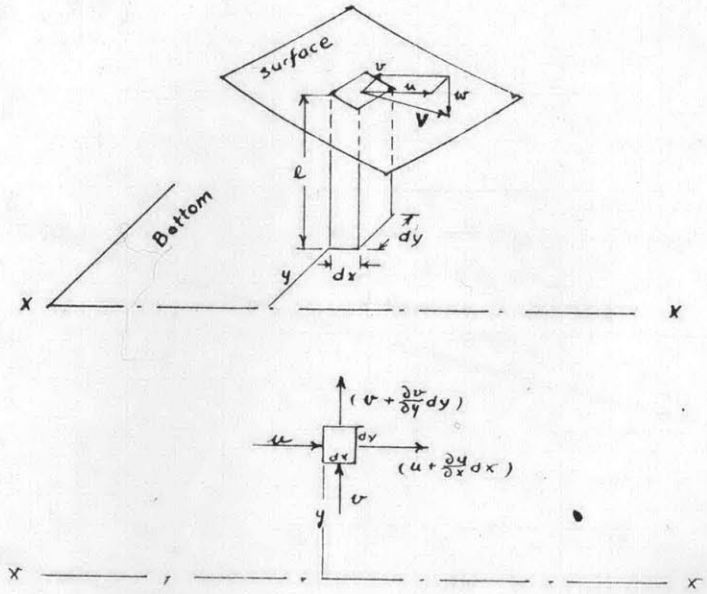

(b)

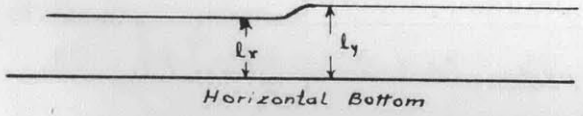

(c)

Hydraulic Jump in Channel of Constant Width

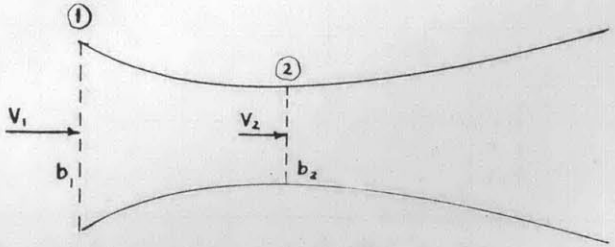

(d)

Fig (28)

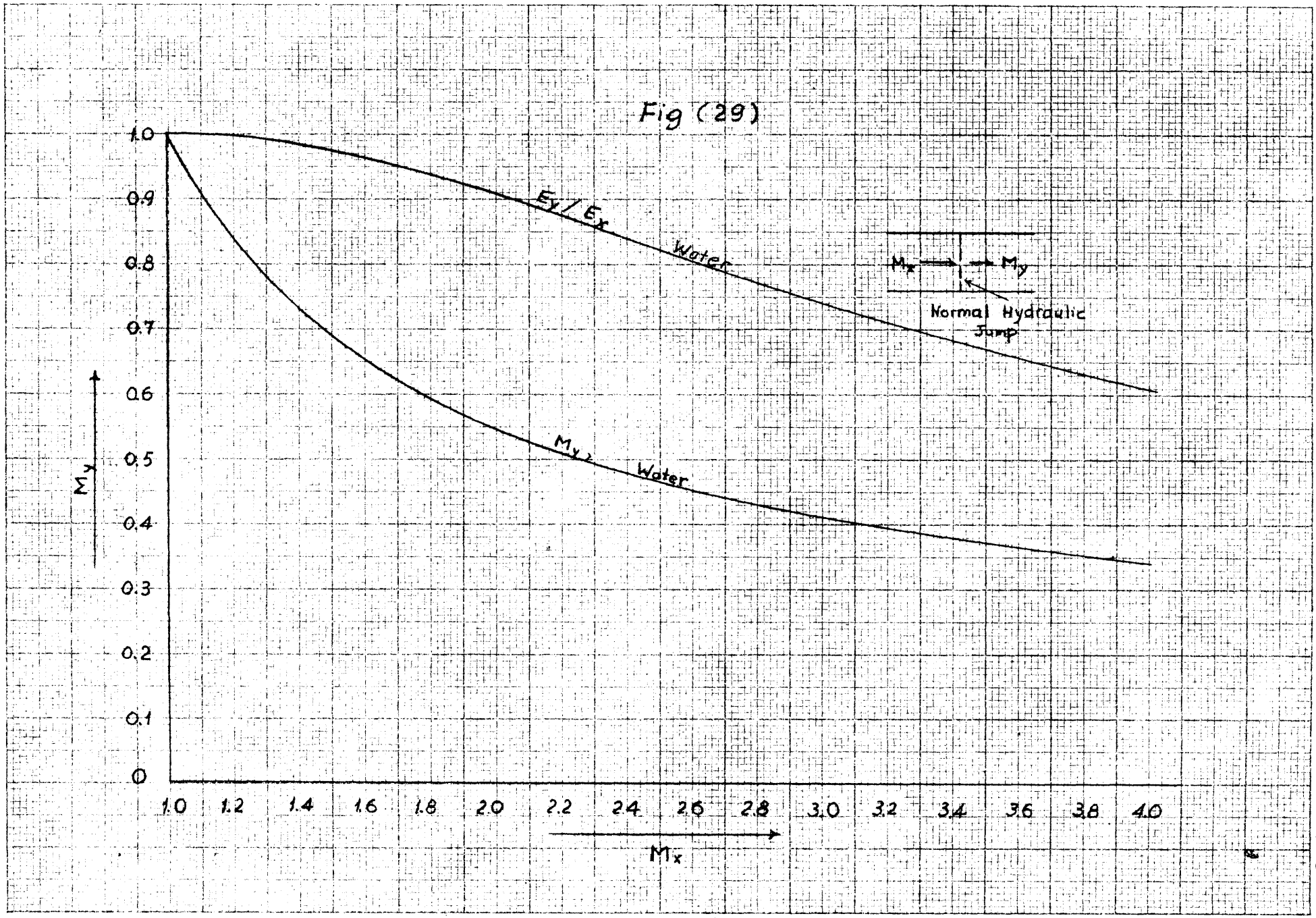
Fig (29)
1.0
0.9
0.8
0.7
0.6
0.5
0.4
0.3
0.2
0.1
0
My
Ey / Ex
Water
My2
Water
Mx
My
Normal Hydraulic Jump
1.0
1.2
1.4
1.6
1.8
2.0
2.2
2.4
2.6
2.8
3.0
3.2
3.4
3.6
3.8
4.0
Mx

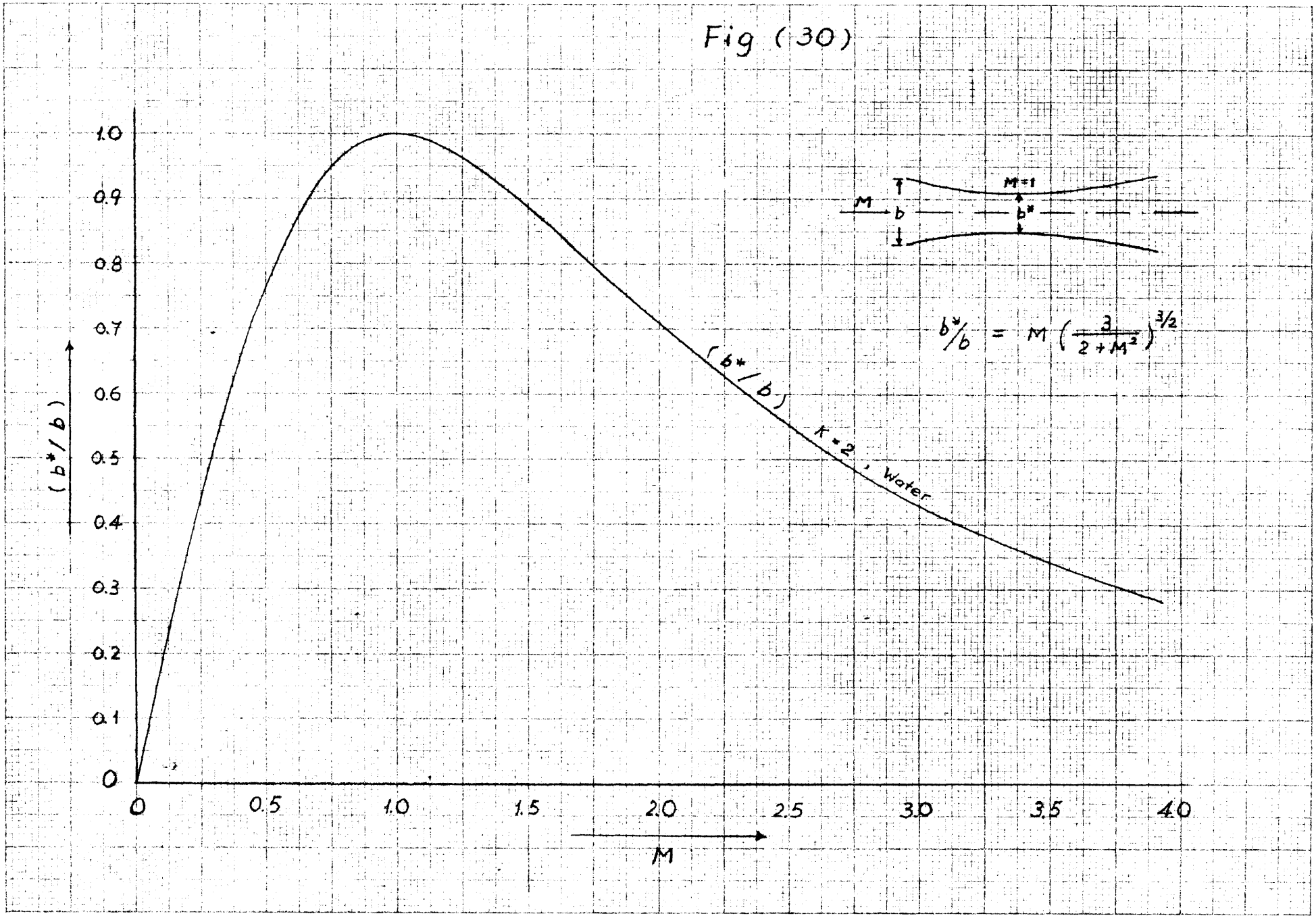
Fig (30)
1.0
0.9
0.8
0.7
0.6
0.5
0.4
0.3
0.2
0.1
0
(b*/b)
0
0.5
1.0
1.5
2.0
2.5
3.0
3.5
4.0
M
(b*/b)
K=2, water
M=1
M
b
b*
b*/b = M (3/(2+M²))^3/2

Fig. (31)

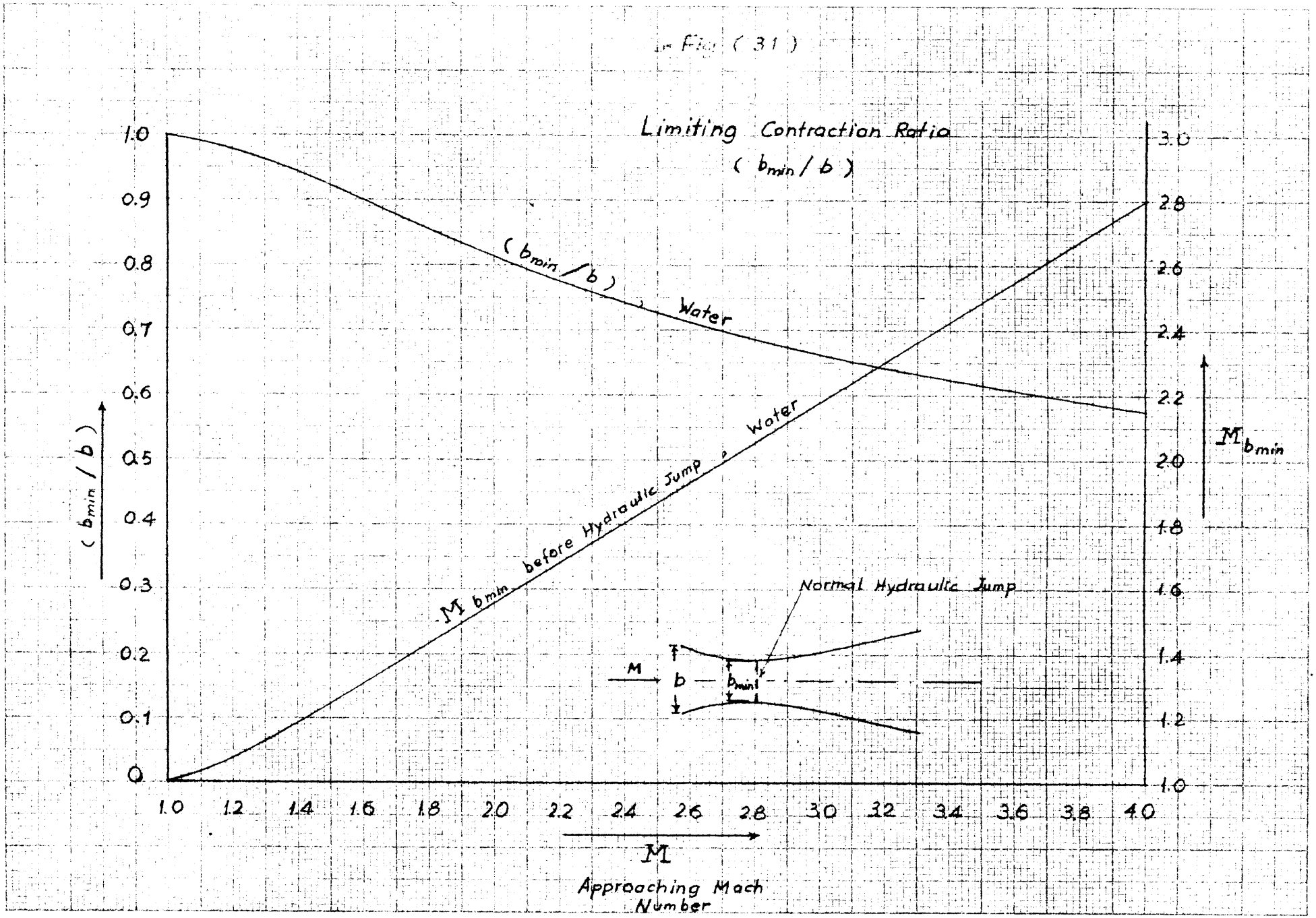
Limiting Contraction Ratio
(bmin / b)
(bmin / b) , Water
M bmin before Hydraulic Jump , Water
Normal Hydraulic Jump
M
b
bmin
(bmin / b)
Mbmin
M
Approaching Mach Number
1.0
0.9
0.8
0.7
0.6
0.5
0.4
0.3
0.2
0.1
0
3.0
2.8
2.6
2.4
2.2
2.0
1.8
1.6
1.4
1.2
1.0
1.0 1.2 1.4 1.6 1.8 2.0 2.2 2.4 2.6 2.8 3.0 3.2 3.4 3.6 3.8 4.0

Fig (32)

Diffusers designed for water channel tests
on the limiting contraction ratios

For approaching Mach Number equal to 2

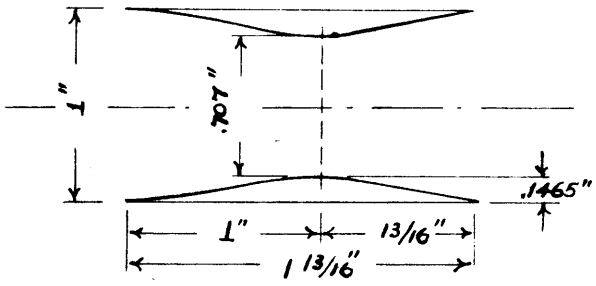

Diffuser tip (1)a

Contraction Ratio

$= b^*/b = .707$

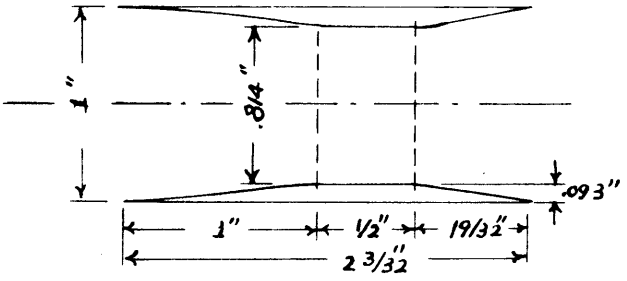

Diffuser tip (1)b

Contraction Ratio

$= b_{min}/b = .814$

2 Diffuser Walls

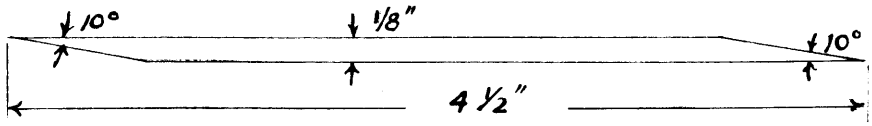

Scale 1:1 Made of 1 inch wide hard brass

Fig (33)

Diffusers designed for water channel tests
on the limiting contraction ratios

For approaching Mach Number equal to 3

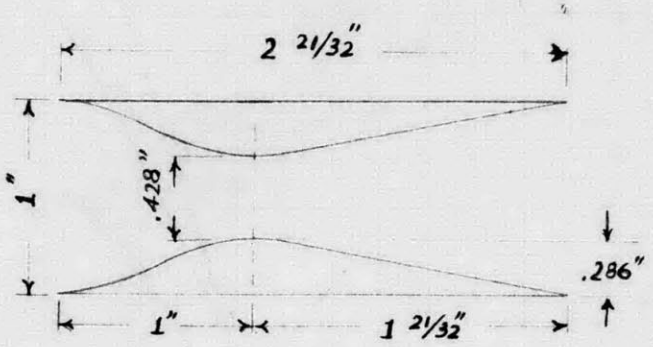

Diffuser tip (2)a

Contraction Ratio

$= b^*/b = .428$

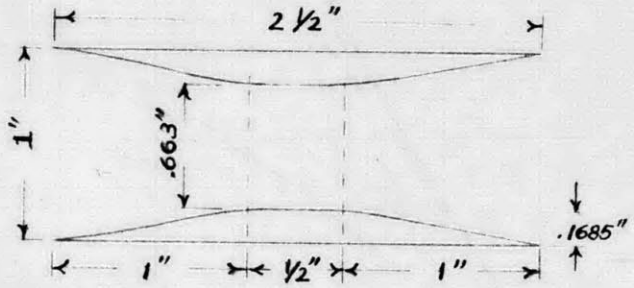

Digfuser tip (2)b

Contraction Ratio

$= b_{min}/b = .663$

2 Diffuser Walls

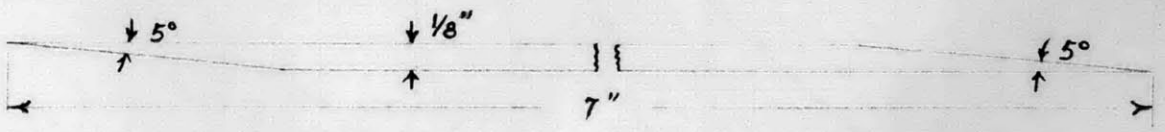

Scale 1;1 Made of 1 inch wide brass

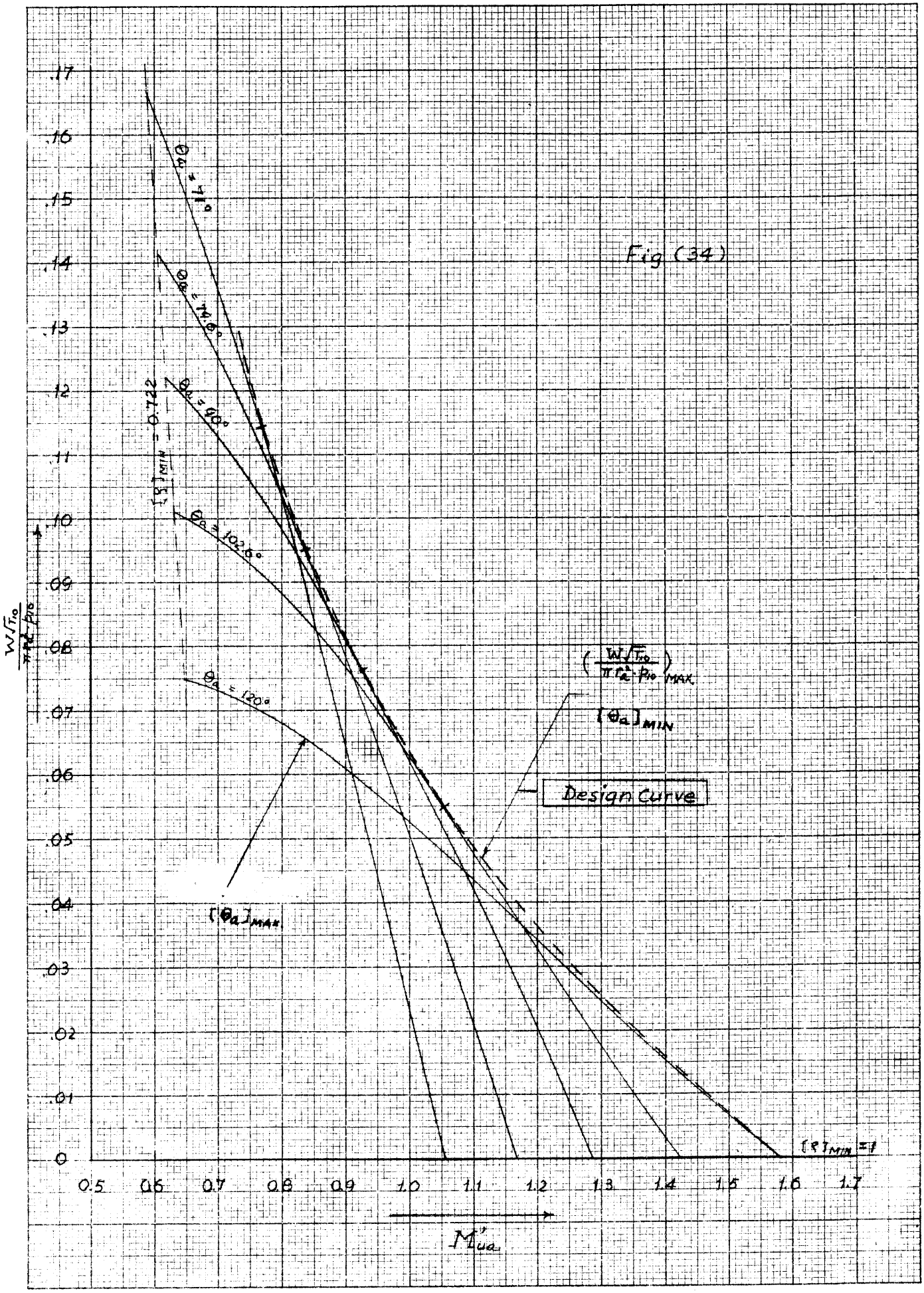
Fig (34)
$\frac{W\sqrt{T_{10}}}{\pi r_2^2 P_{10}}$
M'_{ua}
$[\theta_a]_{MIN}$
$[\theta_a]_{MAX}$
$\left(\frac{W\sqrt{T_{10}}}{\pi r_2^2 P_{10}}\right)_{MAX}$
Design Curve
$[\theta_a]_{MIN} = 0.722$
$[\theta_a]_{MIN} = 1$
$\theta_a = 90°$
$\theta_a = 100°$
$\theta_a = 120°$
0.5
0.6
0.7
0.8
0.9
1.0
1.1
1.2
1.3
1.4
1.5
1.6
1.7
.17
.16
.15
.14
.13
.12
.11
.10
.09
.08
.07
.06
.05
.04
.03
.02
.01
0

Fig (35)

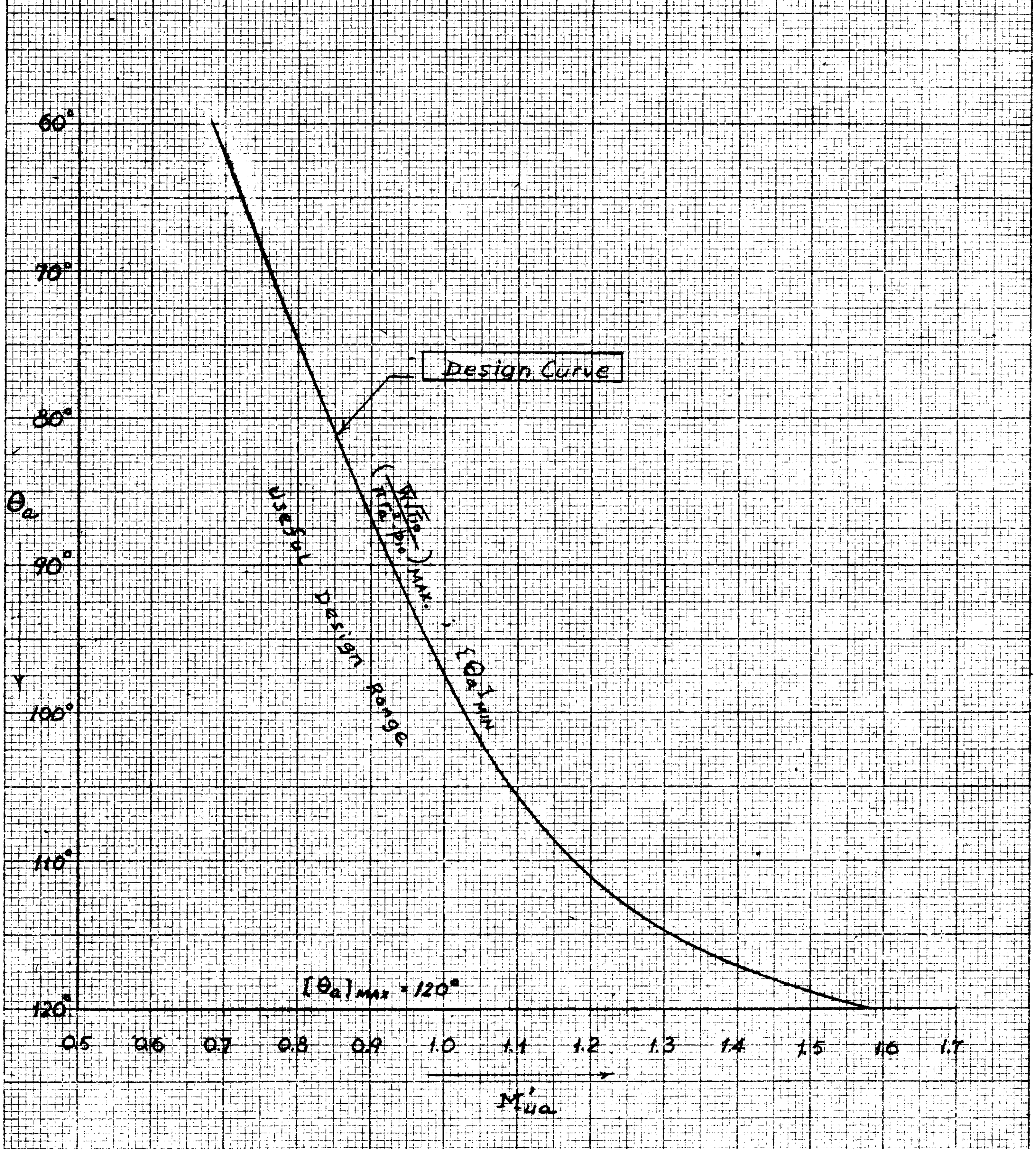
Design Curve
Useful
Design Range
$[\Theta_a]_{MIN}$
$[\Theta_a]_{max} = 120°$
Θ_a
M'_{ua}
60°
70°
80°
90°
100°
110°
120°
0.5
0.6
0.7
0.8
0.9
1.0
1.1
1.2
1.3
1.4
1.5
1.6
1.7

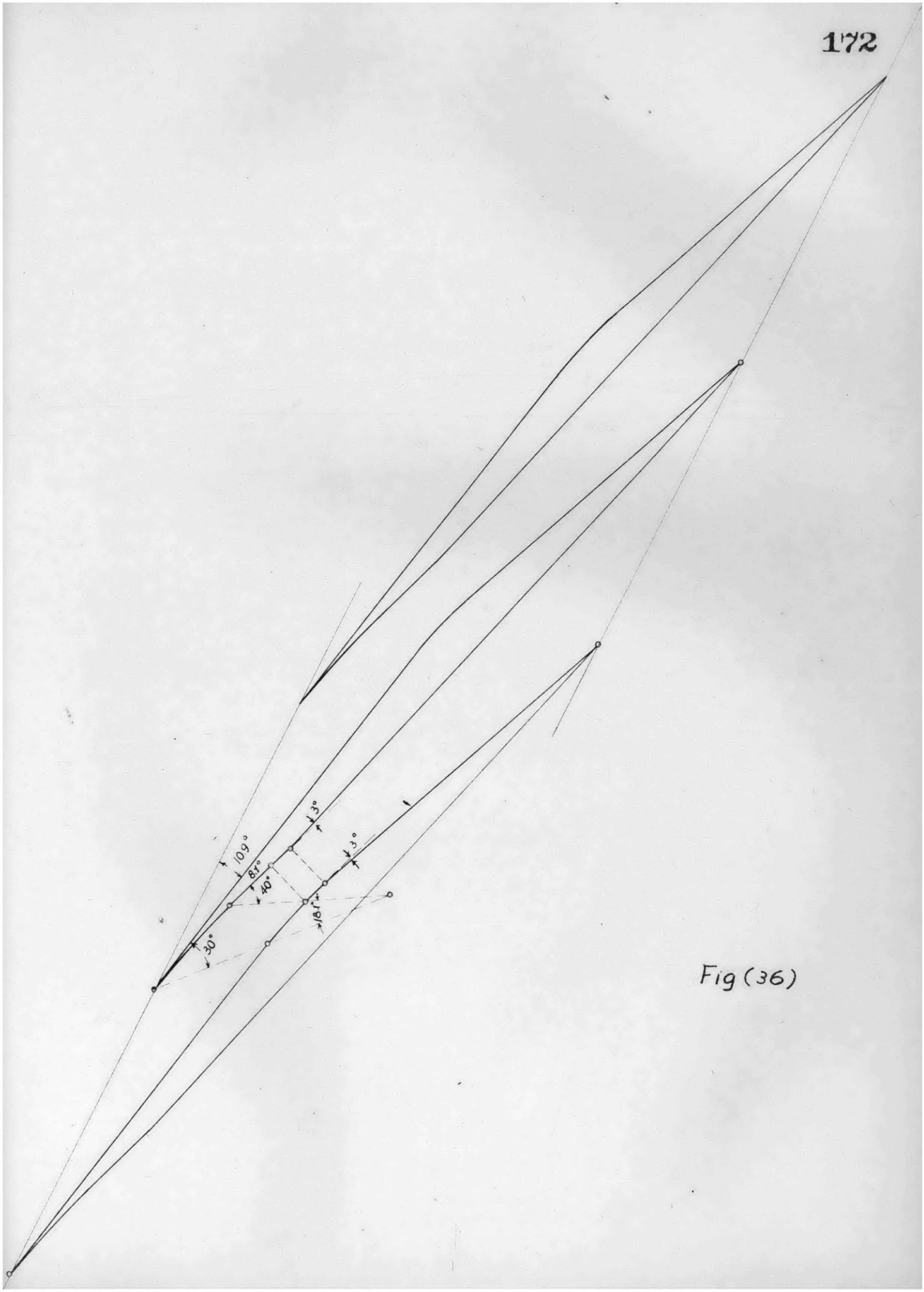

Fig (36)

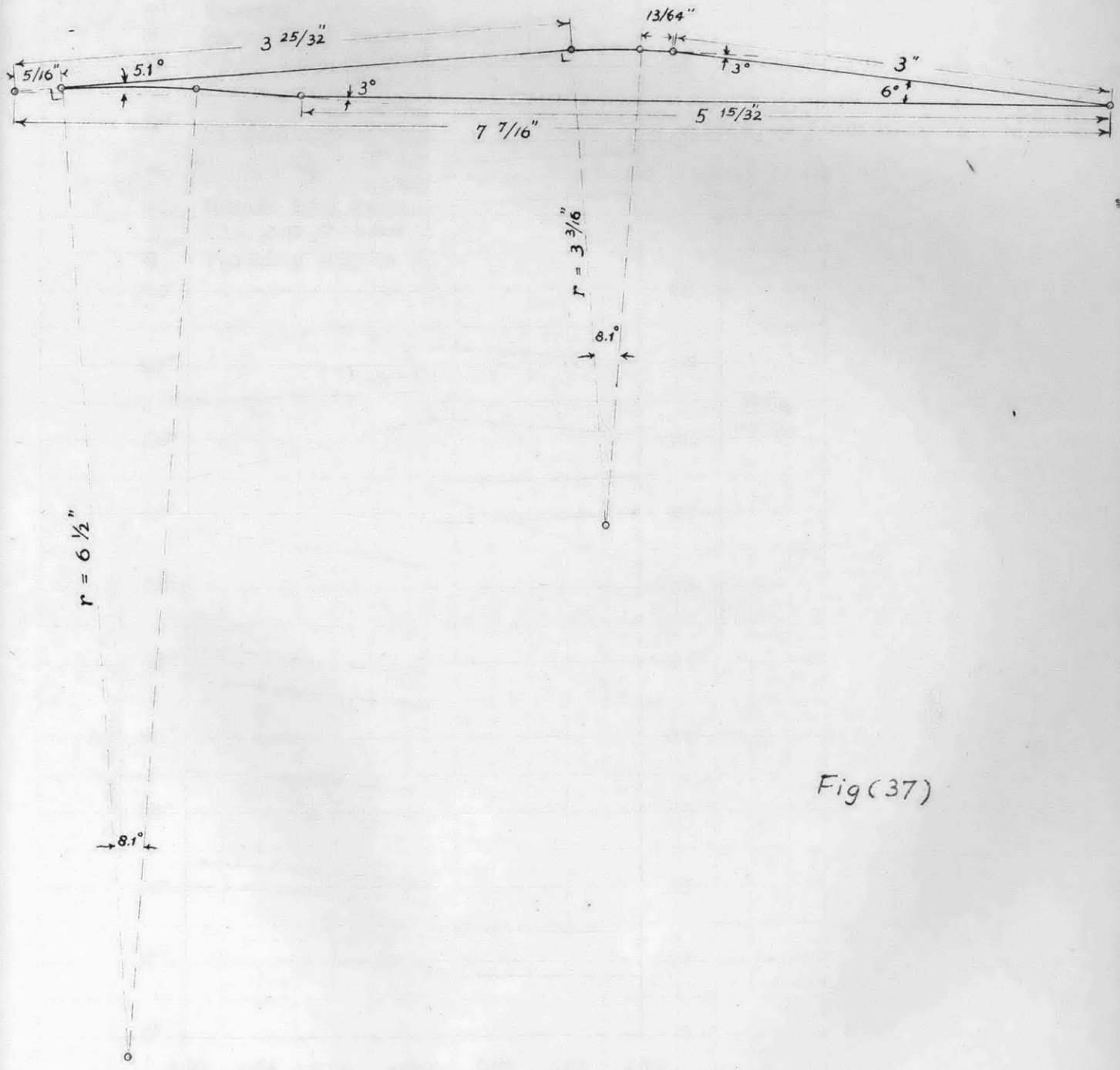

Fig (37)

Design Charts of Single Stage Supersonic Axial Flow Compressors

Fig (38)

Nov. 1948
W. W. CHAO

Supersonic Flow Entering Stator, Constant Circulation, Pure Impulse Blade Design at Tip Radius in Rotor, Perfect Gas, k = 1.4.

R	Total compression ratio.	Normal shock at outlet stator entrance.
η	Thermal efficiency.	
R'	Total compression ratio.	Normal shock at throat section in stator.
η'	Thermal efficiency.	
W	Mass flow rate in lbs/sec.	
M_1	Flow Mach Number before rotor.	
M_2	Flow Mach Number behind rotor.	
p_{to}	Stagnation pressure of gas at compressor inlet in lbs/ft^2.	
T_{to}	Stagnation temperature of gas at compressor inlet, Fabs.	
α_1 ; β_1 ; β_2 ; α_2	Blade angles at guide fan outlet, rotor inlet, rotor exit, outlet stator inlet respectively.	
$r_a = r_{tip}$	Rotor tip radius in ft.	
M'_{ua}	Tip compressor Mach Number = rotor tip speed divided by $\sqrt{kgRT_{to}}$	
θ_a	Turning angle in rotor tip.	

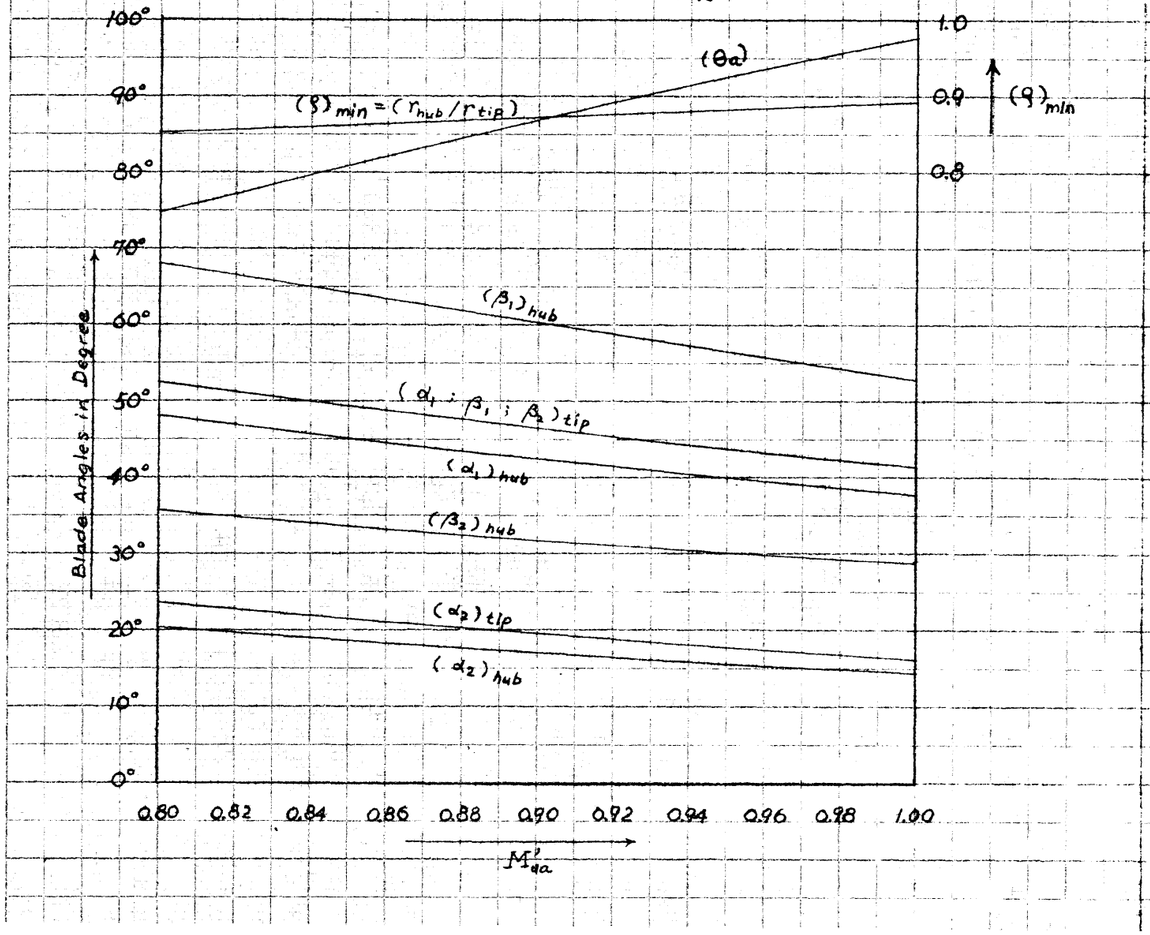

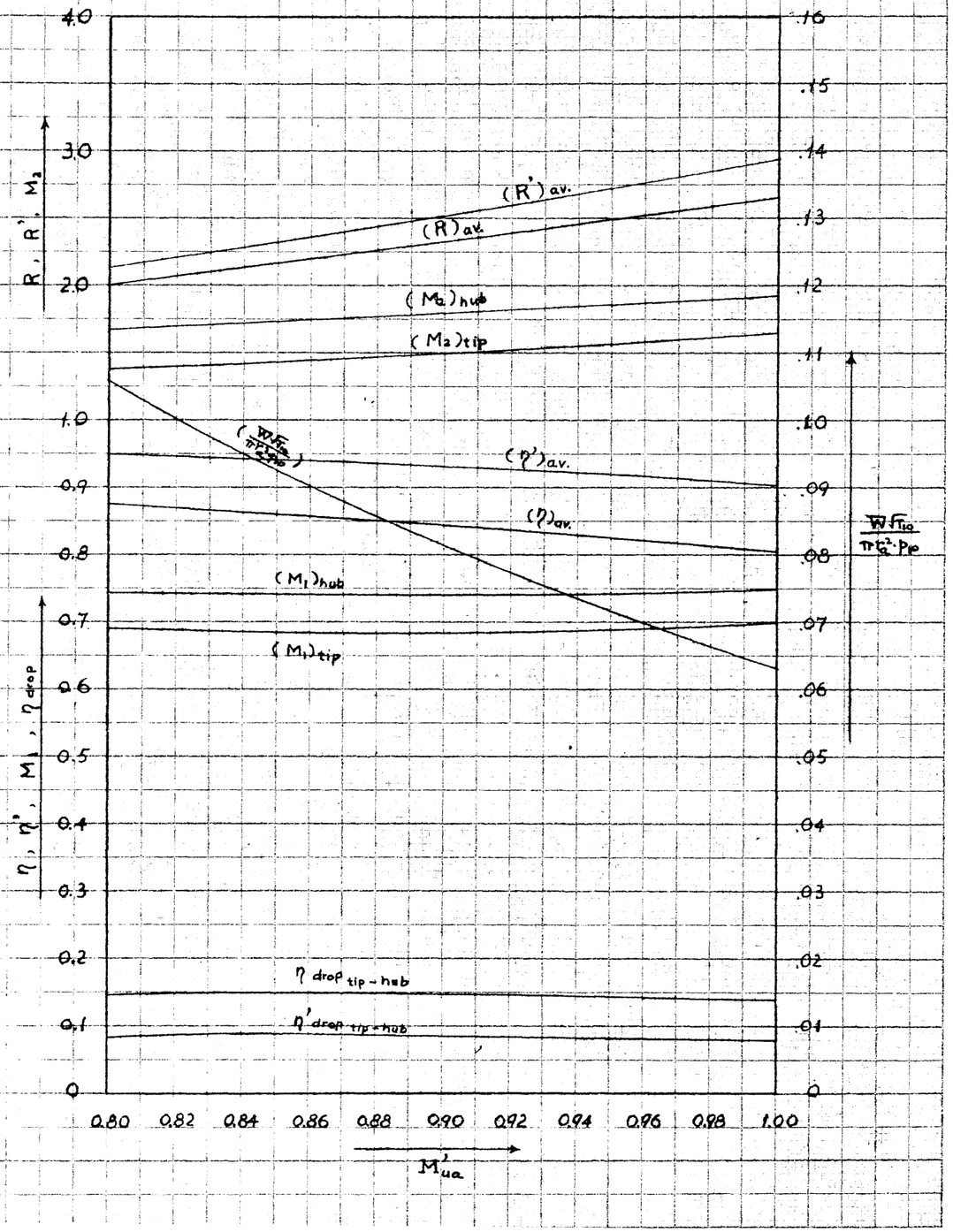

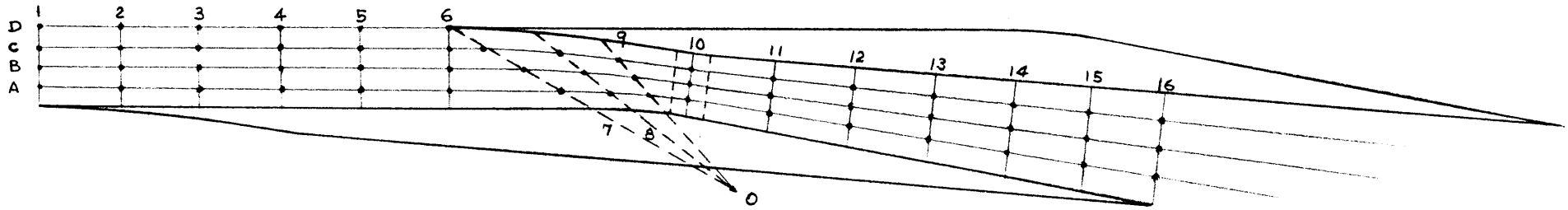

Fig (39)

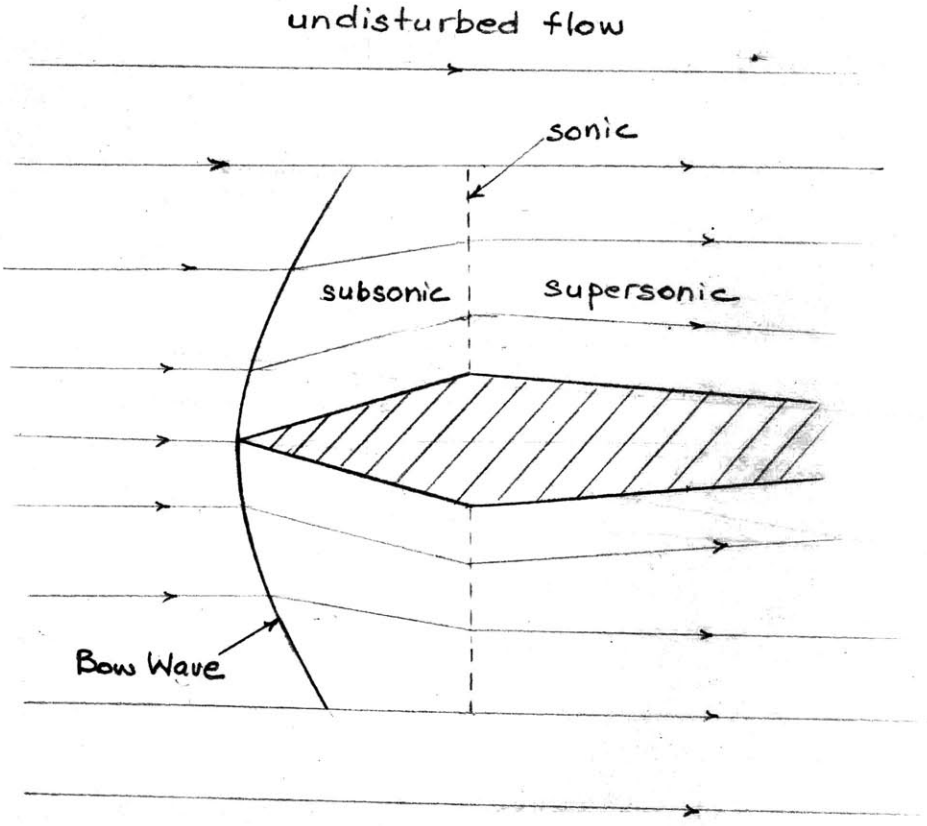

Fig (40)

Bow Wave Attached to An Isolated Body
At Transonic Region

$M \gtrless 1$ Starting Condition

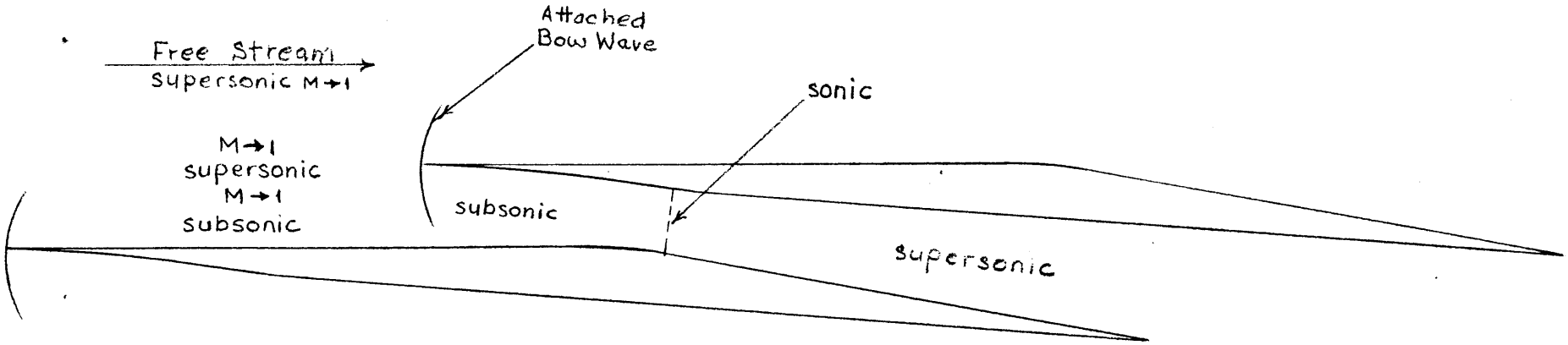

Wave Pattern for the Cascade in the Transonic Region

Fig (41)

Fig (42)

Starting Condition

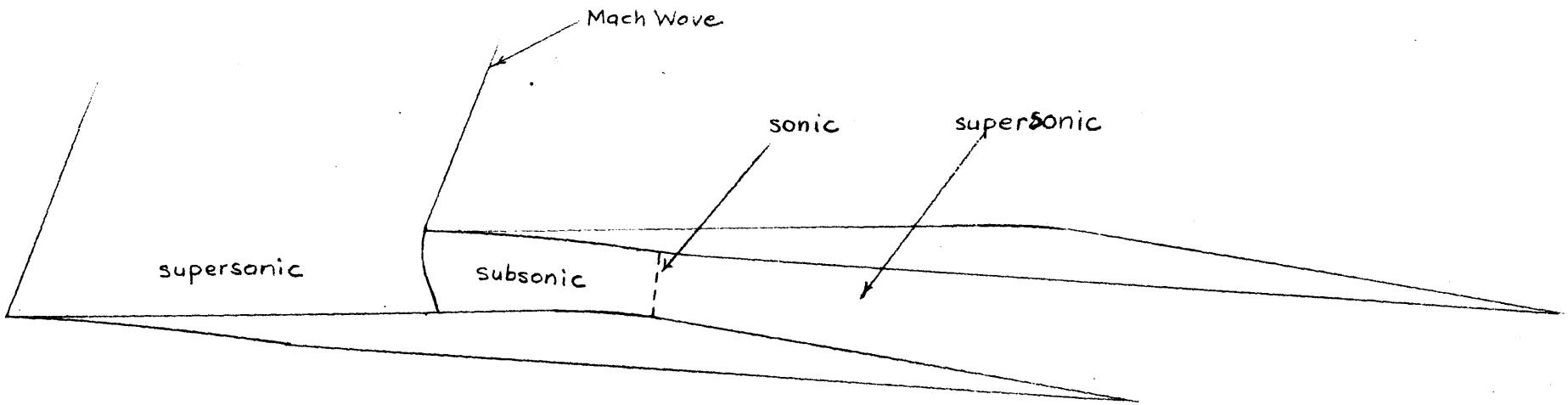

$1 < M << 2$

(undisturbed flow)

Wave Pattern for the Cascade at the End of the Bow Wave System

$1 \ll M < 2$

(undisturbed flow)

Starting Condition

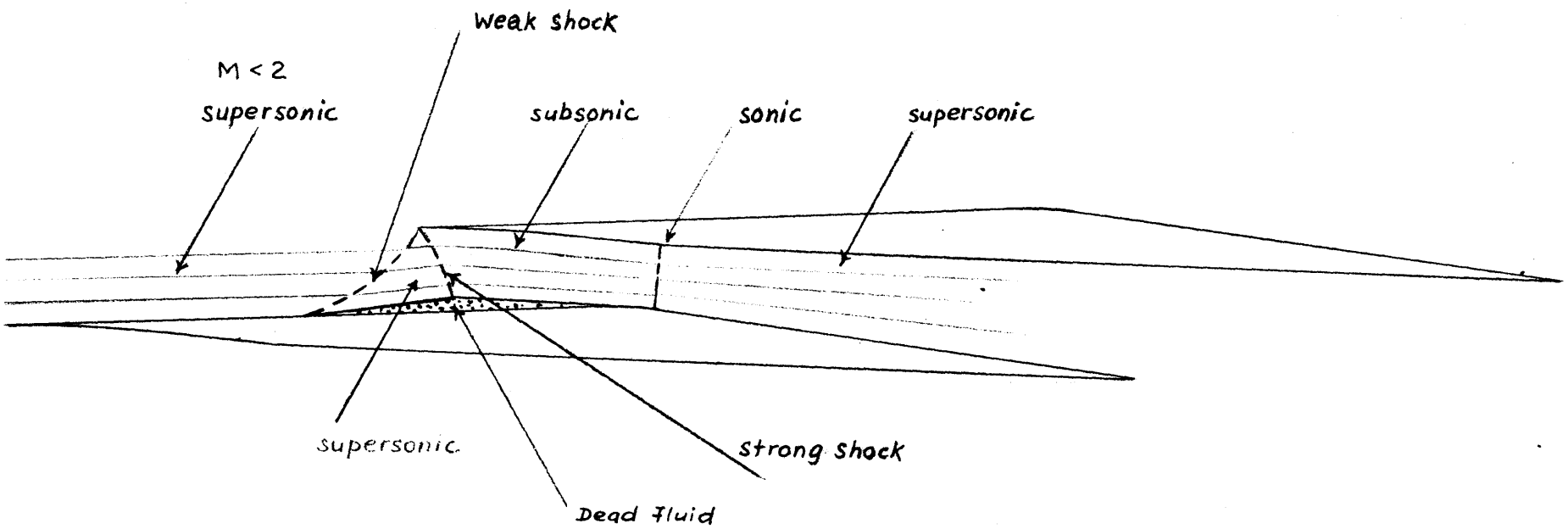

Wave Pattern for the Cascade Before Flow Reaches M = 2. Fork Shock System.

Fig (43)

Fig (44)

Free Stream: $\ell = .302''$ $M = 1.56$

$\ell_o = .670''$

$\ell^* = .446''$ ($M = 1$)

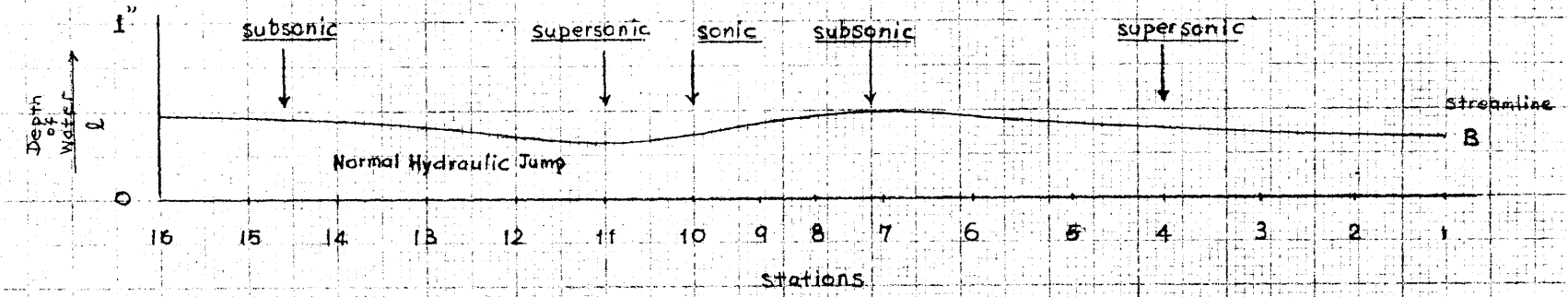

Fig (45)

Free Stream: $l = .238"$ $M = 2.0$

$l_o = .714"$

$l^* = .476"$

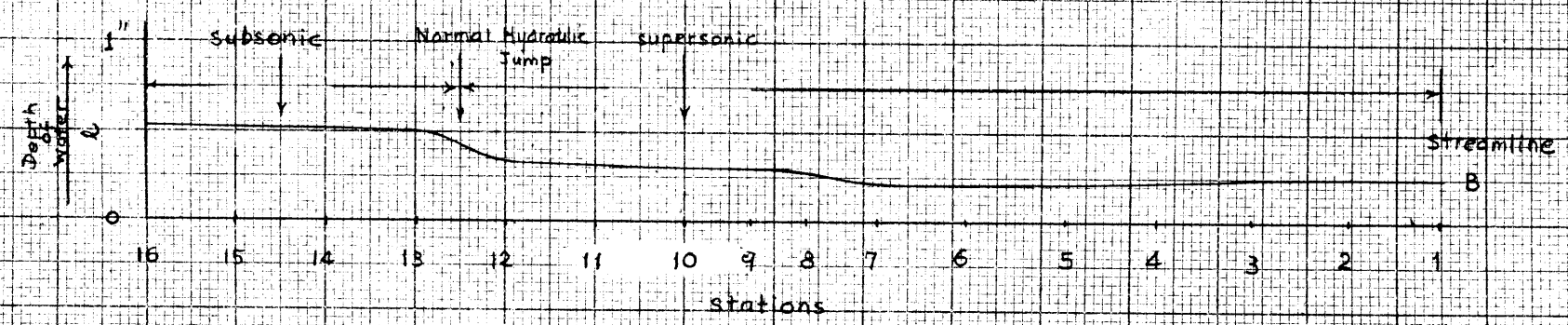

V. TABLES

TABLE (I)

ν	M_1/M_u	M_2/M_u	$(M_u)_{max}$	$(M_u)_{min}$	$\measuredangle\theta$	$\measuredangle\alpha_2$
0.289	0.577	1.528	1.732	0.655	120.00°	10.90°
0.350	0.610	1.540	1.640	0.650	110.00°	13.10°
0.400	0.640	1.550	1.560	0.645	102.60°	14.93°
0.450	0.673	1.570	1.485	0.637	96.00°	16.70°
0.500	0.708	1.582	1.410	0.632	90.00°	18.40°
0.550	0.744	1.600	1.344	0.625	84.40°	20.10°
0.600	0.780	1.615	1.282	0.622	79.60°	21.80°
0.650	0.820	1.635	1.220	0.612	75.00°	23.40°
0.700	0.860	1.660	1.160	0.603	71.00°	25.00°
0.750	0.900	1.689	1.110	0.595	67.40°	26.55°
0.800	0.943	1.700	1.060	0.588	64.00°	28.05°
0.866	1.000	1.732	1.000	0.576	60.00°	30.00°

TABLE (II)

M_u	M_1	M_2	M'_u	R	η	$W\sqrt{T_o}/A_o P_{1o}$
$\measuredangle \theta = 120^\circ$, $\gamma = 0.289$, $\measuredangle \alpha_2 = 10.90^\circ$, $\measuredangle \alpha_1 = 30.00^\circ$						
0.655_{min}	0.377	1.000	0.646_{min}	1.716	1.000	0.159
0.800	0.461	1.223	0.784	2.142	0.988	0.187
1.000	0.577	1.528	0.968	2.910	0.915	0.219
1.200	0.692	1.834	1.148	3.490	0.825	0.242
1.400	0.807	2.140	1.318	4.145	0.720	0.256
1.600	0.922	2.444	1.480	4.710	0.640	0.264
1.732_{max}	1.000	2.650	1.582_{max}	5.010	0.585	0.266
$\measuredangle \theta = 102.6^\circ$, $\gamma = 0.400$, $\measuredangle \alpha_2 = 14.93^\circ$, $\measuredangle \alpha_1 = 38.70^\circ$						
0.645_{min}	0.413	1.000	0.634_{min}	1.680	1.000	0.214
0.800	0.512	1.240	0.779	2.115	0.982	0.253
1.000	0.640	1.550	0.961	2.740	0.903	0.291
1.200	0.768	1.860	1.136	3.350	0.805	0.316
1.400	0.897	2.170	1.300	3.900	0.710	0.330
1.560_{max}	1.000	2.420	1.425_{max}	4.230	0.630	0.332
$\measuredangle \theta = 90^\circ$, $\gamma = 0.500$, $\measuredangle \alpha_2 = 18.40^\circ$, $\measuredangle \alpha_1 = 45.00^\circ$						
0.632_{min}	0.448	1.000	0.620_{min}	1.645	1.000	0.259
0.800	0.567	1.266	0.776	2.095	0.980	0.305
1.000	0.708	1.582	0.953	2.670	0.887	0.345
1.200	0.850	1.900	1.122	3.180	0.783	0.367
1.410_{max}	1.000	2.230	1.288_{max}	3.620	0.675	0.376

(over)

(TABLE II continued)

M_u	M_1	M_2	M'_u	R	η	$W\sqrt{T_{10}}/A_0 p_{10}$
$\measuredangle\theta$ = 79.60 , ν = 0.600 , $\measuredangle\alpha_2$ = 21.80 , $\measuredangle\alpha_1$ = 50.20						
0.620_{min}	0.484	1.000	0.606_{min}	1.620	1.000	0.299
0.800	0.624	1.292	0.770	2.070	0.972	0.353
1.000	0.780	1.615	0.944	2.585	0.870	0.391
1.150	0.898	1.858	1.068	2.940	0.790	0.406
1.282_{max}	1.000	2.070	1.170_{max}	3.170	0.715	0.410
$\measuredangle\theta$ = 71.00 , ν = 0.700 , $\measuredangle\alpha_2$ = 25.00 , $\measuredangle\alpha_1$ = 54.50						
0.603_{min}	0.518	1.000	0.587_{min}	1.582	1.000	0.353
0.800	0.688	1.327	0.765	2.045	0.962	0.393
1.000	0.866	1.660	0.933	2.480	0.855	0.427
1.160_{max}	1.000	1.925	1.060_{max}	2.790	0.755	0.433
$\measuredangle\theta$ = 64.00 , ν = 0.800 , $\measuredangle\alpha_2$ = 28.05 , $\measuredangle\alpha_1$ = 58.00						
0.588_{min}	0.555	1.000	0.571_{min}	1.534	1.000	0.362
0.700	0.660	1.190	0.676	1.775	0.987	0.402
0.800	0.754	1.360	0.758	1.995	0.950	0.426
0.900	0.848	1.530	0.842	2.192	0.880	0.443
1.060_{max}	1.000	1.800	0.968_{max}	2.440	0.785	0.451
$\measuredangle\theta$ = 60.00 , ν = 0.866 , $\measuredangle\alpha_2$ = 30.00 , $\measuredangle\alpha_1$ = 60.00						
0.576_{min}	0.576	1.000	0.558_{min}	1.524	1.000	0.378
0.700	0.700	1.214	0.668	1.768	0.980	0.422
0.800	0.800	1.390	0.753	1.975	0.940	0.444
0.900	0.900	1.560	0.835	2.153	0.875	0.457
1.000_{max}	1.000	1.732	0.913_{max}	2.304	0.805	0.460

TABLE(III)

$\measuredangle\ \theta=120^\circ$, $\gamma = 0.289$, $\measuredangle\ \alpha_2 = 10.90^\circ$, $\measuredangle\ \alpha_1 = 30.00^\circ$

1. $M_1' = 1.190$

M_1	0.300	0.400	0.500	0.600	0.722	0.775
M_{w1}	0.955	0.889	0.827	0.797	0.722	0.715
M_{w2}	0.185	0.270	0.370	0.480	0.722	1.000
M_2	1.275	1.365	1.485	1.620	1.910	2.240
M_1'	0.297	0.394	0.488	0.580	0.687	0.733
M_{w1}'	0.946	0.874	0.807	0.770	0.687	0.675
M_{w2}'	0.199	0.283	0.380	0.482	0.687	0.904
M_2'	1.367	1.435	1.525	1.625	1.820	2.025
$\measuredangle\ \beta_1'$	9.03°	13.02°	17.62°	22.12°	30.00°	32.50°
$\measuredangle\ \alpha_2'$	4.15°	5.70°	7.15°	8.54°	10.90°	12.90°
R	2.130	2.600	2.980	3.320	3.680	4.040
η	0.456	0.600	0.702	0.770	0.797	0.772
$\frac{W\sqrt{T_{10}}}{A_0 p_{10}}$	0.130	0.168	0.199	0.223	0.246	0.254

(over)

(TABLE III continued)

2. $M_1' = 1.095$

M_1	0.400	0.500	0.600	0.658	0.700	0.730
M_{w1}	0.792	0.733	0.684	0.658	0.643	0.635
M_{w2}	0.293	0.406	0.546	0.658	0.780	1.000
M_2	1.315	1.450	1.615	1.745	1.886	2.140
M_1'	0.394	0.488	0.580	0.632	0.668	0.690
M_{w1}'	0.778	0.715	0.660	0.632	0.613	0.600
M_{w2}'	0.304	0.410	0.536	0.632	0.732	0.903
M_2'	1.367	1.464	1.585	1.675	1.770	1.930
$\measuredangle \beta_1'$	14.65°	20.00°	26.10°	30.00°	33.00°	35.10°
$\measuredangle \alpha_2'$	6.38°	8.05°	9.73°	10.90°	11.90°	13.55°
R	2.450	2.840	3.130	3.300	3.440	3.680
η	0.660	0.770	0.834	0.847	0.837	0.804
$\frac{W\sqrt{T_{t0}}}{A_0 p_{t0}}$	0.168	0.199	0.223	0.237	0.243	0.248

(over)

(TABLE III continued)

3. $M_1 = 0.995$

M_1	0.300	0.400	0.500	0.695	0.695
M_{w1}	0.758	0.694	0.636	0.595	0.565
M_{w2}	0.224	0.324	0.445	0.595	1.000
M_2	1.155	1.265	1.405	1.575	2.040
M_1'	0.297	0.394	0.488	0.575	0.664
M_{w1}'	0.752	0.682	0.621	0.575	0.540
M_{w2}'	0.234	0.331	0.443	0.575	0.898
M_2'	1.204	1.292	1.397	1.522	1.830
$\measuredangle \beta_1'$	11.43°	16.80°	23.15°	30.00°	38.60°
$\measuredangle \alpha_2'$	6.30°	7.37°	9.15°	10.90°	14.25°
R	1.930	2.340	2.665	2.910	3.350
η	0.557	0.727	0.848	0.905	0.867
$\frac{W\sqrt{T_{10}}}{A_0 p_{10}}$	0.130	0.168	0.199	0.223	0.242

(over)

(TABLE III continued)

4. $M_u' = 0.895$

M_1	0.300	0.400	0.530	0.600	0.655
M_{w1}	0.664	0.597	0.530	0.505	0.490
M_{w2}	0.241	0.355	0.530	0.670	1.000
M_2	1.082	1.210	1.404	1.560	1.930
M_1'	0.297	0.394	0.516	0.580	0.636
M_{w1}'	0.658	0.587	0.516	0.488	0.469
M_{w2}'	0.248	0.357	0.516	0.636	0.897
M_2'	1.116	1.217	1.365	1.480	1.730
$\measuredangle \beta_1'$	13.06°	19.60°	30.00°	36.40°	43.60°
$\measuredangle \alpha_2'$	6.37°	8.44°	10.90°	12.40°	15.00°
R	1.802	2.190	2.560	2.740	3.110
η	0.595	0.805	0.952	0.975	0.951
$\frac{W\sqrt{T_o}}{A_o p_o}$	0.130	0.168	0.207	0.223	0.237

TABLE (IV)

$\measuredangle\theta = 102.6$, $\gamma = 0.400$, $\measuredangle\alpha_2 = 14.93^\circ$, $\measuredangle\alpha_1 = 38.70^\circ$

1. $M_u' = 1.145$

M_1	0.400	0.500	0.600	0.700	0.775	0.800	0.815
M_{w1}	0.890	0.840	0.810	0.785	0.775	0.765	0.775
M_{w2}	0.270	0.360	0.473	0.615	0.775	0.850	1.000
M_2	1.310	1.410	1.537	1.697	1.875	1.970	2.130
M_1'	0.394	0.488	0.580	0.668	0.732	0.753	0.765
M_{w1}'	0.873	0.822	0.782	0.750	0.732	0.730	0.728
M_{w2}'	0.285	0.371	0.475	0.600	0.732	0.790	0.908
M_2'	1.380	1.455	1.545	1.655	1.772	1.830	1.935
$\measuredangle\beta_1'$	16.40°	21.80°	27.60°	33.80°	38.70°	40.20°	41.00°
$\measuredangle\alpha_2'$	7.43°	9.18°	11.00°	13.12°	14.93°	15.67°	17.00°
R	2.400	2.730	3.010	3.240	3.400	3.470	3.550
η	0.570	0.677	0.755	0.800	0.803	0.798	0.758
$\frac{W\sqrt{T_{10}}}{A_0 p_{10}}$	0.210	0.249	0.280	0.304	0.318	0.321	0.323

(over)

(TABLE IV continued)

2. $M_u' = 1.049$

M_1	0.300	0.400	0.500	0.600	0.705	0.750	0.770
M_{w1}	0.845	0.795	0.755	0.725	0.705	0.700	0.708
M_{w2}	0.205	0.295	0.400	0.520	0.705	0.840	1.000
M_2	1.160	1.260	1.370	1.520	1.710	1.860	2.020
M_1'	0.297	0.394	0.488	0.580	0.672	0.711	0.728
M_{w1}'	0.838	0.782	0.735	0.699	0.672	0.665	0.670
M_{w2}'	0.216	0.310	0.406	0.507	0.672	0.781	0.905
M_2'	1.225	1.307	1.390	1.480	1.630	1.730	1.845
$\alpha\beta_1'$	12.82°	18.36°	24.50°	31.20°	38.70°	42.00°	42.50°
$\alpha\alpha_2'$	6.34°	8.55°	10.55°	12.35°	14.93°	16.40°	17.86°
R	1.840	2.270	2.580	2.840	3.065	3.200	3.230
η	0.458	0.630	0.755	0.830	0.857	0.847	0.812
$\frac{W\sqrt{T_{10}}}{A_e p_{10}}$	0.164	0.210	0.249	0.280	0.305	0.314	0.317

(over)

(TABLE IV continued)

3. $M_u' = 0.957$

M_1	0.300	0.400	0.500	0.600	0.637	0.700	0.730
M_{w1}	0.755	0.707	0.668	0.644	0.637	0.635	0.634
M_{w2}	0.224	0.320	0.423	0.600	0.637	0.790	1.000
M_2	1.103	1.203	1.314	1.500	1.545	1.710	1.945
M_1'	0.297	0.394	0.488	0.580	0.612	0.668	0.694
M_{w1}'	0.747	0.696	0.652	0.622	0.612	0.605	0.603
M_{w2}'	0.233	0.327	0.423	0.583	0.612	0.738	0.903
M_2'	1.148	1.230	1.314	1.460	1.488	1.600	1.755
$\measuredangle \beta_1'$	14.40°	20.70°	27.90°	36.80°	38.70°	43.60°	45.60°
$\measuredangle \alpha_2'$	7.30°	9.55°	11.65°	14.50°	14.93°	16.73°	18.80°
R	1.765	2.137	2.420	2.700	2.750	2.890	2.980
η	0.507	0.695	0.821	0.900	0.908	0.912	0.870
$\frac{W\sqrt{T_{10}}}{A_6 P_{10}}$	0.164	0.210	0.249	0.280	0.290	0.304	0.310

(over)

(TABLE IV continued)

4. $M_1 = 0.860$

M_1	0.300	0.400	0.500	0.567	0.600	0.700
M_{w1}	0.665	0.615	0.585	0.567	0.565	0.575
M_{w2}	0.235	0.345	0.467	0.567	0.628	1.000
M_2	1.030	1.143	1.270	1.375	1.440	1.845
M_1'	0.298	0.394	0.488	0.550	0.579	0.668
M_{w1}'	0.659	0.606	0.570	0.550	0.545	0.548
M_{w2}'	0.242	0.348	0.462	0.550	0.603	0.900
M_2'	1.060	1.153	1.254	1.335	1.383	1.660
$\measuredangle \beta_1'$	16.37°	23.95°	32.30°	38.70°	41.70°	49.60°
$\measuredangle \alpha_2'$	8.22°	10.90°	13.30°	14.93°	15.84°	19.80°
R	1.635	1.960	2.265	2.430	2.530	2.790
η	0.535	0.760	0.903	0.956	0.973	0.945
$\frac{W\sqrt{T_{10}}}{A_0 p_{10}}$	0.164	0.210	0.249	0.270	0.280	0.305

TABLE (V)

$\measuredangle\theta = 90^\circ$, $\nu = 0.500$, $\measuredangle\alpha_2 = 18.40^\circ$, $\measuredangle\alpha_1 = 30.00^\circ$

1. $M_u' = 1.010$

M_1	0.400	0.500	0.600	0.700	0.755	0.800
M_{w1}	0.797	0.767	0.752	0.750	0.755	0.758
M_{w2}	0.294	0.393	0.493	0.650	0.755	1.000
M_2	1.200	1.300	1.407	1.575	1.685	1.970
M_1'	0.394	0.488	0.579	0.668	0.715	0.753
M_{w1}'	0.783	0.748	0.726	0.715	0.715	0.714
M_{w2}'	0.305	0.400	0.492	0.628	0.715	0.908
M_2'	1.247	1.324	1.402	1.522	1.596	1.774
$\measuredangle\beta_1'$	20.80°	27.40°	34.30°	41.30°	45.00°	48.20°
$\measuredangle\alpha_2'$	9.95°	12.32°	14.36°	17.00°	18.40°	21.20°
R	2.050	2.320	2.550	2.770	2.880	3.080
η	0.593	0.712	0.790	0.843	0.850	0.825
$\frac{W\sqrt{T_o}}{A_o p_{to}}$	0.237	0.282	0.316	0.344	0.355	0.363

(over)

(TABLE V continued)

2. $M_u' = 0.925$

M_1	0.400	0.500	0.600	0.685	0.760
M_{w1}	0.715	0.690	0.680	0.685	0.690
M_{w2}	0.318	0.423	0.550	0.685	1.000
M_2	1.155	1.255	1.390	1.530	1.870
M_1'	0.394	0.488	0.579	0.655	0.720
M_{w1}'	0.703	0.673	0.656	0.655	0.653
M_{w2}'	0.326	0.425	0.540	0.655	0.905
M_2'	1.180	1.260	1.362	1.462	1.690
$\alpha\beta_1'$	23.30°	30.80°	38.70°	45.00°	50.60°
$\alpha\alpha_2'$	11.30°	13.80°	16.25°	18.40°	22.20°
R	1.975	2.230	2.420	2.580	2.805
η	0.660	0.785	0.874	0.912	0.880
$\frac{W\sqrt{T}_{10}}{A_o p_{10}}$	0.237	0.282	0.316	0.341	0.356

(over)

(TABLE V continued)

3. $M_1' = 0.835$

M_1	0.400	0.500	0.600	0.650	0.700	0.727
M_{w1}	0.632	0.613	0.609	0.614	0.622	0.630
M_{w2}	0.340	0.455	0.594	0.684	0.850	1.000
M_2	1.087	1.207	1.350	1.445	1.617	1.780
M_1'	0.394	0.488	0.579	0.624	0.668	0.692
M_{w1}'	0.622	0.598	0.588	0.590	0.593	0.600
M_{w2}'	0.344	0.452	0.575	0.652	0.788	0.902
M_2'	1.100	1.197	1.307	1.375	1.500	1.605
$\measuredangle \beta_1'$	26.60°	35.20°	44.10°	48.50°	53.00°	54.40°
$\measuredangle \alpha_2'$	12.77°	15.48°	18.10°	19.56°	21.80°	23.40°
R	1.876	2.100	2.300	2.400	2.502	2.580
η	0.730	0.870	0.953	0.976	0.975	0.943
$\frac{W\sqrt{T_{10}}}{A_0 P_{10}}$	0.237	0.282	0.316	0.332	0.344	0.350

TABLE (VI)

M_{w1}	A^* / A_{w1}	M_1	$\frac{\sin\beta_1'}{\sin\alpha_1}$
0.20	0.3374	0.593	2.960
0.30	0.4914	0.610	2.036
0.40	0.6289	0.636	1.590
0.50	0.7464	0.670	1.340
0.60	0.8416	0.712	1.188
0.70	0.9138	0.766	1.094
0.80	0.9632	0.830	1.039
0.90	0.9912	0.908	1.010
1.00	1.0000	1.000	1.000

TABLE (VII)

M_u'	M_u	M_1	$\frac{W\sqrt{T}_{10}}{A_o P_{10}}$
$\measuredangle\theta = 120°$, $\gamma = 0.289$, $\measuredangle\alpha_2 = 10.90$, $\measuredangle\alpha_1 = 30.00$			
0.763	0.793	0.636	0.232
0.912	0.952	0.670	0.238
1.049	1.099	0.712	0.245
1.188	1.252	0.766	0.252
1.318	1.404	0.830	0.259
1.452	1.565	0.908	0.264
1.732	1.732	1.000	0.266
$\measuredangle\theta = 102.6$, $\gamma = 0.400$, $\measuredangle\alpha_2 = 14.93$, $\measuredangle\alpha_1 = 38.70$			
0.477	0.496	0.636	0.290
0.761	0.795	0.670	0.298
0.915	0.960	0.712	0.306
1.050	1.110	0.766	0.316
1.177	1.255	0.830	0.325
1.308	1.410	0.908	0.330
1.560	1.560	1.000	0.332
$\measuredangle\theta = 90$, $\gamma = 0.500$, $\measuredangle\alpha_2 = 18.40$, $\measuredangle\alpha_1 = 45.00$			
0.612	0.638	0.670	0.337
0.792	0.831	0.712	0.346
0.933	0.987	0.766	0.357
1.060	1.130	0.830	0.366
1.180	1.272	0.908	0.373
1.414	1.414	1.000	0.375

TABLE (VIII)

(p_1/p_{1a})

$\rho \backslash M_{ua}$	0.800	0.900	1.000	1.100	1.200	1.300	1.400
1.000	1.000	1.000	1.000	1.000	1.000	1.000	1.000
0.950	0.988	0.985	0.981	0.977	0.973	0.969	0.964
0.900	0.974	0.967	0.960	0.951	0.942	0.932	0.922
0.850	0.957	0.947	0.934	0.921	0.906	0.891	0.875
0.800	0.938	0.922	0.905	0.886	0.863	0.842	0.820

(p_2/ p_{2a})

$\rho \backslash M_{ua}$	0.800	0.900	1.000	1.100	1.200	1.300	1.400
1.000	1.000	1.000	1.000	1.000	1.000	1.000	1.000
0.950	0.900	0.868	0.840	0.809	0.775	0.741	0.704
0.900	0.783	0.730	0.677	0.620	0.560	0.504	0.444
0.850	0.665	0.590	0.514	0.440	0.368	0.299	0.235
0.800	0.538	0.450	0.362	0.278	0.198	0.104	0.090

$p_{1a} = p_{2a}$

TABLE (IX)

$\angle \alpha_1$

φ	1.000	0.950	0.900	0.850	0.800
$\theta_a = 120.0$	30.00	28.80	27.50	26.20	24.80
$\theta_a = 102.6$	38.65	37.20	25.75	34.20	32.60
$\theta_a = 90.0$	45.00	43.55	42.00	40.40	38.70

$\angle \beta_1$

φ	1.000	0.950	0.900	0.850	0.800
$\theta_a = 120.0$	30.00	34.30	40.00	47.80	58.80
$\theta_a = 102.6$	38.65	43.30	49.20	56.80	66.40
$\theta_a = 90.0$	45.00	49.70	55.40	62.35	70.70

$\angle \beta_2$

φ	1.000	0.950	0.900	0.850	0.800
$\theta_a = 120.0$	30.00	24.70	20.70	17.55	15.05
$\theta_a = 102.6$	38.65	32.50	27.65	23.60	20.14
$\theta_a = 90.0$	45.00	38.50	33.20	28.65	24.95

$\angle \alpha_2$

φ	1.000	0.950	0.900	0.850	0.800
$\theta_a = 120.0$	10.90	10.38	9.85	9.28	8.75
$\theta_a = 102.6$	14.93	14.20	13.50	12.78	12.04
$\theta_a = 90.0$	18.40	17.57	16.70	15.80	14.92

TABLE (X)

M_{ua}	M'_{ua}	$(\rho)_{min}$
$\theta_a = 120^\circ$		
0.655_{min}	0.646_{min}	0.722
0.800	0.784	0.791
1.000	0.968	0.863
1.200	1.148	0.915
1.400	1.318	0.955
1.600	1.480	0.985
1.732_{max}	1.582_{max}	1.000
$\theta_a = 102.6^\circ$		
0.645_{min}	0.634_{min}	0.722
0.800	0.779	0.797
1.000	0.961	0.873
1.200	1.136	0.930
1.400	1.300	0.974
1.560_{max}	1.425_{max}	1.000
$\theta_a = 90^\circ$		
0.632_{min}	0.620_{min}	0.722
0.800	0.776	0.811
1.000	0.953	0.890
1.200	1.122	0.948
1.410_{max}	1.288_{max}	1.000

M_{ua}	M'_{ua}	$(\rho)_{min}$
$\theta_a = 79.6^\circ$		
0.620_{min}	0.606_{min}	0.722
0.800	0.770	0.824
1.000	0.944	0.910
1.150	1.068	0.962
1.282_{max}	1.170_{max}	1.000
$\theta_a = 71^\circ$		
0.603_{min}	0.587_{min}	0.722
0.800	0.765	0.842
1.000	0.933	0.939
1.160_{max}	1.060_{max}	1.000
$\theta_a = 64^\circ$		
0.588_{min}	0.571_{min}	0.722
0.700	0.676	0.802
0.800	0.758	0.863
0.900	0.842	0.922
1.060_{max}	0.968_{max}	1.000
$\theta_a = 60^\circ$		
0.576_{min}	0.558_{min}	0.722
0.700	0.668	0.815
0.800	0.753	0.883
0.900	0.835	0.945
1.000_{max}	0.913_{max}	1.000

TABLE (XI)

$\measuredangle\theta_a = 120^\circ$, $\gamma_a = 0.289$, $\alpha_{1a} = 10.9^\circ$, $\alpha_{1a}, \beta_{1a}, \beta_{2a} = 30^\circ$

ξ	M_1	M_2	R	η
$M'_{ua} = 0.784$				
1.000	0.461	1.223	2.142	0.988
0.950	0.482	1.304	2.115	0.972
0.900	0.503	1.400	2.070	0.940
0.850	0.528	1.515	2.000	0.890
0.800	0.556	1.660	1.885	0.806
0.791_{min}	0.560	1.700	1.870	0.790
$M'_{ua} = 0.877$				
1.000	0.520	1.374	2.460	0.955
0.950	0.542	1.472	2.393	0.922
0.900	0.566	1.593	2.290	0.870
0.850	0.595	1.735	2.142	0.792
0.830_{min}	0.610	1.800	2.080	0.752
$M'_{ua} = 0.968$				
1.000	0.577	1.528	2.810	0.915
0.950	0.602	1.645	2.680	0.867
0.900	0.630	1.790	2.490	0.795
0.863_{min}	0.650	1.920	2.320	0.725

(over)

(TABLE XI continued)

ς	M_1	M_2	R	η
$M'_{ua} = 1.060$				
1.000	0.635	1.680	3.150	0.866
0.950	0.663	1.820	2.930	0.804
0.900	0.695	1.992	2.640	0.715
0.891_{min}	0.700	2.020	2.580	0.695
$M'_{ua} = 1.148$				
1.000	0.692	1.834	3.490	0.825
0.950	0.724	1.995	3.160	0.742
0.915_{min}	0.750	2.120	2.870	0.670
$M'_{ua} = 1.235$				
1.000	0.750	1.985	3.830	0.770
0.950	0.785	2.180	3.360	0.681
0.937_{min}	0.790	2.230	3.230	0.650
$M'_{ua} = 1.318$				
1.000	0.807	2.140	4.145	0.720
0.955_{min}	0.845	2.320	3.580	0.635

TABLE (XII)

$\times \theta_a = 102.6^\circ$; $\gamma_a = 0.400$, $\times d_{2a} = 14.93^\circ$; $\times d_{1a}, \beta_{1a}, \beta_{2a} = 38.7^\circ$

ϱ	M_1	M_2	R	η
$M'_{ua} = 0.779$				
1.000	0.512	1.240	2.115	0.982
0.950	0.530	1.325	2.085	0.960
0.900	0.550	1.425	2.040	0.930
0.850	0.573	1.535	1.965	0.877
0.800	0.599	1.680	1.850	0.790
0.797_{min}	0.600	1.700	1.840	0.785
$M'_{ua} = 0.871$				
1.000	0.576	1.395	2.430	0.950
0.950	0.597	1.495	2.360	0.915
0.900	0.620	1.615	2.250	0.860
0.850	0.645	1.760	2.100	0.776
0.838_{min}	0.650	1.800	2.050	0.750
$M'_{ua} = 0.961$				
1.000	0.640	1.550	2.740	0.903
0.950	0.663	1.670	2.610	0.855
0.900	0.690	1.815	2.422	0.778
0.873_{min}	0.706	1.900	2.310	0.725
$M'_{ua} = 1.050$				
1.000	0.705	1.710	3.050	0.855
0.950	0.730	1.845	2.840	0.788
0.903_{min}	0.755	2.000	2.570	0.703

(over)

(TABLE XII continued)

$M'_{ua} = 1.136$

1.000	0.768	1.860	3.350	0.805
0.950	0.797	2.030	3.020	0.723
0.930_{min}	0.810	2.110	2.850	0.680

TABLE (XIII)

$\measuredangle \theta_a = 90°$; $\gamma_a = 0.500$, $\measuredangle \alpha_{2a} = 18.4°$, $\measuredangle \alpha_{1a}, \beta_{1a}, \beta_{2a} = 45°$

ς	M_1	M_2	R	η
$M'_{ua} = 0.776$				
1.000	0.567	1.266	2.095	0.980
0.950	0.582	1.345	2.062	0.958
0.900	0.601	1.445	2.013	0.920
0.850	0.621	1.555	1.940	0.867
0.811_{min}	0.640	1.660	1.860	0.802
$M'_{ua} = 0.865$				
1.000	0.636	1.420	2.385	0.940
0.950	0.655	1.485	2.320	0.900
0.900	0.677	1.640	2.200	0.844
0.853_{min}	0.695	1.770	2.080	0.768
$M'_{ua} = 0.953$				
1.000	0.708	1.582	2.670	0.887
0.950	0.728	1.700	2.535	0.835
0.900	0.752	1.830	2.365	0.767
0.890_{min}	0.760	1.850	2.320	0.745
$M'_{ua} = 1.040$				
1.000	0.778	1.740	3.090	0.842
0.950	0.800	1.880	2.860	0.776
0.929_{min}	0.810	1.950	2.750	0.740

TABLE (XIV)

M_2	p_{30}/p_{20}	A_{min}/A_2	$(M)_{A_{min}}$	p'_{30}/p_{20}	p'_{30}/p_{30}
1.000	1.000	1.000	1.000	1.000	1.000
1.200	0.993	0.978	1.095	0.999	1.005
1.400	0.958	0.936	1.240	0.988	1.031
1.600	0.895	0.893	1.405	0.957	1.070
1.800	0.813	0.855	1.575	0.904	1.112
2.000	0.721	0.822	1.750	0.835	1.158
2.200	0.628	0.794	1.930	0.754	1.200
2.400	0.540	0.771	2.110	0.670	1.240
2.600	0.460	0.750	2.290	0.588	1.277
2.800	0.390	0.733	2.470	0.511	1.311
3.000	0.328	0.720	2.655	0.440	1.340
3.200	0.276	0.706	2.835	0.378	1.370
3.400	0.232	0.695	3.015	0.324	1.395
3.600	0.195	0.687	3.200	0;276	1.415
3.800	0.165	0.678	3.380	0.236	1.435
4.000	0.139	0.672	3.566	0.201	1.445

TABLE (XV)

M'_u	R'	η'
$\theta = 120^\circ$		
0.646_{min}	1.716	1.000
0.784	2.190	0.997
0.968	2.980	0.966
1.148	3.910	0.909
1.318	4.880	0.835
1.480	5.820	0.752
1.582_{max}	6.450	0.695
$\theta = 102.6^\circ$		
0.634_{min}	1.680	1.000
0.779	2.180	0.993
0.961	2.930	0.962
1.136	3.780	0.902
1.300	4.620	0.823
1.425_{max}	5.260	0.752
$\theta = 90^\circ$		
0.620_{min}	1.645	1.000
0.776	2.130	0.992
0.953	2.860	0.956
1.122	3.630	0.888
1.288_{max}	4.370	0.794

M'_u	R'	η'
$\theta = 79.6^\circ$		
0.606_{min}	1.620	1.000
0.770	2.120	0.990
0.944	2.780	0.950
1.068	3.300	0.893
1.170_{max}	3.720	0.835
$\theta = 71^\circ$		
0.587_{min}	1.582	1.000
0.765	2.075	0.987
0.933	2.685	0.937
1.060_{max}	3.180	0.870
$\theta = 64^\circ$		
0.571_{min}	1.534	1.000
0.676	1.760	0.994
0.758	2.020	0.984
0.842	2.310	0.960
0.968_{max}	2.720	0.892
$\theta = 60^\circ$		
0.558_{min}	1.524	1.000
0.668	1.730	0.993
0.753	1.980	0.980
0.835	2.240	0.953
0.913_{max}	2.500	0.913

TABLE (XVI)

M_x	M_y	n	E_y/E_x
1.0	1.000	1.600	1.000
1.2	0.835	1.274	0.998
1.4	0.730	1.545	0.986
1.6	0.653	1.818	0.967
1.8	0.594	2.092	0.940
2.0	0.547	2.370	0.908
2.2	0.510	2.650	0.875
2.4	0.479	2.930	0.840
2.6	0.453	3.210	0.807
2.8	0.430	3.490	0.775
3.0	0.410	3.770	0.740
3.2	0.393	4.050	0.713
3.4	0.377	4.330	0.685
3.6	0.362	4.620	0.657
3.8	0.350	4.910	0.633
4.0	0.339	5.180	0.608

TABLE(XVII)

M	b*/b	b_{min}/b	Mb_{min}
0	0	-	-
0.1	0.189	-	-
0.2	0.367	-	-
0.3	0.516	-	-
0.4	0.656	-	-
0.5	0.770	-	-
0.6	0.862	-	-
0.7	0.928	-	-
0.8	0.972	-	-
0.9	0.995	-	-
1.0	1.000	1.000	1.000
1.2	0.977	0.983	1.075
1.4	0.925	0.945	1.185
1.6	0.853	0.900	1.310
1.8	0.780	0.855	1.435
2.0	0.707	0.814	1.555
2.2	0.643	0.778	1.680
2.4	0.577	0.745	1.805
2.6	0.524	0.714	1.930
2.8	0.472	0.687	2.050
3.0	0.428	0.663	2.175
3.2	0.386	0.642	2.300
3.4	0.355	0.623	2.425
3.6	0.324	0.605	2.550
3.8	0.299	0.590	2.670
4.0	0.273	0.575	2.800

TABLE (XVIII)

M'_{ua}	$\frac{W\sqrt{T_{1o}}}{\pi r_a^2 \cdot p_{1o}}$
$\theta_a = 120^\circ$	
0.646_{min}	0.0749
0.784	0.0690
0.968	0.0548
1.148	0.0393
1.318	0.0228
1.480	0.0079
1.582_{max}	0.0000
$\theta_a = 102.6^\circ$	
0.634_{min}	1.0100
0.779	0.0906
0.961	0.0685
1.136	0.0422
1.300	0.0164
1.425_{max}	0.0000
$\theta_a = 90^\circ$	
0.620_{min}	0.1220
0.776	0.1025
0.963	0.0707
1.122	0.0374
1.288_{max}	0.0000
$\theta_a = 79.6^\circ$	
0.606_{min}	0.1412
0.770	0.1115
0.944	0.0666
1.068	0.0303
1.170_{max}	0.0000
$\theta_a = 71^\circ$	
0.587_{min}	0.1668
0.765	0.1124
0.933	0.0504
1.060_{max}	0.0000

TABLE (XIX)

Free stream stagnation height = 0.670"

Free stream water height = 0.302"

Calculated Mach Number of free stream = 1.560

Depth Measurements in Inches

line / station	A	B	C	D
1	0.312	0.302	0.292	0.292
2	0.347	0.327	0.322	0.317
3	0.376	0.344	0.362	0.337
4	0.400	0.390	0.388	0.388
5	0.444	0.437	0.416	0.436
6	0.474	0.464	0.476	-
7	-	0.482	-	-
8	-	0.477	-	-
9	-	0.416	-	-
10	-	0.366	-	-
11	-	0.296	-	-
12	-	0.348	-	-
13	-	0.415	-	-
14	-	0.432	-	-
15	-	0.452	-	-
16	-	0.454	-	-

TABLE (XX)

Free stream stagnation height = 0.714"

Free stream water height = 0.238"

Calculated Mach Number of free stream = 2.000

Depth Measurements in inches

line / station	A	B	C	D
1	0.231	0.237	0.237	0.237
2	0.248	0.227	0.212	0.232
3	0.256	0.240	0.204	0.215
4	0.237	0.215	0.222	0.222
5	0.242	0.207	0.201	0.202
6	0.237	0.206	0.202	-
7	0.237	0.202	0.202	-
8	0.277	0.280	0.287	-
9	0.277	0.302	0.337	-
10	0.289	0.297	0.332	-
11	-	0.307	-	-
12	-	0.327	-	-
13	-	0.512	-	-
14	-	0.513	-	-
15	-	0.517	-	-
16	-	0.542	-	-

REFERENCES

1. A. Weise : A Supersonic Axial Flow Compressor. From Report No.171 of the Lilienthal Society.
2. A. Kantrowitz : The Supersonic Axial Flow Compressor. NACA ACR No. L6d02,1946
3. A. Kantrowitz and Coleman duP. Donaldson : Preliminary Investigation of Supersonic Diffusers. NACA ACR No. L5D20, 1945
4. E. Preiswerk : Anwendung Gasdynamischer Methoden auf Wasserstroemungen mit freier Oberflaeche. Mitteilungen aus dem Institut fuer Aerodynamik, Nr.7, 1938, Eidgenoessische Technische Hochschuele, Zuerich.
5. A. Weise : Ueber die Stroemungsabloesung durch Verdichtungsstoesse. Technische Berichte, Band 10, Heft 2, 1943, pp 59 - 61.
6. Eggink : Ueber Verdichtungsstoesse bei abgeloester Stroemung. Deutsche Luftfahrtforschung, Forschungsbericht Nr.1850.
7. R. Sauer : Theoretische Einfuehrung in die Gasdynamik. Springer-Verlag, 1943.

8. J.Erwin, L.Wright and A.Kantrowitz : Investigation of An Experimental Supersonic Axial Flow Compressor. NACA RM No.L6J01b, 1947.

9. W.R.Hawthorne and A.H.Shapiro : Report on present Status of Compressor Development with Special Reference to the Prospects for Supersonic Compressors. 1946.

BIOGRAPHY OF AUTHOR

In 1922, I was born in Shanghai, China. My childhood and early adolescent years were fairly uneventful. Then war came to Shanghai just as I had started in the preparatory school to National Tung-Chi University. (which maintains both a prep school and a college) So when the institution had to be moved to interior China, I, like most of the students, left home and moved with it. From then on, I was more or less on my own. I received my B.S. degree in 1943 from Tung-Chi. Then with the idea of furthering my studies in mechanical engineering, I came to America in 1944, and enrolled for graduate work at M.I.T.. I received my M.S. in 1945. The following year I stopped studying long enough to be an observer at Whitin Machine Work at Whitinsville, Mass. because my family had always been interested in textile industry and also to be an assistant at M.I.T. The latter project started me once more in scholastic work. I decided to concentrate on getting my doctorate and studied for the examination in 1947. Ever since, I have been working on the various aspects of my thesis.

W.W.Chao

December,1948